



National Library  
of Canada

Acquisitions and  
Bibliographic Services Branch

395 Wellington Street  
Ottawa, Ontario  
K1A 0N4

Bibliothèque nationale  
du Canada

Direction des acquisitions et  
des services bibliographiques

395, rue Wellington  
Ottawa (Ontario)  
K1A 0N4

*Notice à l'attention de*

*Notice à l'attention de*

## **NOTICE**

The quality of this microform is heavily dependent upon the quality of the original thesis submitted for microfilming. Every effort has been made to ensure the highest quality of reproduction possible.

If pages are missing, contact the university which granted the degree.

Some pages may have indistinct print especially if the original pages were typed with a poor typewriter ribbon or if the university sent us an inferior photocopy.

Reproduction in full or in part of this microform is governed by the Canadian Copyright Act, R.S.C. 1970, c. C-30, and subsequent amendments.

## **AVIS**

La qualité de cette microforme dépend grandement de la qualité de la thèse soumise au microfilmage. Nous avons tout fait pour assurer une qualité supérieure de reproduction.

S'il manque des pages, veuillez communiquer avec l'université qui a conféré le grade.

La qualité d'impression de certaines pages peut laisser à désirer, surtout si les pages originales ont été dactylographiées à l'aide d'un ruban usé ou si l'université nous a fait parvenir une photocopie de qualité inférieure.

La reproduction, même partielle, de cette microforme est soumise à la Loi canadienne sur le droit d'auteur, SRC 1970, c. C-30, et ses amendements subséquents.

**Canada**

UNIVERSITY OF ALBERTA

**Atmospheric Refraction and its Effects on Sunrise and Sunset**

by



**Russell Dean Sampson**

A thesis submitted to the Faculty of Graduate Studies and Research in partial fulfillment of the requirements for the degree of Master of Science.

Department of Geography

Edmonton, Alberta

Fall, 1994



National Library  
of Canada

Acquisitions and  
Bibliographic Services Branch

395 Wellington Street  
Ottawa, Ontario  
K1A 0N4

Bibliothèque nationale  
du Canada

Direction des acquisitions et  
des services bibliographiques

395, rue Wellington  
Ottawa (Ontario)  
K1A 0N4

*Your file* *Votre référence*

*Your file* *Notre référence*

THE AUTHOR HAS GRANTED AN  
IRREVOCABLE NON-EXCLUSIVE  
LICENCE ALLOWING THE NATIONAL  
LIBRARY OF CANADA TO  
REPRODUCE, LOAN, DISTRIBUTE OR  
SELL COPIES OF HIS/HER THESIS BY  
ANY MEANS AND IN ANY FORM OR  
FORMAT, MAKING THIS THESIS  
AVAILABLE TO INTERESTED  
PERSONS.

L'AUTEUR A ACCORDE UNE LICENCE  
IRREVOCABLE ET NON EXCLUSIVE  
PERMETTANT A LA BIBLIOTHEQUE  
NATIONALE DU CANADA DE  
REPRODUIRE, PRETER, DISTRIBUER  
OU VENDRE DES COPIES DE SA  
THESE DE QUELQUE MANIERE ET  
SOUS QUELQUE FORME QUE CE SOIT  
POUR METTRE DES EXEMPLAIRES DE  
CETTE THESE A LA DISPOSITION DES  
PERSONNE INTERESSEES.

THE AUTHOR RETAINS OWNERSHIP  
OF THE COPYRIGHT IN HIS/HER  
THESIS. NEITHER THE THESIS NOR  
SUBSTANTIAL EXTRACTS FROM IT  
MAY BE PRINTED OR OTHERWISE  
REPRODUCED WITHOUT HIS/HER  
PERMISSION.

L'AUTEUR CONSERVE LA PROPRIETE  
DU DROIT D'AUTEUR QUI PROTEGE  
SA THESE. NI LA THESE NI DES  
EXTRAITS SUBSTANTIELS DE CELLE-  
CI NE DOIVENT ETRE IMPRIMES OU  
AUTREMENT REPRODUITS SANS SON  
AUTORISATION.

ISBN 0-612-01786-9

Canada

Name Russell Dean Sampson

Dissertation Abstracts International is arranged by broad, general subject categories. Please select the one subject which most nearly describes the content of your dissertation. Enter the corresponding four-digit code in the spaces provided

0608

U·M·I

SUBJECT TERM

SUBJECT CODE

Subject Categories

THE HUMANITIES AND SOCIAL SCIENCES

COMMUNICATIONS AND THE ARTS

Architecture	0729
Art History	0377
Cinema	0900
Dance	0378
Fine Arts	0357
Information Science	0723
Journalism	0391
Library Science	0399
Mass Communications	0708
Music	0413
Speech Communication	0459
Theater	0465

EDUCATION

General	0515
Administration	0514
Adult and Continuing	0516
Agricultural	0517
Art	0273
Bilingual and Multicultural	0282
Business	0688
Community College	0275
Curriculum and Instruction	0727
Early Childhood	0518
Elementary	0524
Finance	0277
Guidance and Counseling	0519
Health	0680
Higher	0745
History of	0520
Home Economics	0278
Industrial	0521
Language and Literature	0279
Mathematics	0280
Music	0522
Philosophy of	0998
Physical	0523

Psychology	0525
Reading	0535
Religious	0527
Sciences	0714
Secondary	0533
Social Sciences	0534
Sociology of	0340
Special	0529
Teacher Training	0530
Technology	0710
Tests and Measurements	0288
Vocational	0747

LANGUAGE, LITERATURE AND LINGUISTICS

Language	
General	0679
Ancient	0289
Linguistics	0290
Modern	0291
Literature	
General	0401
Classical	0294
Comparative	0295
Medieval	0297
Modern	0298
African	0516
American	0521
Asian	0375
Canadian (English)	0352
Canadian (French)	0355
English	0593
Germanic	0311
Latin American	0312
Middle Eastern	0315
Romance	0313
Slavic and East European	0314

PHILOSOPHY, RELIGION AND THEOLOGY

Philosophy	0422
Religion	
General	0318
Biblical Studies	0321
Clergy	0319
History of	0320
Philosophy of	0322
Theology	0469

SOCIAL SCIENCES

American Studies	0323
Anthropology	
Archaeology	0324
Cultural	0326
Physical	0327
Business Administration	
General	0310
Accounting	0272
Banking	0770
Management	0454
Marketing	0338
Canadian Studies	0385
Economics	
General	0501
Agricultural	0503
Commerce-Business	0505
Finance	0508
History	0509
Labor	0510
Theory	0511
Folklore	0358
Geography	0366
Gerontology	0351
History	
General	0578

Ancient	0579
Medieval	0581
Modern	0582
Black	0328
African	0331
Asia, Australia and Oceania	0322
Canadian	0324
European	0325
Latin American	0336
Middle Eastern	0333
United States	0337
History of Science	0585
Law	0398
Political Science	
General	0615
International Law and Relations	0616
Public Administration	0617
Recreation	0814
Social Work	0452
Sociology	
General	0626
Criminology and Penology	0627
Demography	0938
Ethnic and Racial Studies	0631
Individual and Family Studies	0628
Industrial and Labor Relations	0629
Public and Social Welfare	0630
Social Structure and Development	0700
Theory and Methods	0344
Transportation	0709
Urban and Regional Planning	0999
Women's Studies	0453

THE SCIENCES AND ENGINEERING

BIOLOGICAL SCIENCES

Agriculture	
General	0473
Agronomy	0285
Animal Culture and Nutrition	0475
Animal Pathology	0476
Food Science and Technology	0359
Forestry and Wildlife	0478
Plant Culture	0479
Plant Pathology	0480
Plant Physiology	0817
Range Management	0777
Wood Technology	0746
Biology	
General	0306
Anatomy	0287
Biostatistics	0308
Botany	0309
Cell	0379
Ecology	0329
Entomology	0353
Genetics	0369
Limnology	0793
Microbiology	0410
Molecular	0307
Neuroscience	0317
Oceanography	0416
Physiology	0433
Radiation	0821
Veterinary Science	0778
Zoology	0472
Biophysics	
General	0786
Medical	0760

Geodesy	0370
Geology	0372
Geophysics	0373
Hydrology	0388
Mineralogy	0411
Paleobotany	0345
Paleoecology	0426
Paleontology	0418
Paleozoology	0985
Palynology	0427
Physical Geography	0368
Physical Oceanography	0415

HEALTH AND ENVIRONMENTAL SCIENCES

Environmental Sciences	0768
Health Sciences	
General	0566
Audiology	0300
Chemotherapy	0992
Dentistry	0567
Education	0350
Hospital Management	0769
Human Development	0758
Immunology	0982
Medicine and Surgery	0564
Mental Health	0347
Nursing	0569
Nutrition	0570
Obstetrics and Gynecology	0380
Occupational Health and Therapy	0354
Ophthalmology	0381
Pathology	0571
Pharmacology	0419
Pharmacy	0572
Physical Therapy	0382
Public Health	0573
Radiology	0574
Recreation	0575

Speech Pathology	0460
Toxicology	0383
Home Economics	0386

PHYSICAL SCIENCES

Pure Sciences	
Chemistry	
General	0485
Agricultural	0749
Analytical	0486
Biochemistry	0487
Inorganic	0488
Nuclear	0738
Organic	0490
Pharmaceutical	0491
Physical	0494
Polymer	0495
Radiation	0714
Mathematics	0415
Physics	
General	0605
Acoustics	0986
Astronomy and Astrophysics	0606
Atmospheric Science	0608
Atomic	0748
Electronics and Electricity	0607
Elementary Particles and High Energy	0798
Fluid and Plasma	0759
Molecular	0609
Nuclear	0610
Optics	0752
Radiation	0756
Solid State	0611
Statistics	0463
Applied Sciences	
Applied Mechanics	0346
Computer Science	0984

Engineering	
General	0537
Aerospace	0538
Agricultural	0539
Automotive	0540
Biomedical	0541
Chemical	0542
Civil	0543
Electronics and Electrical	0544
Heat and Thermodynamics	0348
Hydraulic	0545
Industrial	0546
Marine	0547
Materials Science	0794
Mechanical	0548
Metallurgy	0743
Mining	0551
Nuclear	0552
Packaging	0549
Petroleum	0765
Sanitary and Municipal	0554
System Science	0790
Geotechnology	0428
Operations Research	0796
Plastics Technology	0795
Textile Technology	0994

PSYCHOLOGY

General	0621
Behavioral	0384
Clinical	0622
Developmental	0620
Experimental	0623
Industrial	0624
Personality	0625
Physiological	0989
Psychobiology	0349
Psychometrics	0632
Social	0451



UNIVERSITY OF ALBERTA

RELEASE FORM

NAME OF AUTHOR: **Russell Dean Sampson**

TITLE OF THESIS: **Atmospheric Refraction and its Effects on Sunrise and Sunset.**

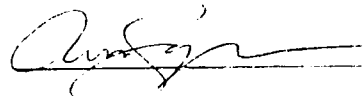
DEGREE: **Master of Science.**

YEAR THIS DEGREE GRANTED: **1994.**

Permission is hereby granted to the University of Alberta Library to reproduce single copies of this thesis and to lend or sell copies for private, scholarly or scientific research purposes only.

The author reserves all other publication and other rights in association with the copyright in the thesis and except as hereinbefore provided neither the thesis nor any substantial portion thereof may be printed or otherwise reproduced in any material form whatever without the author's prior written permission.

(signed):



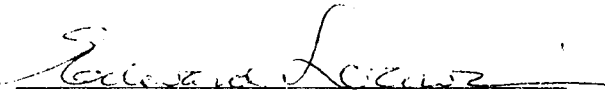
apt. 902, 9947 Saskatchewan Dr.  
Edmonton, Alberta, Canada  
T6E 4R3

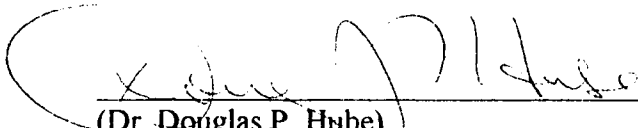
Date: October 3 1994.

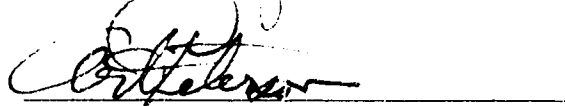
UNIVERSITY OF ALBERTA


FACULTY OF GRADUATE STUDIES AND RESEARCH

The undersigned certify that they have read, and recommend to the Faculty of Graduate Studies and Research for acceptance, a thesis entitled **Atmospheric Refraction and its Effects on Sunrise and Sunset** submitted by Russell Dean Sampson in partial fulfillment of the requirements for the degree of Master of Science.

  
(Supervisor: Dr. Edward P. Lozowski)

  
(Dr. Douglas P. Hube)

  
(Prof. Arthur Peterson)

  
(Dr. Gerhard W. Reuter)

Date: October 3 1994.

**To Susan**

## ABSTRACT

Observed timings of 244 sunrises and 125 sunsets were used to determine the astronomical refraction of the Sun's upper limb at the moment of sunrise and sunset on a zero horizon. Mean astronomical refraction was found to be  $0.669^\circ$  with a standard deviation of  $0.175^\circ$  and a total range of between  $0.402^\circ$  and  $2.081^\circ$ . Mean sunrise astronomical refraction was found to be  $0.714^\circ$  with a standard deviation of  $0.184^\circ$  while the mean sunset astronomical refraction was  $0.579^\circ$  with a standard deviation of  $0.108^\circ$ . There appears to be a strong seasonal effect on the monthly mean and standard deviation of the astronomical refraction. Both the monthly mean and standard deviations of the sunrise and sunset astronomical refraction appear to reach a maximum during the colder months. Astronomical refraction appears to be strongly correlated with surface temperature and the surface vertical temperature gradient. The standard deviation of the astronomical refraction also appears to be strongly correlated with the standard deviation in the surface vertical temperature gradient. All, except one anomalous event, took place during surface inversion conditions and are typically, but not exclusively, a cold weather phenomenon. The observed azimuthal location of a selection of sunrises around the winter solstice, appear to show the possible existence of systematic horizontal refraction of  $0.19^\circ \pm 0.1^\circ$ . Comparison of the astronomical refraction found in the present study and that predicted by the Astronomical Almanac, shows a strong correlation with the difference between the observed and predicted refraction and the surface vertical temperature gradient. The monthly standard deviation of the astronomical refraction appears to place severe restrictions on claims regarding the astronomical knowledge of Neolithic people. Specifically, the claims of A. Thom (1971), that Neolithic observers could determine the obliquity of the ecliptic to an accuracy of  $0.01^\circ$  and determine the exact date of the solstice. The results also suggest that the alignment of the Egyptian Pyramids with the cardinal points could have been achieved using the azimuthal position of summer solstice sunrise and sunset.



## ACKNOWLEDGMENTS

I would like to express my sincere gratitude to Professor Edward P. Lozowski for his untiring guidance and support throughout this project. His confidence in an unknown and unproven undergraduate student helped inspire me to achieve the things I have done. I would like to thank Professor Douglas Hube for his friendship, counseling and encouragement; Professor Arthur Peterson for his direction and confidence in my abilities, without which, this thesis would not have occurred; and Dr. Gerhard Reuter for his useful suggestions.

Even though he was not on my committee, I would like to extend many thanks to Dr. David Halliwell for countless hours of fruitful conversation.

The project got early encouragement and valuable advice from Dr. Bradley Schaefer of NASA's Goddard Space Flight Center and Stephen J. O'Meara of Sky & Telescope magazine. Valuable assistance was also provided by Dr. Stephen Haack of the University of Nebraska, Robert H. Myrick of Alberta Environment, Dr. Geoff Strong of the Atmospheric Environment Service in Saskatoon and the many people at the Edmonton office of the Atmospheric Environment Service.

Thanks also go out to fellow graduate students Raymond Beaubien, Randal Barrett, Victor Chung, Karen Harper, Bruno Larochelle, and Brian Wiens for their assistance, suggestions and companionship.

Finally, a special thanks to Terry Thompson for his assistance, advice and good humor.

## TABLE OF CONTENTS

CHAPTER	PAGE
1. INTRODUCTION .....	1
1.1 Introduction .....	1
2. EXPERIMENTAL PROCEDURE .....	3
2.1 Calculating Astronomical Refraction from the Times of Sunrise and Sunset .....	4
2.2 Observing Sites .....	7
2.3 Observational Technique .....	8
2.4 Measurement of Horizon Altitude .....	9
2.5 Terrestrial Refraction and Horizon Altitude .....	11
2.6 Measurement of Horizon Azimuth .....	19
3. RESULTS AND ANALYSIS .....	21
3.1 Sunrise and Sunset Data .....	21
3.2 Correction of Astronomical Refraction to a Zero Horizon .....	22
3.3 Overall Astronomical Refraction .....	26
3.4 Seasonal Differences in Astronomical Refraction .....	27
3.5 Surface Atmospheric Conditions and Astronomical Refraction .....	33
3.6 Anomalous Astronomical Refractive Events: The Novaya Zemlya Effect .....	59
3.7 Horizontal Astronomical Refraction .....	61
3.8 Comparison of Present Results with Other Predictive Formula .....	67

<b>CHAPTER</b>	<b>PAGE</b>
4. APPLICATIONS TO ARCHEOASTRONOMY .....	77
4.1 Neolithic Stone Monuments .....	77
4.2 The Pyramids of Egypt .....	85
5. DISCUSSION AND CONCLUSION .....	87
BIBLIOGRAPHY .....	92
APPENDIX A: GLOSSARY OF TERMS .....	95
APPENDIX B: STATISTICAL METHODS .....	98
APPENDIX C: DISTANCE TO THE HORIZON .....	99
APPENDIX D: SUNRISE AND SUNSET DATA .....	100

## LIST OF TABLES

TABLE	PAGE
2.4.1	Altitude measurements of standard horizon reference points ..... 10
2.4.2	Comparison between the trigonometric and theodolite method of horizon measurement ..... 11
2.5.1	Comparison of three methods for determining the terrestrial refraction of a distant horizon ..... 14
2.5.2	Calculated local horizon distances ..... 16
2.5.3	Local Horizon distance regimes ..... 17
2.6.1	Comparison of three methods for calculating the azimuth of the old international airport radome as seen from the apartment site ..... 20
3.2.1	Slopes of the linear regression of the astronomical refraction and horizon altitude ..... 25
3.2.2	Results of zero horizon correction ..... 26
3.3.1	Comparison of Schaefer and Liller's results (1990) with corrected sunrise and sunset refraction results from the present investigation ..... 27
3.3.2	Comparison of Schaefer and Liller's results (1990) results with current results uncorrected for horizon refraction ..... 27
3.4.1	Monthly refraction statistics ..... 30
3.5.1	Linear regression analysis of refraction data with respect to surface meteorological parameters ..... 46
3.5.2	Comparison of propagated uncertainties in determining the surface vertical temperature gradient ..... 47
3.5.3	Comparison of Stony Plain radiosonde surface vertical temperature gradients with those derived from the Ft. Saskatchewan minisonde data ..... 50
3.5.4	Comparison of error propagation through Equations (3.5.5) to (3.5.7) ..... 51

<b>TABLE</b>	<b>PAGE</b>
3.5.5 Linear regression analysis of the monthly standard deviations of the observed refraction of sunrises and sunsets versus the corresponding monthly standard deviations of surface temperature and surface lapse rate .....	52
3.6.1 Anomalous astronomical refraction events and corresponding surface meteorological conditions .....	60
3.7.1 Azimuth measurements for a sample of sunrises around the winter solstice .....	62
3.8.1 Linear regression results for surface temperature and deviation between Equation (3.8.1) and the astronomical refraction found in this study .....	76
3.8.2 Linear regression results for surface pressure and deviation between Equation (3.8.1) and the astronomical refraction found in this study .....	76
3.8.3 Linear regression results for vertical temperature gradient and deviation between Equation (3.8.1) and the astronomical refraction found in this study .....	76
4.1.1 Standard deviations and half ranges for azimuth and declinations due to the standard deviation and range in refraction .....	79
4.1.2 The estimated uncertainties in the solstitial solar azimuth and declination for Ballochroy and Kintraw .....	80
4.1.3 The estimated uncertainty in determining the date of the solstice at Edmonton's geographical location and climate, using the most northerly or southerly sunrise or sunset to indicate the date of solstice .....	83
4.1.4 The estimated uncertainty in determining the date of the solstice from Thom's Neolithic solstitial sites .....	83
4.2.1 The error in alignment of five of the pyramids of Egypt .....	85
C.1 Altitude of contour lines .....	99
D.1 Sunrise data .....	101
D.2 Sunset data .....	116

## LIST OF FIGURES

FIGURE	PAGE
1.1.1 Schematic of horizon with geometric and refracted sun at moment of sunrise or sunset .....	2
1.1.2 Schematic showing astronomical refraction at sunrise or sunset.....	3
1.1.3 Schematic showing the variation in sunrise time and azimuth as a function of atmospheric refraction .....	3
2.1.1 Horizontal or diurnal parallax.....	4
2.1.2 Parameters involved in determining astronomical refraction at sunrise or sunset .....	5
2.1.3 Observer's view of parameters involved in determining astronomical refraction at sunrise or sunset .....	6
2.5.1 Schematic showing terrestrial refraction and the refracted Sun at sunrise or sunset .....	12
2.5.2 Horizon regime boundaries .....	15
2.5.3 A possible example of anomalous terrestrial refraction .....	18
3.2.1 Horizon altitude and astronomical refraction of sunrises .....	23
3.2.2 Horizon altitude and astronomical refraction of sunset .....	24
3.4.1 Sunrise astronomical refraction versus time of year .....	28
3.4.2 Sunset astronomical refraction versus time of year .....	29
3.4.3 Monthly mean astronomical refraction .....	31
3.4.4 Monthly standard deviation of the astronomical refraction compared to the time of year .....	32
3.5.1 Surface atmospheric density versus surface vertical temperature gradient ....	35
3.5.2 Surface temperature versus sunrise astronomical refraction .....	36

<b>FIGURE</b>	<b>PAGE</b>
3.5.3 Surface temperature versus sunset astronomical refraction .....	37
3.5.4 Surface pressure versus sunrise astronomical refraction .....	38
3.5.5 Surface pressure versus sunset astronomical refraction .....	39
3.5.6 Surface density versus sunrise astronomical refraction .....	40
3.5.7 Surface density versus sunset astronomical refraction .....	41
3.5.8 Surface vertical temperature gradient versus sunrise astronomical refraction .....	42
3.5.9 Surface vertical temperature gradient versus sunset astronomical refraction .....	43
3.5.10 Surface vertical temperature gradient versus sunset and sunset astronomical refraction.....	44
3.5.11 Uncertainty in the sunrise surface vertical temperature gradient versus the sunrise surface vertical temperature gradient .....	48
3.5.12 Uncertainty in the sunset surface vertical temperature gradient versus the sunset surface vertical temperature gradient .....	49
3.5.13 Sunrise surface temperature versus time of year .....	53
3.5.14 Sunset surface temperature versus time of year .....	54
3.5.15 Sunrise surface vertical temperature gradient versus time of year .....	55
3.5.16 Sunset surface vertical temperature gradient versus time of year .....	56
3.5.17 Standard deviation of monthly surface temperature versus the standard deviation of the monthly refraction .....	57
3.5.18 Standard deviation of monthly surface vertical temperature gradient versus the standard deviation of the monthly refraction .....	58
3.7.1 Plan view showing the sense of horizontal refraction due to a meridional temperature gradient .....	63
3.7.2 Horizontal deviation versus astronomical refraction .....	65

<b>FIGURE</b>	<b>PAGE</b>
3.7.3 Histogram of horizontal deviation .....	66
3.8.1 Observed minus calculated sunrise astronomical refraction versus surface temperature .....	70
3.8.2 Observed minus calculated sunset astronomical refraction versus surface temperature .....	71
3.8.3 Observed minus calculated sunrise astronomical refraction versus surface pressure .....	72
3.8.4 Observed minus calculated sunset astronomical refraction versus surface pressure .....	73
3.8.5 Observed minus calculated sunrise astronomical refraction versus surface vertical temperature gradient .....	74
3.8.6 Observed minus calculated sunset astronomical refraction versus surface vertical temperature gradient .....	75
4.1.1 Azimuth of the setting Sun around the date of summer solstice, as seen from Edmonton .....	82
4.1.2 Summer solstice sunset as seen from Edmonton .....	84
A.1 Equatorial coordinate system .....	96



## NOMENCLATURE

$R_v$	astronomical refraction ( $^{\circ}$ )
$R'_v$	astronomical refraction corrected to a zero horizon ( $^{\circ}$ )
$R_h$	refraction of the local horizon ( $^{\circ}$ )
$s$	solar semidiameter ( $^{\circ}$ )
$A$	azimuth ( $^{\circ}$ )
$h$	elevation (m)
$r_e$	radius of the Earth (m)
$d$	horizontal distance from observer (km)
$a$	altitude ( $^{\circ}$ )
$R_t$	terrestrial refraction ( $^{\circ}$ )
$K$	Thom's refractive coefficient
$\gamma_{F/ft}$	lapse rate ( $^{\circ}$ F/ft)
$w$	wind speed (Beaufort scale)
$d_{ft}$	horizontal distance from observer (ft.)
$p_{inHg}$	surface pressure (inches of Hg)
$T_f$	temperature ( $^{\circ}$ F)
$k$	radius of curvature (m)
$p$	surface pressure (mb)
$T$	surface air temperature ( $^{\circ}$ C)
$\Lambda_{12}$	oblateness correction factor.
$\epsilon, e$	oblateness
$a$	mean equatorial radius of the Earth (m)
$b$	mean polar radius of the Earth (m)
$Z$	zenith angle ( $^{\circ}$ )
$\delta$	solar declination ( $^{\circ}$ )
$\alpha$	solar right ascension ( $^{\circ}$ )
$\lambda$	geographic longitude ( $^{\circ}$ )
$\phi$	geographic latitude ( $^{\circ}$ )
$H$	hour angle ( $^{\circ}$ )
$t$	time (hours)
$t_s$	sidereal time (hours)
$\rho$	air density ( $kgm^{-3}$ )
$R$	Gas Constant ( $J^{\circ} K^{-1} kg^{-1}$ )
$a_h$	corrected altitude of the horizon at sunrise or sunset ( $^{\circ}$ )
$a_0$	altitude of the centre of the geometric Sun ( $^{\circ}$ )
<b>SD</b>	population standard deviation
<b>SSD</b>	sample standard deviation
$m$	vapor pressure (mm Hg)
$n$	refractive index
$\gamma$	surface lapse rate ( $^{\circ}$ C/m)
$\omega$	angle between horizon and circle of declination ( $^{\circ}$ )

# CHAPTER 1.

## INTRODUCTION

### 1.1 Introduction

This investigation originated as an amateur study into the frequency of anomalous sunrise and sunset timings. Sunrise and sunset are defined as the moment at which the upper limb of the sun appears or disappears on the horizon of the observer (see Figure 1.1.1) (readers that are unfamiliar with the astronomical or meteorological terminology used in this study, should refer to the glossary in Appendix A). The equatorial coordinates of the Sun are known to an accuracy of about  $0.1''$  ( $3 \times 10^{-5}$  degrees) and the semidiameter to about  $0.01''$  ( $3 \times 10^{-6}$  degrees or  $10^{-5}$  % of the semidiameter of the Sun) (The Astronomical Almanac, 1992). Therefore, the rising and setting time of the geometric Sun should be predictable to less than a second. Yet, before the sunrise or sunset can be observed, the light of the Sun must pass through the atmosphere of the Earth. As sunlight traverses the atmosphere it passes through a gradient of atmospheric density and, following Snell's Law, the rays of sunlight are refracted before they reach the observer (see Figure 1.1.2). The refractive behavior of light from astronomical objects at zenith angles less than  $75^\circ$  (greater than  $15^\circ$  in altitude) is well understood and quite predictable (Humphreys, 1964 pp. 454-462), yet at zenith angles greater than this, the amount of refraction is highly variable and is only known through observation and approximate empirical expressions (The Astronomical Almanac, 1992, p. B62).

Published times of sunrise and sunset are usually determined using a fixed value for the amount of astronomical refraction  $R_0$  experienced by the Sun at the moment of sunrise or sunset. For simplicity, most computer programs use  $0.57^\circ$  (Green, 1985, p. 95) as the assumed astronomical refraction at the moment of sunrise or sunset on a zero horizon. Previous investigations have found the amount of refraction at sunset, taken from a number of geographical sites looking at a sea horizon, varies with a total range of between  $0.234^\circ$  and  $1.678^\circ$  and a standard deviation of  $0.16^\circ$  (Schaefer and Liller, 1990). Since computer programs require decimal degrees and Schaefer and Liller's results were also given in such units, the astronomical refraction found in this work shall be given in decimal degrees.

In this investigation, the astronomical refraction  $R_0$  at the moment of sunrise and sunset has been determined for a large number of both sunrises and sunsets as observed from two geographical locations separated by about 2 km. All observations were performed by the author using the same technique. The overall variation in astronomical refraction at sunrise and sunset is determined and then compared with the published results of Schaefer and Liller. The possibility of significant horizontal refraction is also explored for a sample of observations. Seasonal variations in astronomical refraction are determined by examining the amount and variability as a function of the time of year. Diurnal variations in astronomical refraction are also explored through differences between sunrise and sunset data. To further develop a

simple predictive model based on the physical principles of refraction, the amount of astronomical refraction is compared to the surface temperature, surface pressure and the surface vertical temperature gradient.

The results are then used to examine the claims that certain Neolithic structures in the British Isles were deliberately aligned with the exact azimuthal location of the summer solstice sunrise or sunset or other celestial rising and setting points. (Thom, 1971 pp. 36-44, Mackie, 1974, Heggie, 1981). As illustrated in Figure 1.1.3, a variation in the amount of astronomical refraction will lead to a corresponding variation in the observed azimuth of the rising or setting sun. This variation in observed azimuth will place restrictions on the accuracy of these observations and the validity of the subsequent claims. These results can also be applied to the problem of the accurate alignment of the pyramids of Egypt to the geographical cardinal points (Haack, 1984).

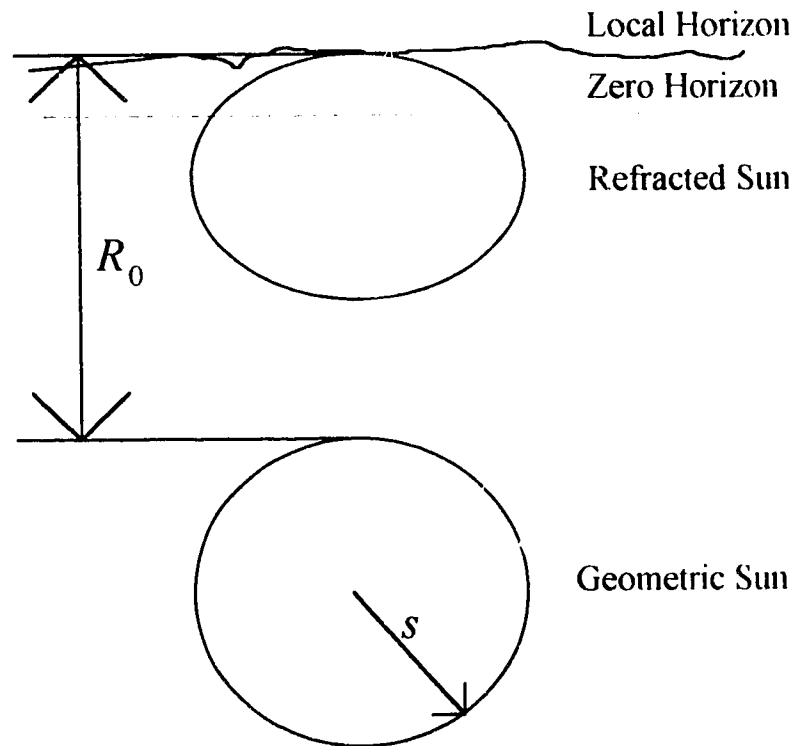


**Figure 1.1.1:** The moment of sunrise or sunset as observed from a particular geographical site, is the time at which the upper limb of the refracted Sun meets the local horizon. The zero horizon is a hypothetical horizon at an altitude of  $0^\circ$  or a zenith angle of  $90^\circ$ . The geometric Sun is the unrefracted image of the Sun. The angle,  $R_0$ , is the amount of astronomical refraction while,  $s$ , is the semidiameter of the Sun. The refracted Sun appears oblate due to the lower limb of the Sun experiencing more refraction than the upper limb.

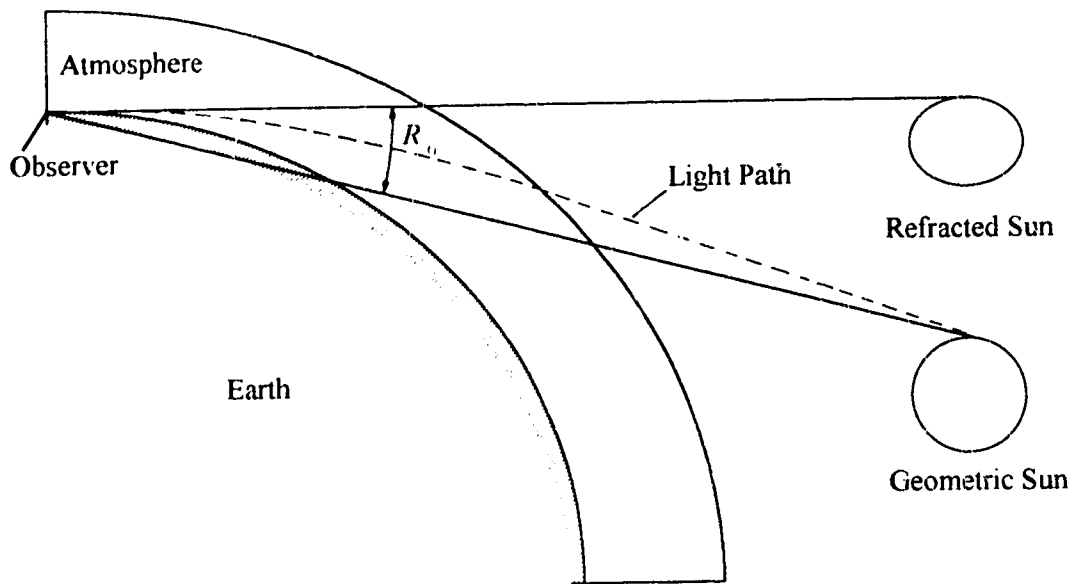


**Figure 1.1.2:** A schematic diagram showing astronomical refraction  $R_0$  and the relationship between the light path and the position of the geometric and refracted Sun at the moment of sunrise or sunset on a zero horizon.

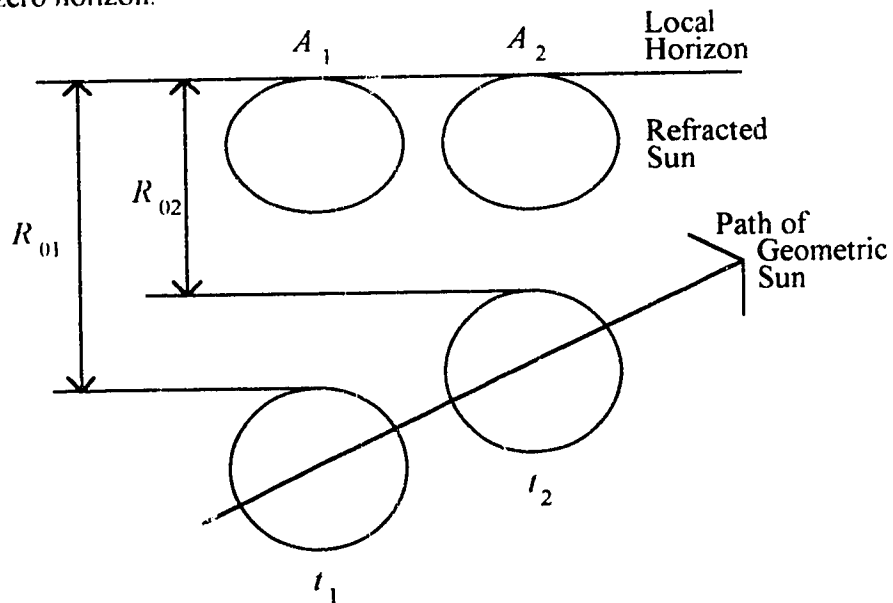


**Figure 1.1.3:** The time and azimuthal position of sunrise (or sunset) is a function of the amount of atmospheric refraction. This schematic diagram shows the path of the geometric Sun below the horizon as it approaches sunrise. If the amount of atmospheric refraction is  $R_{01}$  then sunrise occurs at time  $t_1$  and at azimuth  $A_1$ . If the refraction is  $R_{02}$  then sunrise occurs at time  $t_2$  and at azimuth  $A_2$ .

## CHAPTER 2

### EXPERIMENTAL PROCEDURE

#### 2.1 Calculating Astronomical Refraction from the Time of Sunrise and Sunset.

If the altitude of the geometric Sun can be found for the moment of sunrise or sunset, then the amount of astronomical refraction  $R_0$  can be found through the formula:

$$R_0 = a_s - a_0 - s + \pi \quad (2.1.1)$$

where  $s$  is the semidiameter of the geometric Sun,  $a_s$  is the altitude of the horizon at the point of sunrise or sunset (adjusted for the effects of terrestrial refraction as outlined in Section 2.5) and,  $a_0$  is the altitude of the centre of the geometric Sun above or below the zero horizon (see Figures 2.1.2 and 2.1.3). The variable  $\pi$  is the solar horizontal or diurnal parallax (Illingworth, 1980, p. 206). Since the equatorial coordinates of the Sun are geocentric (i.e., as seen from the centre of the Earth) a correction must be made to the altitude of the Sun as seen from the surface of the Earth. At the time of sunrise and sunset, the distance from the centre of the Earth to an observer at the surface, is at right angles to the line joining the centre of the Earth and the Sun and therefore, the parallax is at a maximum (see Figure 2.1.1).

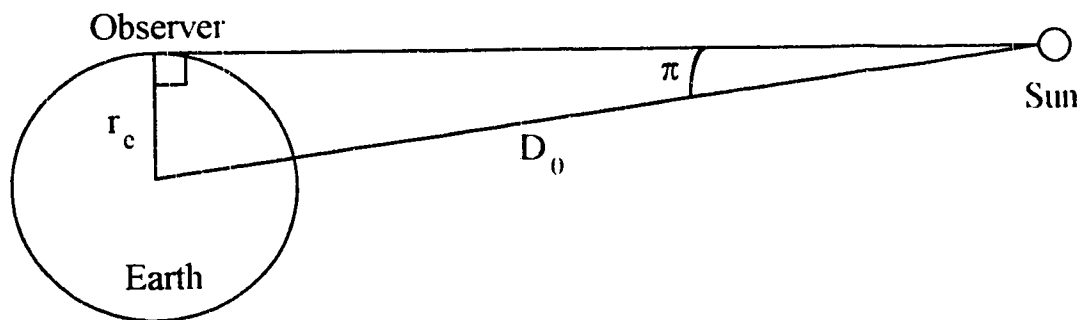


**Figure 2.1.1:** Horizontal or diurnal parallax at sunrise or sunset (not to scale).

The global maximum value for the solar horizontal parallax is found through the formula: (Green, 1985, p. 102)

$$\sin \pi = \frac{r_e}{D_0} \quad (2.1.2)$$

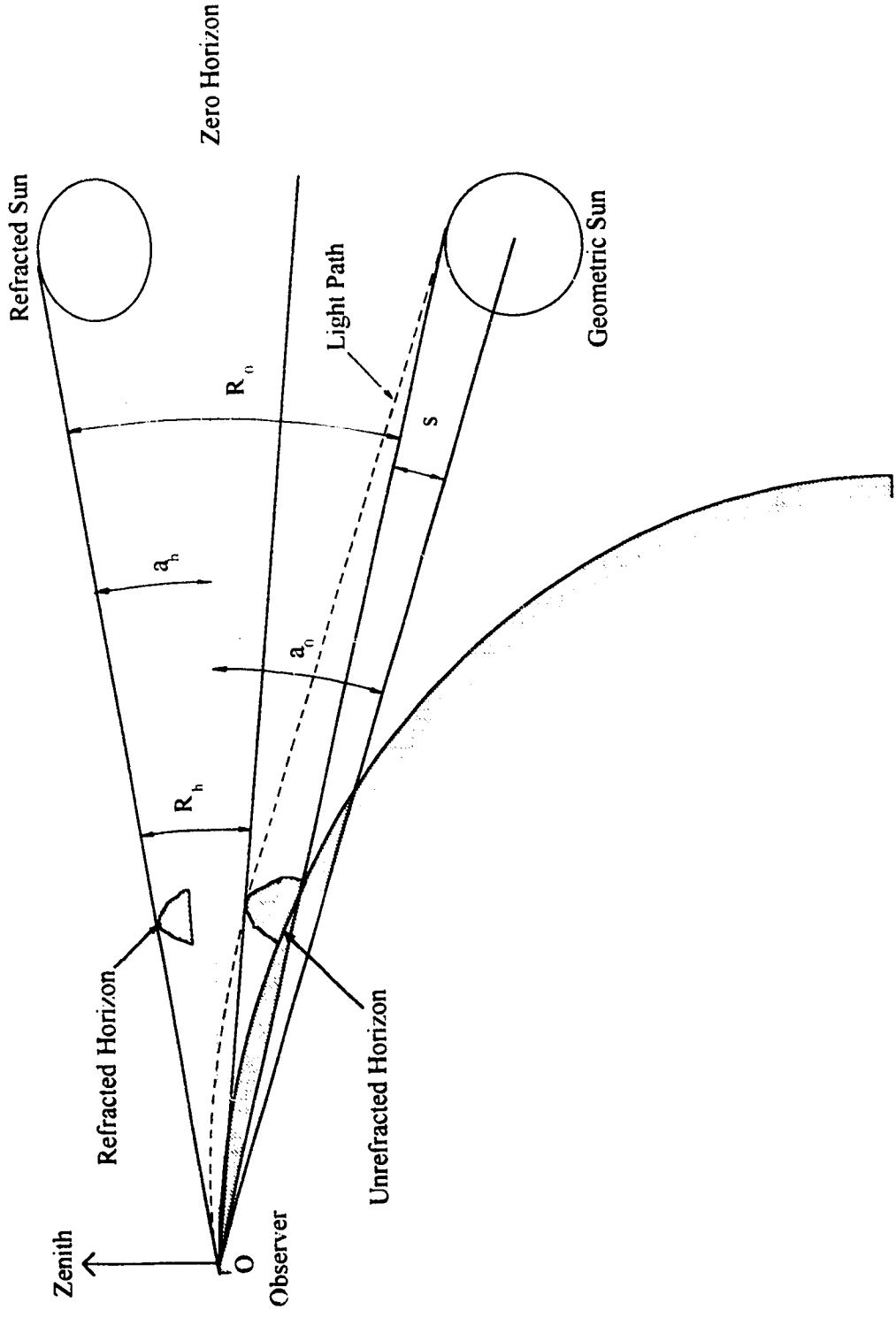
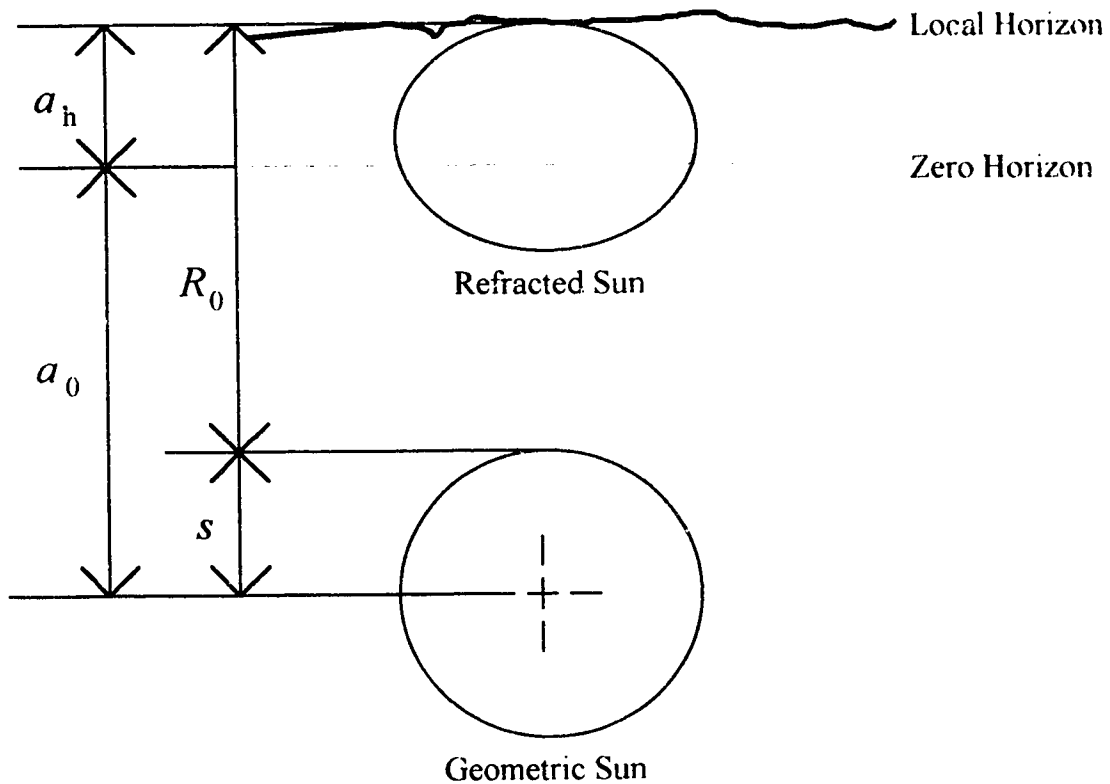


Figure 2.1.2: Parameters necessary to determine astronomical refraction at sunrise or sunset.

Where  $r_e$  is the mean radius of the Earth and,  $D_0$  is the distance to the Sun. The maximum solar horizontal parallax varies between  $0.00248^\circ$  at perihelion (the moment when the Earth is at its closest to the Sun, occurring in early January) and  $0.00240^\circ$  at aphelion (early July). An average value of  $0.00244^\circ$  is used in this study.



**Figure 2.1.3:** The relationship between the astronomical refraction  $R_0$ , horizon altitude  $a_h$ , altitude of the centre of the geometric solar disc  $a_0$  and the semidiameter of the geometric Sun,  $s$ .

If the time, equatorial coordinates of the geometric Sun, and geographical coordinates of the observer are known (see Section 2.2 for geographic coordinates), then the altitude  $a_0$  of the geometric Sun above or below a zero horizon can be determined from the formula (Green, 1985, p. 28):

$$\sin a_0 = \sin \delta \sin \phi + \cos H \cos \delta \cos \phi \quad (2.1.3)$$

where  $\phi$  is the geographic latitude of the observer,  $\delta$  is the declination of the centre of the solar disc and,  $H$  is the hour angle.

The declination  $\delta$  for the centre of the disc of the geometric Sun was found using formulae developed by Meeus (1988, pp. 79-82). The accuracies of the

resulting sample values were checked against selected values in the tables of the *Astronomical Almanac* (1992, pp. C4-C19) and were found to vary by no more than  $\pm 0.0003^\circ$  or 0.056% of the solar semidiameter.

The hour angle  $H$  can be found from the formula:

$$H = t_s - \alpha \quad (2.1.4)$$

where  $t_s$  is the sidereal time of the observation (expressed in degrees), and  $\alpha$  is the right ascension of the object. The right ascension of the centre of the solar disc was again calculated from the formulation by Meeus (1988). Test values were found to be within 1 arc second of selected values in the *Astronomical Almanac*. The sidereal time was also found through a series of formulae described in Meeus (1988, pp. 39-41). Selected test results were checked against selected values derived from tables in the *Royal Astronomical Society of Canada's Observer's Handbook* and were found to differ by no more than 0.5 seconds.

The semidiameter of the disc of the geometric Sun  $s$  was also found from a series of formulae in Meeus (1988, pp. 79-82 and p. 185). These were checked against selected values in the *Astronomical Almanac* and were found to differ by no more than 0.01 arc seconds.

To examine the effect of the above discrepancies on the computer model, values of solar declination, right ascension and semidiameter from the tables in the *Astronomical Almanac*, were placed into the computer model. The almanac values changed a selected sunrise and sunset time by about 0.6 seconds and the altitude of the geometric Sun by no more than  $0.002^\circ$ . This is well within the timing uncertainty of the observed sunrises and sunsets which was typically about  $\pm 2$  seconds.

## 2.2 Observing Sites

Edmonton has a continental climate with no large bodies of water nearby. The local topography is relatively flat with the foothills of the Rocky Mountains approximately 80 km to the west and the Rocky Mountains starting about 200 km further west. The climate is classified as Dfc in the Köppen classification system, where the average temperature of the warmest month is greater than  $10^\circ\text{C}$  but below  $22^\circ\text{C}$  and the coldest month is below  $0^\circ\text{C}$  (Henderson-Sellers and Robinson, 1986, pp. 210-214). The lowest winter temperature in Edmonton was  $-49.4^\circ\text{C}$  (January 19, 1886 and February 3, 1893) and the highest summer temperature was  $37.2^\circ\text{C}$  (June 29, 1937).

Two observing sites were used, both in central Edmonton. The first site was an apartment building with an unobstructed view of the eastern horizon and a partially obstructed western horizon. Three locations in the building were used depending on the time of year and whether a sunset or sunrise was to be observed. Two indoor locations, both at an elevation of  $687 \pm 1\text{m}$  (22m above the ground level), were used to observe sunrises from about November 3 to February 2 and sunsets between April



3 and May 1 and between August 10 and September 11. A roof-top site in the same building with an elevation of  $704 \pm 1\text{m}$  was also used to observe sunrises from February 3 to November 2 and sunsets from about September 14 to October 3. The latitude and longitude of the site used to observe sunrises between November 3 and February 2 were determined by measuring the distance from a survey monument located about 20 m northwest of the apartment building :

$$53^{\circ}31'33".57 \pm 0.06", 53.52599^{\circ} \pm 0.00002^{\circ} \text{ N}$$

$$113^{\circ}29'14".35 \pm 0.10", 113.48732^{\circ} \pm 0.00003^{\circ} \text{ W}$$

The second site was located 2240 m to the west, on the roof of the Henry Marshall Tory Building on the campus of the University of Alberta. The elevation of this site is  $728 \pm 1\text{m}$ . From this site, sunsets could be observed throughout the year on an unobstructed western horizon. Sunsets were observed from this site between October 5, 1992 and March 26, 1993 and between May 10 and July 17, 1993. Using a 1:40000 map (Alberta Bureau of Surveying and Mapping, 1982), the geographic coordinates of this site were determined to be:

$$53^{\circ}31'41" \pm 1", 53.5281^{\circ} \pm 0.0003^{\circ} \text{ N}$$

$$113^{\circ}31'10" \pm 1", 113.5194^{\circ} \pm 0.0003^{\circ} \text{ W}$$

The higher accuracy of the apartment coordinates was required for the azimuthal survey discussed in Section 2.6.

### 2.3 Observational Technique

Sunrises and sunsets were observed using a pair of 7x20 binoculars and, when appropriate, a number 14 welding filter. Timings were performed with an electronic timer synchronized with a digital quartz watch. The watch in turn was synchronized with the time signal from radio station WWV. Errors in synchronizing the timer with the digital watch and the radio time signals, plus uncertainties in the timing of the sunrise or sunset event, were estimated to produce a total uncertainty of about 2 seconds for each observation. The observational uncertainties are consistent with those estimated by Schaefer and Liller. Observations with a suspected uncertainty greater than about 10 seconds were discarded. The larger uncertainties were usually produced when cirrus clouds near the horizon scattered sunlight near the disc of the Sun thus obscuring the limb.

At the moment of sunrise or sunset, when only a small point of sunlight was visible, no optical filtering was necessary. A number 14 or 13 welding filter was used to view the sun at higher altitudes.

The azimuthal location of sunrise could be predicted by observing the intensity of scattered light in the twilight sky. A minute or two before the sunrise, a bright red or orange hemispheric glow about  $1^{\circ}$  in diameter would mark the location of the Sun below the horizon. A few seconds before sunrise, sunlight could sometimes be seen

outlining trees and other distant horizon objects immediately above the position of the Sun. This appeared to be caused by diffraction of sunlight around the sharp edges of distant objects. Once the sunlight reaches the Earth it is essentially a plane wave front. When a plane wave front encounters an obstacle, a circular wave front spreads out from its edges. Therefore, a portion of the sunlight will be directed away from the original line of motion and, as a result, a glow can be seen around the edges of the obstacle.

A sketch of the relative location of sunrise or sunset on the horizon was made when convenient landmarks were available. The horizon from both sites had few featureless portions.

## 2.4 Measurement of Horizon Altitude

As outlined in Section 2.1, the amount of astronomical refraction derived from the time of sunrise and sunset depends on  $a_h$ , the altitude of the local horizon at the time of the sunrise or sunset. The topography of Edmonton and the surrounding terrain is relatively flat but it shows enough variation from a zero horizon to produce a measurable effect on the time of sunrise or sunset.

The local horizon for the sunrise or sunset events observed from each site was established using measurements made with a Wild Heerbrugg theodolite. The theodolite was set up at the same location and at the same eye-level as used at the moment of the sunrise and sunset observation. In order to standardize the data, measurements were made during mid-day when abnormal refractive conditions were assumed to be minimized and relatively constant. This assumption was based on the understanding that abnormal refraction is most common during surface temperature inversion conditions (Bomford, 1980 pp. 237-241 and Schaefer, 1989). These conditions are most common during the night and early morning when radiative cooling of the Earth's surface produces a surface inversion layer (Wallace and Hobbs, 1977, pp. 342-344). From extensive observations of horizon mirages taken during the same period as the study, it appears that abnormal refractive phenomena typically take place during the morning and during calmer conditions. As the day progressed these mirages would typically diminish and eventually disappear. Therefore, attempts were made to take horizon altitude measurement only during periods of warmer temperatures and moderate wind speed, in order to ensure boundary layer mixing. To check the validity of the above assumptions and the consistency of the altitude measurement, a distant reference point on the horizon was measured at the beginning and the end of each session of observations. The measured altitude of these standard reference points appeared to have an uncertainty of no more than  $0.0008^\circ$  (see Table 2.4.1).

Standard surveying techniques were used to measure 170 horizon points. Each point was measured 6 to 10 times depending on the unevenness and thus the suspected uncertainty of the profile. The standard deviation of the measurements ranged from  $0.001^\circ$  to  $0.012^\circ$  with a mean of  $0.0013^\circ$  which is similar to, though higher than, the standard deviation for the reference points listed in Table 2.4.1.

<b>Reference Point</b>	<b><i>a</i> (<sup>o</sup>)</b>	<b>SD (<sup>o</sup>)</b>
Horizon directly behind CFRN	0.0715	
TV Antenna (west horizon)	0.0717	
	0.0728	
Mean:	<b>0.0720</b>	0.0007
Horizon directly behind old International Airport Radome	0.2072	
	0.2075	
	0.2069	
Mean:	<b>0.2069</b>	0.0003
Horizon directly behind Bonnie Doon Radio Antenna (near equinox sunrise)	0.1636	
	0.1628	
	0.1628	
	0.1617	
	0.1617	
	0.1633	
	0.1619	
	0.1619	
Mean:	<b>0.1625</b>	0.0008
Radio antenna near winter solstice sunset from Tory	-0.0947	
	-0.0922	
Mean:	<b>-0.0934</b>	0.0012

**Table 2.4.1:** Altitude measurements of standard horizon reference points. Each measurement is the average of 6 to 10 theodolite readings. The radome used in this survey was dismantled in May of 1994. The first three reference landmarks were measured from the apartment site. Both reference measurements from the Henry Marshall Tory building were performed on the same day.

To check the validity of the theodolite method, the altitude of two reference landmarks was measured using an independent trigonometric method. The horizon directly behind the CFRN TV antenna in the east end of Edmonton and the old international airport Radome southeast of Edmonton were approximately 20 kilometers distant and could be easily identified on 1:50000 topographic maps (Surveys and Mapping Branch, Department of Energy Mines and Resources, 1980). The altitude  $\alpha$  of the landmark (ignoring the effects of terrestrial refraction) is found using the law of cosines:

$$\sin \alpha = -\frac{(r_e + h_2)^2 - (r_e + h_1)^2 - d^2}{2d(r_e + h_1)} \quad (2.4.1)$$

where  $r_e$  is the mean radius of the Earth ( $6.371004 \times 10^6 \text{ m}$ ),  $d$  is the distance from the observer to the landmark in m,  $h_1$  is the elevation of the observer in m and,  $h_2$  is the elevation of the landmark in m. The results of this test were in good agreement with the values found from the theodolite and are shown in Table 2.4.2.

Reference Point (from apt. bldg.)	Trig. Method ( $^{\circ}$ )	Theodolite ( $^{\circ}$ )
CFRN tower	$0.08 \pm 0.02$	$0.0720 \pm 0.001$
Radome	$0.18 \pm 0.02$	$0.2072 \pm 0.0003$

**Table 2.4.2:** Comparison between the trigonometric and theodolite method of horizon measurement. The uncertainty in the trigonometric method was determined through an error propagation method outlined in Appendix A (Taylor, 1982 p. 73) while uncertainties in the theodolite measurements are standard deviations from a series of measurements.

## 2.5 Terrestrial Refraction and Horizon Altitude.

The measured altitude of a distant horizon is also affected by atmospheric refraction. The tendency will be to increase the apparent altitude of the horizon. The vertical refraction of the geometric Sun must therefore, include the increase in the apparent altitude of the horizon (see Figure 2.1.2 and 2.5.1). To distinguish this from the effects of refraction on the position of the Sun, refraction of the horizon shall be referred to as terrestrial refraction while refraction of the Sun shall be called astronomical refraction.

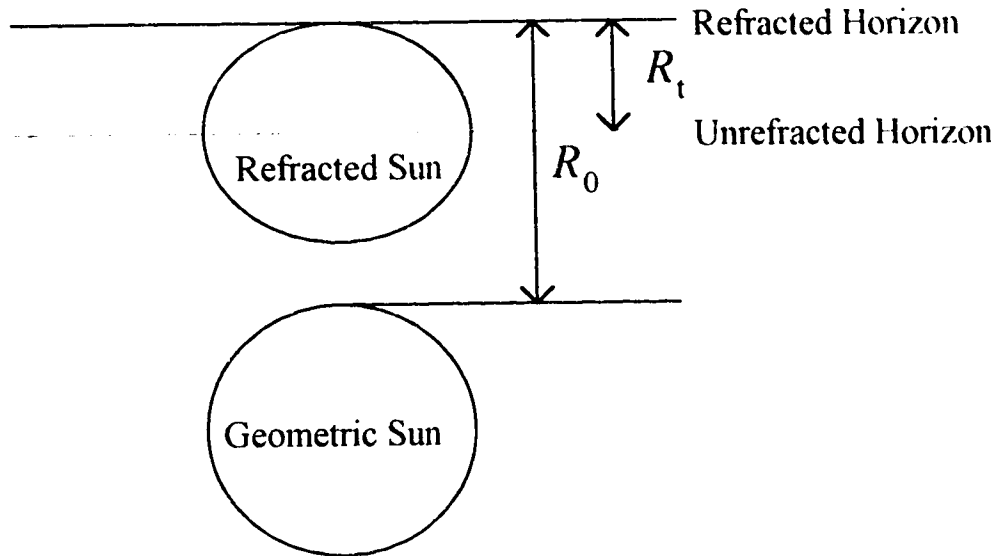


**Figure 2.5.1:** Terrestrial refraction and the resulting position of the refracted Sun at sunrise or sunset. Astronomical refraction is labeled  $R_0$ , while terrestrial refraction is  $R_t$ .

Changes in the vertical density distribution of the atmosphere lead to changes in the vertical gradient of the index of refraction. The optical path length to the horizon is substantially shorter than the total path length for sunlight at the moment of sunrise or sunset. At the same time, the elevation difference between the observer and the horizon, during this experiment, is assumed to be relatively small and therefore the optical path length to the horizon traverses a nearly homogeneous layer of atmospheric density. Hence, it is assumed that the amount of refraction of the horizon will be correspondingly smaller.

A number of approximate, empirical expressions have been developed to estimate terrestrial refraction. Brinker and Wolf (1984, pp. 102) provide the simple expression:

$$R_t = 0.011d^2 \quad (2.5.1)$$

where  $R_t$  is the refraction measured in m, at distance  $d$  from the observer, in km. This appears to assume a parabolic ray trajectory, since the amount of refraction depends on the square of the distance. This is also the method used by Lehn (1983) where the ray trajectory is assumed to be a parabola through a layer of air with a linear temperature distribution specified by the temperatures at the two boundaries.

For a distance of 20 km, Equation (2.5.1) produces a result of 4.4 m, which corresponds to an angular displacement of  $0.0126^\circ$ . This method ignores the effects of any changes in the vertical density distribution and thus ignores the effects of abnormal atmospheric refraction.

An empirical method is outlined in Thom (1958) where extensive surveys of distant hilltops produced the following expression for a refractive coefficient  $K$ :

$$K = 8.8 + 14\gamma_{F/\text{ft}} - 0.37w - 0.22\gamma_{F/\text{ft}}w \quad (2.5.2)$$

where  $\gamma_{F/\text{ft}}$  is the measured surface lapse rate (in degrees Fahrenheit per foot and negative for an inversion) and  $w$  is the wind speed on the Beaufort scale. Although Thom does not give a physical explanation for the connection between the wind speed and refraction, it appears reasonable that increased wind speed could assist in mixing the surface temperature inversion layer and thus reducing the refraction. The amount of terrestrial atmospheric refraction  $R_t$  in seconds of arc, is found from the formula

$$R_t = \frac{Kd_{\text{ft}}p_{\text{inHg}}}{T_F^2} \quad (2.5.3)$$

where  $d_{\text{ft}}$  is the length of the ray path in feet,  $p_{\text{inHg}}$  is the surface pressure in inches of Mercury and,  $T_F$  is the surface temperature in absolute degrees Fahrenheit. For a temperature of 518.7 F (15 °C), a pressure of 27.4 inches of Mercury (930 mb, a typical value for Edmonton), a lapse rate of 0.0055 °F/ft (0.01 °C/m), wind speed of 3 on the Beaufort scale (about 6 m/s) and a distance of 65620 feet (20 km) the resulting refraction is 51.9".

Bomford (1980, pp. 233-243) also attempts to find the standard amount of terrestrial refraction (in radians) through the formula:

$$R_t = \frac{kd}{r_e} \quad (2.5.4)$$

where  $d$  is the distance between the observer and the horizon in m,  $r_e$  the radius of the Earth ( $6.371004 \times 10^6$  m) and  $k$  is the radius of curvature of the light ray found through the expression:

$$k = \frac{252p}{T^2} \left( 0.0342 + \frac{dT}{dh} \right) \quad (2.5.5)$$

where  $p$  is the pressure in millibars,  $T$  is the absolute temperature in degrees Kelvin, and  $dT/dh$  is the vertical temperature gradient in degrees per m (positive for an inversion). Using the same values as in the previous example, the resulting refraction at 20 km is 44.3". The results of the three methods are summarized in Table 2.5.1.

Method	Terrestrial Refraction	
	(")	(°)
Brinker and Wolf	45.4	0.0126
Thom	51.9	0.0144
Bomford	44.3	0.0123

**Table 2.5.1:** Comparison of three methods for determining the terrestrial refraction of a distant horizon. Horizon distance 20 km, surface temperature 15°C, surface pressure 930 mb, wind speed 20 kph, and surface vertical temperature gradient -0.01°C/m (lapse rate of 0.01°C/m). Brinker and Wolf's method does not use any meteorological data. The second and third columns show the calculated terrestrial refraction in seconds of arc and degrees.

Thom felt that his empirical method was incomplete. The use of the Beaufort scale and British units in Thom's formulae also makes calculation somewhat cumbersome. Brinker and Wolf's method makes no allowances for changes in atmospheric conditions and is therefore, also unsuitable. Consequently, Bomford's method was adopted for this investigation.

For this investigation Equation (2.4.1) was used to estimate the distance to the horizon from each observing site. Distances and elevations along a particular sight-line were derived from 1:50000 topographic maps (Surveys and Mapping Branch, Department of Energy Mines and Resources, 1980). A series of sight-lines were drawn on the map separated by about 10°. The distance to each contour line (representing an elevation change of 25 ft or 7.62 m) and its corresponding elevation, was substituted into Equation (2.4.1). The location of the maximum altitude along the sight-line then determined the distance to the local horizon (see Appendix C for an example).

The results were checked by comparing the corresponding location of two horizon landmarks on the topographic map (the old International Airport radome at azimuth 129.6° from the apartment site and a microwave transmission tower between Edmonton and the town of Sherwood Park at azimuth 90.0°, also observed from the apartment site). The numerical method outlined above, gave the same horizon distance for the radome as the distance found on the topographic map (the radome was located on a contour line). The two methods differed by 2.6% for the microwave tower.

Relatively large differences in horizon distance were revealed by using a pair of 7x20 binoculars to examine the overall visual contrast between the horizon features and the adjacent sky. As the distance to the horizon increases scattered light reduces the observed contrast. From this analysis, a number of horizon distance regimes became apparent. Average distances to each horizon regime were determined by taking the average of a number of calculated horizon distances along different sight lines within the regime. The boundary between two adjacent regimes was located by noting the location of the change in visual contrast with respect to prominent horizon

landmarks (see Figure 2.5.2). The azimuthal position of the regime boundaries established which sunrise or sunset events would occur in a particular horizon regime.

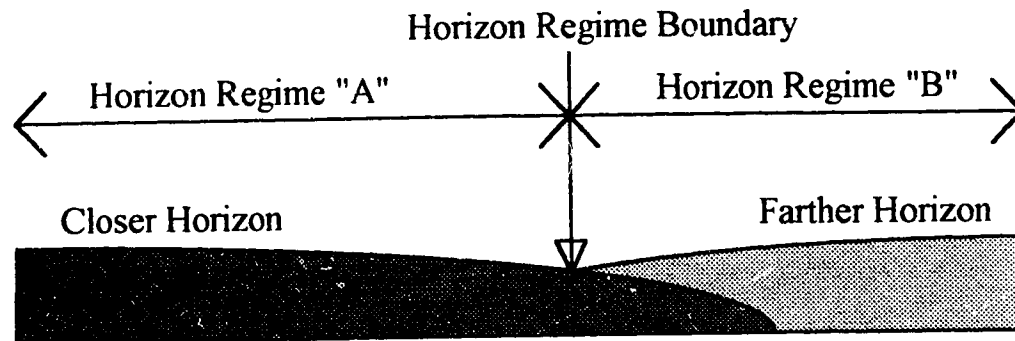


**Figure 2.5.2:** Horizon regime boundary. Horizon regime "A" appears darker and is therefore closer than horizon regime "B".

Three regimes were established for the sunrise horizon and five for the sunset horizon. The sunset horizon between azimuth  $230^\circ$  and  $270^\circ$  shows a relatively high degree of variability due to numerous small hills over relatively flat terrain. The standard deviation of the five horizon distances for the  $230^\circ$  to  $270^\circ$  regime is 3.0 km. A visual examination of this horizon regime with 7x20 binoculars showed the apparent horizon distance varying noticeably and frequently over relatively small azimuthal distances (i.e. less than a degree of azimuth).

A summary of the calculated horizon distances appear in Table 2.5.2 and the corresponding regimes in Table 2.5.3.

The estimated altitude of the horizon at the time of the sunrise and sunset events  $a_h$  was determined through the following expression:

$$a_h = a_t - R_{t1} + R_{t2} \quad (2.5.6)$$

Where  $a_t$  is the altitude of the horizon as measured by the theodolite. The variable  $R_{t1}$  is the terrestrial refraction of the horizon during the time of the theodolite horizon survey and is found by substituting the estimated horizon distances and meteorological conditions at the time of the theodolite horizon survey into Equations (2.5.4) and (2.5.5). The variable  $R_{t2}$  is the terrestrial refraction at the time of the sunrise or sunset event, estimated by substituting the meteorological conditions at the time of the observed sunrise and sunset event into Equations (2.5.4) and (2.5.5).

The average terrestrial refraction of the horizon for all of the sunrises in the data set was found to be  $0.033^\circ$ , with a minimum value of  $0.008^\circ$  and a maximum of  $0.123^\circ$ . For sunsets, the average was  $0.013^\circ$ , the minimum  $-0.003^\circ$  and the maximum  $0.035^\circ$ .



<b>Observing Site</b>	<b>Azimuth (°)</b>	<b>Horizon Distance (km)</b>
Apartment roof top (sunrise)	45.6	23.0
	60.5	26.6
	72.0	27.5
	85.5	11.9
	90.0	9.7
	96.0	11.8
	117.6	12.0
Apartment kitchen window (sunrise)	124.6	12.0
	129.5	18.8
Tory roof top (sunset)	230.0	18.9
	240.0	20.3
	250.0	12.3
	260.0	14.1
	270.0	14.4
Apartment roof top (sunset)	270.4	14.0
Apartment balcony (sunset)	280.5	16.1
	286.0	15.4
	291.1	36.4
	295.9	11.6
Tory roof top (sunset)	301.0	32.3
	319.0	32.8

**Table 2.5.2:** Calculated local horizon distances.

<b>Observing Site (event)</b>	<b>Dates</b>	<b>Mean Distance to Horizon (km)</b>
Apartment (sunrise)	Dec. 3 to Jan. 9	18.8
	Jan. 10 to Apr. 4	11.4
	Apr. 5 to Sept. 7	25.7
	Sept. 8 to Dec. 2	11.4
Tory (sunset)	Oct. 5 to Mar. 26	16.0
Apartment (sunset)	Mar. 21 to 23, 1992	14.0
	Sept. 14 to 30	14.0
	Sept. 18 to Oct. 3	14.0
	Mar. 27 to Apr. 14	15.8
	Apr. 15 to 20	36.4
	Apr. 21 to May 3	11.6
Tory (sunset)	May 4 to Aug. 11	34.9
Apartment (sunset)	Aug. 12 to 14	11.6
	Aug. 15 to 20	34.9
	Aug. 30 to Sept. 10	15.8

**Table 2.5.3:** Local horizon distance regimes for particular observing sites and dates of sunrise or sunset observations. Column 2 give the dates of sunrise or sunset visible over the particular horizon regime. Dates with years indicate those periods where observations were made from either the apartment or the Tory sites.

Ideally, the altitude of the horizon should be measured at the moment of sunrise or sunset. Refractive conditions producing anomalous sunrise and sunset times such as those described by Lehn (1979) may also produce correspondingly anomalous horizon altitudes that may not conform to Bomford's formulation. The results in Lehn's work suggests that a mirage phenomenon like the Novaya Zemlya effect, would tend to increase the horizon altitude even more than is predicted by Bomford's formula. A possible example of this effect occurred during the sunset on January 14, 1993 (Universal Time) when the Sun set about 7 minutes later than predicted (see Figure 2.5.3). This mirage phenomenon appears to be relatively rare, occurring only on one other occasion during this study (sunrise on July 24, 1992). This event showed a similar amount of vertical displacement of the horizon as the January 14, 1993 event. Due to the rarity of the phenomenon, the statistical results of this study should not be greatly affected, but in further studies of sunrise and sunset refraction one should consider measuring the altitude of the horizon at the time of sunrise or sunset.

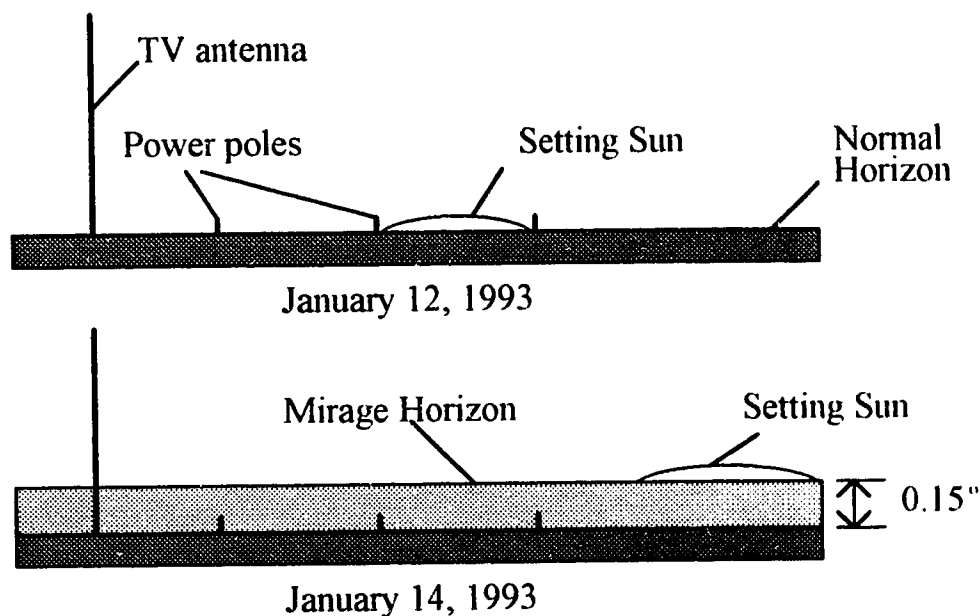


**Figure 2.5.3:** A possible example of anomalous terrestrial refraction. On January 14, 1993 the sunset occurred on a different horizon appearing behind and higher than the normally observed horizon. The TV antenna and power poles, which are normally silhouetted against the sky, were seen in front of the new horizon. This event appeared to be a sunset on a more distant horizon which was refracted to an altitude above the normal horizon. The altitude of the mirage was estimated by comparing the new horizon's position with respect to the TV antenna. The horizon appeared about one quarter the height of the tower, which was at a distance of 13.4 km and 137 m tall.

## 2.6 Measurement of Horizon Azimuth.

In order to measure directly the amount of observed variation in azimuth,  $A$ , due to possible horizontal astronomical refraction, it was necessary to determine the azimuth of the sunrise or sunset. The point on the horizon where sunrise and sunset occurred was found by comparing its relative position to distant horizon landmarks like power poles and radio antennae. This was achieved by sketching the observed position of sunrise or sunset with respect to the nearest horizon landmarks on either side of the sunrise or sunset. The uncertainty in this positioning was greatest when the reference landmarks were farthest from the point of sunrise or sunset. When landmarks were plentiful (for example, around the winter solstice sunrise), the uncertainty was estimated to be no more than  $\pm 0.13^\circ$ . Azimuthal positions of these sunrise and sunset points were found by measuring the horizontal angular displacement of the landmarks from a reference horizon landmark. This was performed with the same theodolite used in the horizon altitude survey. The precision of this measurement was estimated to be about  $\pm 0.5'$  or about  $\pm 0.01^\circ$ . The azimuth of the landmarks was then found by adding the angular displacement to the azimuth of a reference horizon landmark.

The azimuthal position of the reference horizon landmark was determined using a technique based on the Sun's hour angle (personal communication, Peterson, 1993). This value was also estimated using Cunningham's azimuth formula (Bomford, 1980, p. 120). In Peterson's method, a theodolite is used to measure the position of the Sun, with respect to the radome, as seen from the apartment site. A computer program calculates the azimuth by requesting input of the geographic coordinates of the observer, the time of the sun-shot (a projected transit of the trailing edge of the Sun across the vertical cross hair of the theodolite), the azimuthal displacement of the theodolite with respect to the horizon landmark, the declination of the Sun, the rate of change of declination, the equation of time, the rate of change of the equation of time, and the Sun's semidiameter. The accuracy of this method may have been limited by the constrained sight lines of the observing site. Through a south facing window (the window itself was removed for all theodolite readings), the Sun could be measured only around local noon when the Sun's azimuthal motion is the greatest. Higher accuracy is achieved if the Sun can be measured after about 15:00 local time or prior to 09:00 when the azimuthal motion is less.

Cunningham's method of calculating azimuth uses the longitude and latitude of the observer and the target. The coordinates of the centre of the radome were provided by Transport Canada ( $53^\circ 25' 05''.03$  latitude and  $113^\circ 16' 09''.96$  longitude) and the azimuth,  $A$ , found through the equation:

$$\cot A = (\Lambda_{12} - \cos \Delta\lambda) \sin \phi_1 \operatorname{cosec} \Delta\lambda \quad (2.6.1)$$

where  $\Delta\lambda$  is the difference in longitude between the observer and the target,  $\phi_1$  is the latitude of the observer, and  $\Lambda_{12}$  is the correction due to the oblateness of the Earth which is calculated from the equation:

$$\Lambda_{12} = \frac{\tan \phi_2}{(1 + \varepsilon) \tan \phi_1} + e^2 \sqrt{\frac{(1 + \varepsilon) + \tan^2 \phi_2}{(1 + \varepsilon) + \tan^2 \phi_1}} \quad (2.6.2)$$

where  $\phi_2$  is the longitude of the target, and  $\varepsilon$  is found through the formula:

$$\varepsilon = \frac{e^2}{(1 - e^2)} \quad (2.6.3)$$

where  $e$  is the eccentricity of the Earth and is found from:

$$e = \frac{1}{a} \sqrt{a^2 - b^2} \quad (2.6.4)$$

where  $a$  is the mean equatorial radius of the Earth ( $6.37814 \times 10^6$  m), and  $b$  is the mean polar radius ( $6.356755 \times 10^6$  m) (Royal Astronomical Society of Canada Observer's Handbook, 1993, p. 16).

A summary of the different methods is given in Table 2.6.1. The approximate azimuth of the radome was also found using a protractor graduated in  $0.5^\circ$  increments and a 1:50000 topographic map (Surveys and Mapping Branch, Department of Energy Mines and Resources, 1980).

Method	Azimuth ( $^\circ$ )
Solar observation	$129.65 \pm 0.01$
Cunningham	$129.61 \pm 0.02$
Topographic map	$129.5 \pm 0.2$

**Table 2.6.1:** Comparison of three methods for calculating the azimuth of the old international airport radome as seen from the apartment site. The uncertainty in the Solar observation method was provided by the computer program and is based on the standard deviation of 6 measurements. The uncertainty in Cunningham's method was determined by calculating the range in azimuthal angle produced by  $\pm 2$  m (about  $0.06''$  of latitude or  $0.10''$  longitude) at a distance of 18.9 km (the distance to the radome). The uncertainty of  $\pm 2$  m is due to the recent removal of the survey marker used to determine the geographic coordinates of the observing site. A physical description of the location of the monument, provided by the Government of Alberta, was used to find its approximate position.

## CHAPTER 3

### RESULTS AND ANALYSIS

#### 3.1. Sunrise and Sunset Data

Timings began at sunrise on December 29, 1990 and finished at sunrise February 4, 1994. A total of 244 sunrises and 125 sunsets were successfully timed. Sunrise and sunset observations are listed in Appendix D.

The first and second columns contain the date and time of the observed sunrise or sunset in Universal Time (for example: sunset at 19:00 Mountain Standard Time on April 1 is 02:00 April 2 Universal Time).

The third and fourth columns give the temporally interpolated surface temperature  $T$  in degrees Celsius, and the temporally interpolated surface pressure  $p$  in millibars at the approximate time of the observed sunrise or sunset. Temperature and pressure records used to determine these values were recorded on the hour. Surface temperatures and pressure occurring between these times were assumed to vary linearly between the previous and next hourly value. Sunrise and sunset times rounded to the nearest tenth of an hour were used for the interpolation of surface temperature and pressure data. Meteorological data were obtained from the hourly records from Canadian Forces Base Namao located in north suburban Edmonton, about 16.5 km north of the two observing sites. The path of the sunlight through the surface layers of the atmosphere during sunrise and sunset was estimated to be greater than 20 km. From the two observing sites in central Edmonton it was assumed that most of the light path would pass through the surface layers above suburban or rural Edmonton. In order to avoid the effects of urban heating it was decided to use suburban meteorological data which should approximate the mean surface temperature along the total light path.

The fifth column is the estimated surface vertical temperature gradient  $dT/dh$ . This value was calculated from the data from the radiosonde balloon launched from the Stoney Plain upper air station located 30 km west of Edmonton. Launches are conducted twice daily at 00:00 and 12:00 U.T. (17:00 and 05:00 M.S.T. or 18:00 and 06:00 M.D.T.). Vertical temperature gradients were calculated from the balloon launch closest to the time of sunrise or sunset. The average time difference between the balloon launch and sunrise observations was 1.81 hours with the maximum time difference of 3.85 hours occurring around winter solstice sunrise. The average time difference for sunsets was 1.82 hours with a maximum difference of 4.14 hours occurring around summer solstice sunset. The difference between the surface temperature and the second recorded temperature was divided by the estimated height of the balloon at the second height level. Missing data were either not archived or were not received due to lost tephigrams or equipment failure.

The sixth column is the thickness  $h$  of the layer used to determine the surface vertical temperature gradient

The seventh, eighth, ninth and tenth columns are the meteorological conditions at the time of the theodolite survey. These values were used to determine the terrestrial refraction at the time of the survey (see Equations (2.5.4) and (2.5.5)). The surface vertical temperature gradient  $dT/dh$  was found from the 00:00 U.T. radiosonde closest to the time of the survey.

The eleventh column is the measured altitude of the horizon at the azimuthal location of sunrise or sunset (in degrees). These measurements have not been corrected for the effects of terrestrial refraction which occurred during the survey or at the time of the observed sunrise or sunset. This was done in order to provide an unaltered data set that could be more easily reanalysed by other investigators. As mentioned previously, these measurements were taken on warm and clear summer or fall days, during early to mid-afternoon when the surface vertical temperature gradient is usually adiabatic and refraction is minimized.

The twelfth column is the calculated distance  $d$  to the horizon at the point of sunrise or sunset.

The thirteenth column gives the astronomical refraction  $R'_0$  which has been corrected to a zero horizon as outlined in Section 3.2.

### 3.2 Correction of Astronomical Refraction to a Zero Horizon.

The amount of astronomical refraction the Sun will experience is a function of its zenith angle or altitude above the zero horizon (Green, 1985, pp.82-95). The horizon from both observing sites showed measurable variation from the zero horizon. In order to isolate the effects of meteorological conditions on atmospheric refraction and make valid comparisons with the work of Schaefer and Liller, who worked with an ocean horizon, the sunset and sunrise refraction data must be corrected to a zero horizon.

Through a visual examination of a plot of the astronomical refraction against horizon altitude (see Figure 3.2.1 and 3.2.2) it appears that a linear relationship could be fit to the data. It also appeared that the relationship between the horizon altitude and astronomical refraction differed between the sunrise and sunset data. No obvious explanation can be provided for this apparent difference. Much of the scatter is assumed to be a result of anomalous refractive conditions and in order to isolate the effect of horizon altitude, the data were truncated by eliminating refraction values greater than a specified truncation limit.

A series of truncation limits  $L$  was based on the mean and standard deviation of the sunrise or sunset refraction data and takes the form:

$$L = \bar{R}_0 - nSD \quad (3.2.1)$$

where  $\bar{R}_0$  is the mean sunrise or sunset astronomical refraction ( $0.710^\circ$  for sunrise and  $0.581^\circ$  for sunset),  $n$  is in increments of 0.1 between 0.0 and 0.7 (beyond  $n = 0.7$ , the data set appeared to become too small for proper analysis), and  $SD$  is the

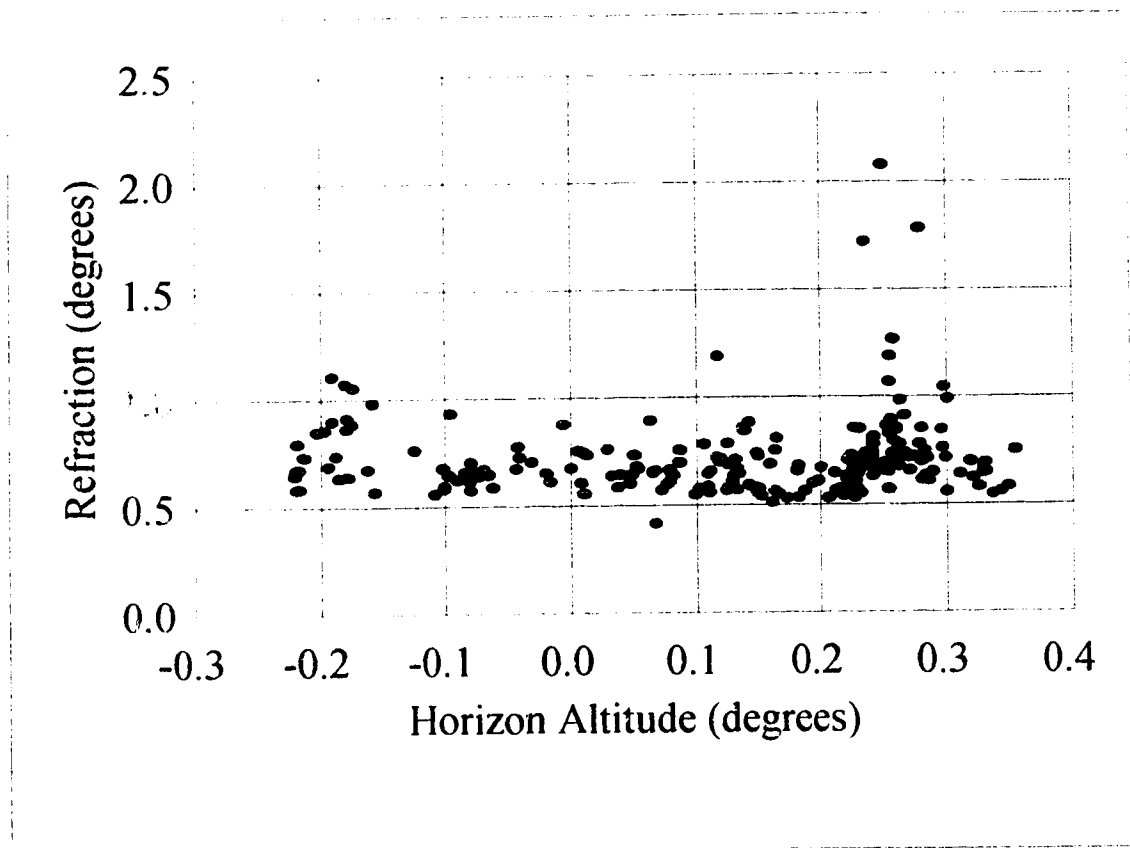


Figure 3.2.1: Horizon altitude versus sunrise astronomical refraction.



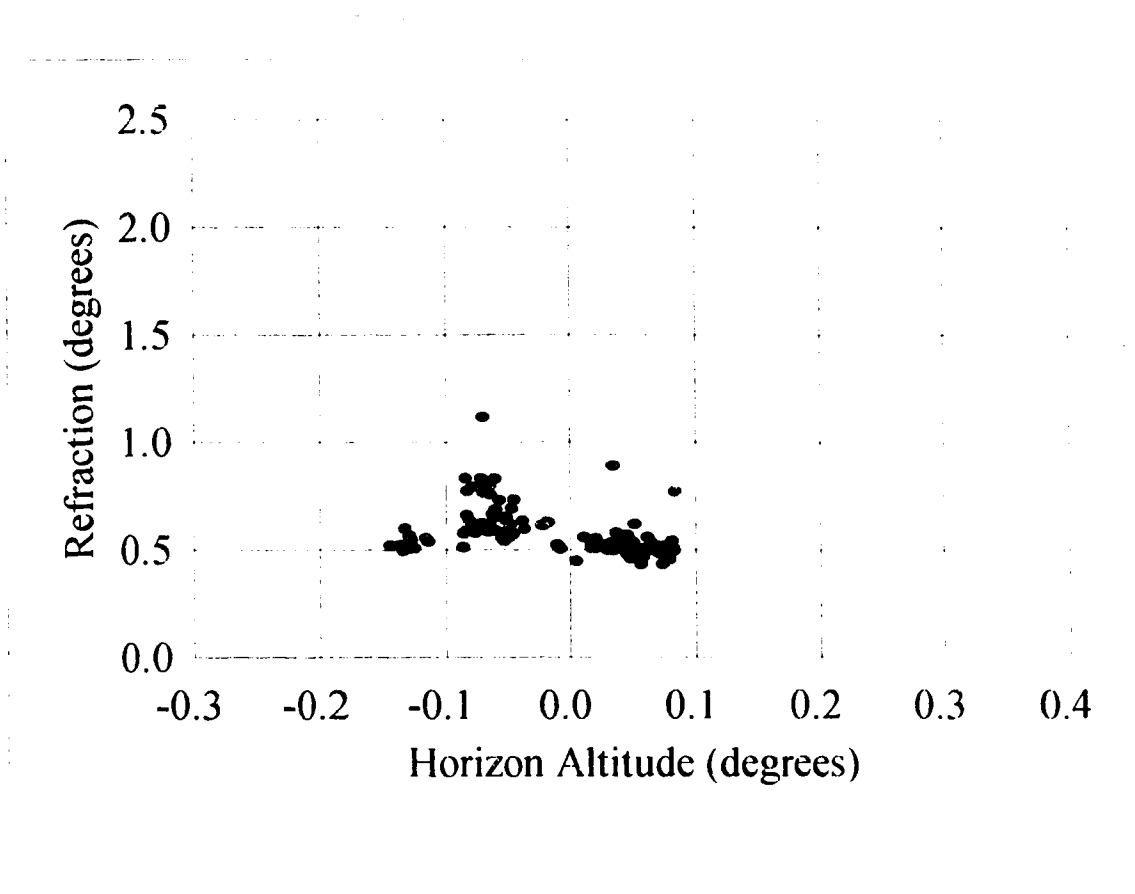


Figure 3.2.2: Horizon altitude versus sunset astronomical refraction.

standard deviation of the sunrise or sunset astronomical refraction ( $0.184^\circ$  for sunrise and  $0.113^\circ$  for sunset).

All data with astronomical refraction greater than  $L$  were deleted from the data set. A linear regression routine was then applied to each of the eight truncated data sets. An average of the eight slopes for sunrise and sunset was then determined. The average was then used as a correction value for the sunrise and sunset astronomical refraction values. The results of the truncations appear in Table 3.2.1 and the resulting absolute mean, minimum and maximum corrections appear in Table 3.2.2.

n	Slope (sunrise)	Slope (sunset)
0.0	-0.014	-0.145
0.1	-0.030	-0.118
0.2	-0.031	-0.109
0.3	-0.031	-0.091
0.4	-0.013	-0.089
0.5	-0.016	-0.124
0.6	-0.024	-0.127
0.7	-0.008	-0.091
<b>Average:</b>	<b>-0.021 <math>\pm</math>0.003</b>	<b>-0.112 <math>\pm</math>0.007</b>

**Table 3.2.1:** The slopes from the linear regression of the astronomical refraction versus horizon altitude. The first column is the multiplier of the standard deviation used in determining the truncation value. The second and third columns are the slopes found from the linear regression, in degrees of refraction per degree of horizon altitude gained. The uncertainties in the averages are standard deviations of the mean.

The value for the astronomical refraction corrected to a zero horizon was determined through the formula:

$$R'_0 = R_0 + ma_h \quad (3.2.2.)$$

Where  $m$  is the average slope from Table 3.2.1. The absolute mean, maximum and minimum resulting corrections are outlined in Table 3.2.2.

<b>Zero Horizon Correction</b>	<b>Sunrise</b>	<b>Sunset</b>
Abs. Mean Correction ( $^{\circ}$ )	0.007	0.017
Min. Correction ( $^{\circ}$ )	-0.012	0.001
Max. Correction ( $^{\circ}$ )	0.016	0.055

**Table 3.2.2:** The results of the zero horizon corrections. The first row is the absolute mean correction in degrees. The second and third rows show the range of the correction.

The astronomical refraction values were then corrected and plotted. The mean correction is 1.0% for the mean sunrise refraction and 2.9% for the mean sunset refraction.

### 3.3 Overall Astronomical Refraction.

The first results of the investigation appear in Tables 3.3.1 and 3.3.2. The original data of Schaefer and Liller (1990) was filtered to produce a more consistent comparison with the present investigation. All lunar and planetary events (the setting of the Moon or the planet Venus) were removed from Schaefer and Liller's data set. As well, all observations with a noted uncertainty greater than 10 seconds were also removed. In the Schaefer and Liller study it appears that no correction was made for terrestrial refraction of the horizon. Therefore, two tables are shown comparing the results of this study corrected and uncorrected for horizon refraction.

There appears to be an obvious difference between the mean sunrise refraction and sunset refraction. The mean refraction and the variability appear to be less during sunset than at sunrise. The mean corrected sunset refraction was found to be  $0.135^{\circ}$  less than the mean sunrise refraction (18.9%). The mean sunset refraction in the Schaefer and Liller study is very similar to that of this study,  $0.016^{\circ}$  or 2.8% less than the mean corrected sunset refraction found in this study and  $0.001^{\circ}$  or 0.2% less than the uncorrected value. The population standard deviation of the corrected refraction shows a far greater difference, and was found to be  $0.075^{\circ}$  or 69.4% greater in the Schaefer and Liller study. The possible reasons for this difference are somewhat uncertain. Schaefer and Liller's study used 9 observers and 11 observing sites with elevations from 3 to 4205 m above the sea level horizon where the sunsets were observed. It is, therefore, not unreasonable to assume that other variables, such as human error and the effects of terrestrial refraction, especially in the higher altitude observing sites, may have contributed to the differences in uncertainty between the two data sets.

Since the results show variability in the astronomical refraction rather than measurement uncertainty, the results have three significant digits even though the population standard deviation is two orders of magnitude larger.

Author	Event	# Obs.	Mean ( $^{\circ}$ )	SD ( $^{\circ}$ )	Min. ( $^{\circ}$ )	Max. ( $^{\circ}$ )
Schaefer and Liller	sunset	97	0.563	0.183	0.234	1.678
Sampson	sunset	115	0.579	0.108	0.442	1.085
Sampson	sunrise	234	0.714	0.184	0.402	2.081
Sampson	both	349	0.669	0.175	0.402	2.081

**Table 3.3.1:** Comparison of Schaefer and Liller's results (1990) with corrected sunrise and sunset astronomical refraction results from the present investigation. The third column is the number of observations. The fifth column is the population standard deviation. The sixth and seventh columns show the range of the observed refraction.

Author	Event	# Obs.	Mean ( $^{\circ}$ )	SD ( $^{\circ}$ )	Min. ( $^{\circ}$ )	Max. ( $^{\circ}$ )
Schaefer and Liller	sunset	97	0.563	0.183	0.234	1.678
Sampson	sunset	125	0.564	0.106	0.421	1.081
Sampson	sunrise	244	0.680	0.177	0.403	2.034
Sampson	both	369	0.641	0.166	0.403	2.034

**Table 3.3.2:** Comparison of Schaefer and Liller's (1990) results with current results uncorrected for horizon refraction.

### 3.4 Seasonal Differences in Astronomical Refraction.

The variation in astronomical refraction with the time of year was also examined. A plot of the data appears in Figures 3.4.1 and 3.4.2. Previous experiments have found seasonal variations in astronomical refraction (Sugawa, 1955). Sugawa performed numerical ray tracing for altitudes of  $5^{\circ}$  to  $85^{\circ}$  through monthly mean atmospheric density profiles. The mean profiles were constructed of layers 1 km thick with the maximum height ranging from 16 to 20 km. Temperature and pressure data were obtained from 323 radiosonde launches which took place at 00:00 and 12:00 Japanese Standard Time. Sugawa found the maximum amount of astronomical refraction occurred during the colder months and the minimum in the warmer months. The maximum monthly refraction occurred in December and the minimum in August. The maximum value was 13% greater than the minimum. A visual examination of the time series from the present study appears to show a similar overall relationship.

To help examine these seasonal variations, refraction values were placed into 12 equal bins of 30.44 days. Each bin represents approximately a single calendar month (see Table 3.4.1 for results). For each bin the mean refraction and the

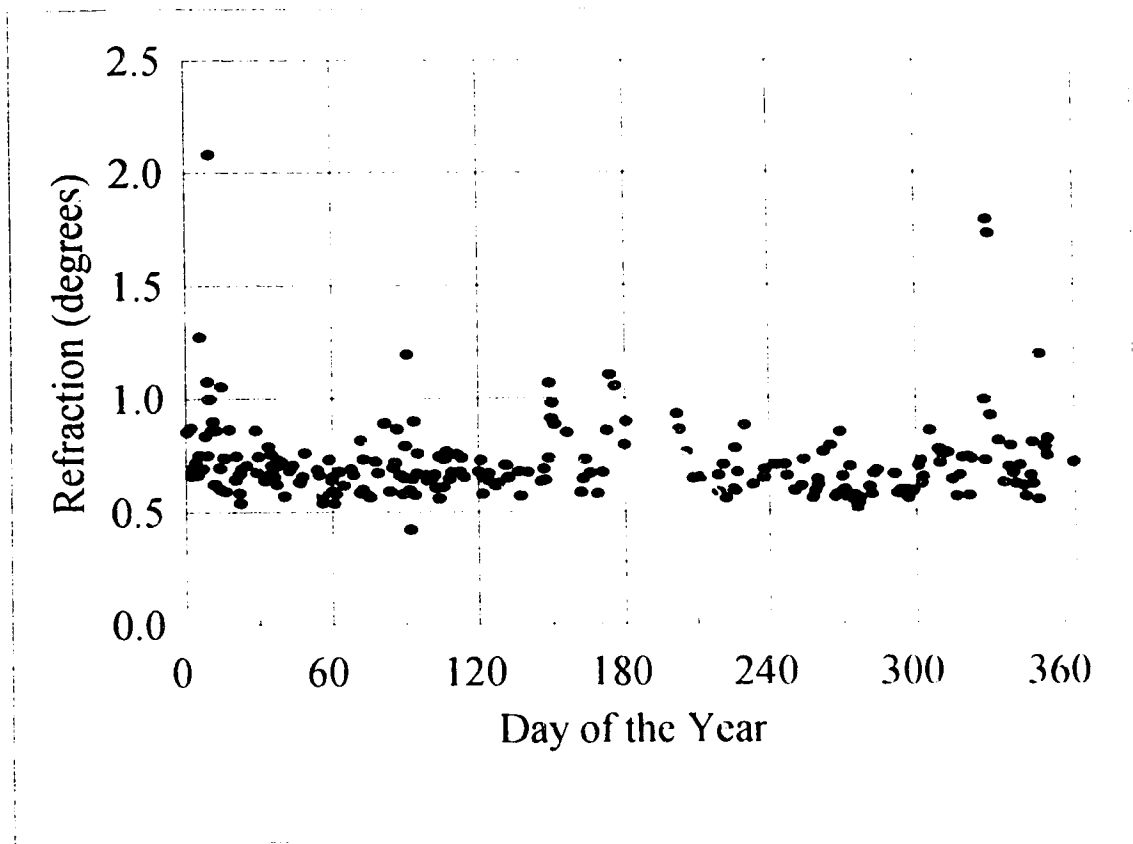


Figure 3.4.1: Time of year versus sunrise astronomical refraction

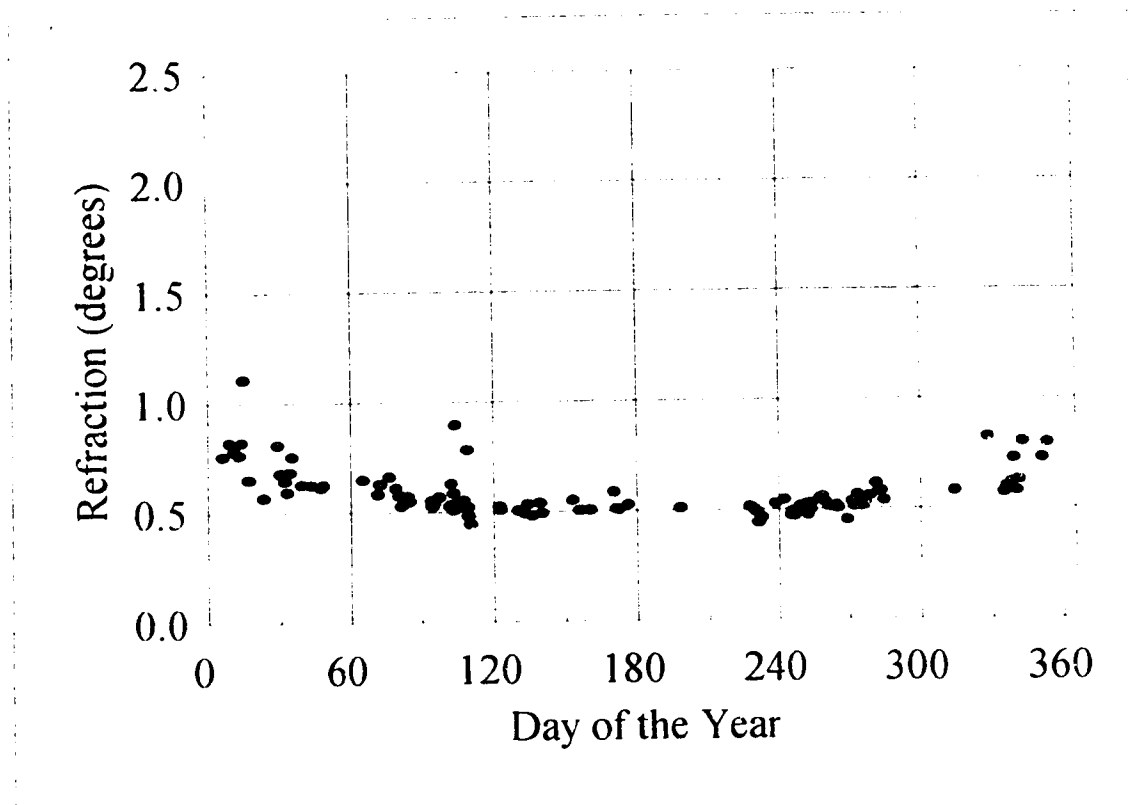


Figure 3.4.2: Time of year versus sunset astronomical refraction.

	J	F	M	A	M	J	J	A	S	O	N	D
<b>BOTH</b>												
Mean	0.802	0.665	0.663	0.629	0.612	0.681	0.740	0.606	0.572	0.587	0.841	0.694
SD	0.247	0.059	0.129	0.103	0.099	0.183	0.151	0.108	0.092	0.056	0.324	0.129
SSD	0.249	0.060	0.131	0.104	0.101	0.188	0.168	0.110	0.093	0.057	0.332	0.131
Min.	0.538	0.537	0.528	0.443	0.482	0.502	0.507	0.442	0.449	0.512	0.564	0.548
Max.	2.082	0.788	1.194	0.897	0.908	1.102	0.929	0.878	0.850	0.722	1.788	1.192
Num.	44	34	34	46	23	18	5	20	41	29	20	27
<b>SUNRISE</b>												
Mean	0.810	0.670	0.693	0.679	0.667	0.779	0.798	0.666	0.647	0.603	0.857	0.713
SD	0.270	0.061	0.140	0.074	0.077	0.171	0.107	0.085	0.083	0.056	0.335	0.144
SSD	0.274	0.063	0.143	0.075	0.080	0.180	0.124	0.088	0.085	0.058	0.345	0.149
Min.	0.538	0.537	0.536	0.557	0.568	0.578	0.644	0.557	0.553	0.517	0.564	0.548
Max.	2.082	0.788	1.194	0.897	0.908	1.102	0.929	0.878	0.850	0.722	1.788	1.192
Num.	34	26	24	26	15	11	4	13	19	20	18	17
<b>SUNSET</b>												
Mean	0.777	0.647	0.590	0.564	0.509	0.526		0.496	0.507	0.550	0.701	0.662
SD	0.136	0.048	0.044	0.100	0.019	0.029		0.033	0.029	0.032	0.122	0.087
SSD	0.143	0.051	0.046	0.102	0.020	0.031		0.035	0.029	0.034	0.172	0.091
Min.	0.568	0.593	0.528	0.443	0.482	0.502		0.442	0.449	0.512	0.580	0.571
Max.	1.108	0.755	0.661	0.894	0.538	0.586	0.507	0.543	0.563	0.613	0.823	0.801
Num.	10	8	10	20	8	7	1	7	22	9	2	10

**Table 3.4.1:** Monthly mean astronomical refraction, population standard deviation (SD), minimum and maximum astronomical refraction, and number of observations. For comparison, the sample standard deviation (SSD) is also included.

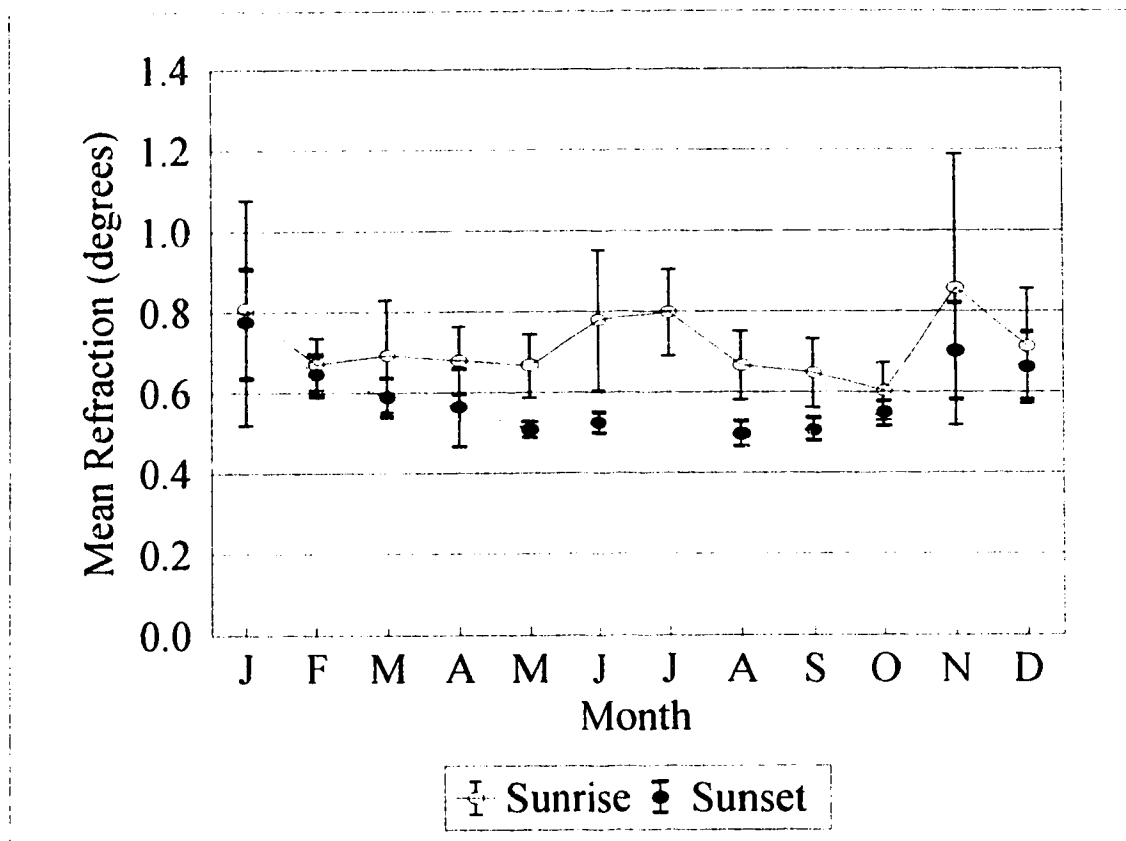


Figure 3.4.3: Mean monthly astronomical refraction for sunrise and sunset. Due to a lack of data, no mean value for the July sunset astronomical refraction is given. Error bars are the standard deviation (see Figure 3.4.4).



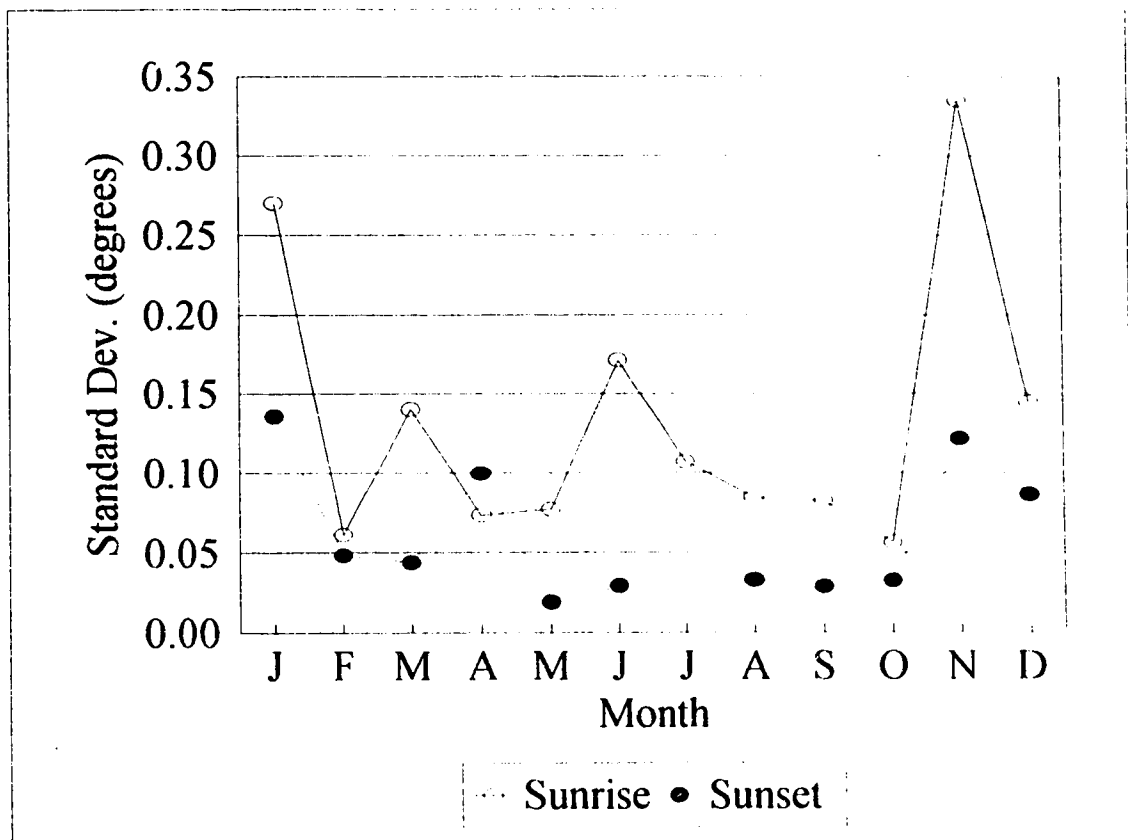


Figure 3.4.4: Monthly standard deviation of the astronomical refraction.

population standard deviation were calculated and plotted (see Figures 3.4.3 and 3.4.4).

It is apparent from the graphs that there is a systematic difference between the mean refraction at sunrise and at sunset. The mean sunset refraction appears to follow the results of Sugawa's work with a maximum during the colder months and a minimum in the warmer months. The maximum sunset astronomical refraction occurs in January ( $0.774^\circ$ ) and minimum in August ( $0.494^\circ$ ). The maximum is 57% greater than the minimum value. The relative difference between the minimum and maximum mean values is four times the value found by Sugawa.

Only one sunset data point was obtained in the month of July. The scarcity of data during this period is a result of summer convective cloud formation near the foothills of the Rocky Mountains which obscured the sunset observations.

The mean sunrise refraction data follow the sunset data only for the monthly bins of December, January and February. For the rest of the year the sunrise refraction is consistently greater than the sunset refraction, reaching a maximum difference of  $0.253^\circ$  in the month of June.

Mean sunrise refraction also shows a maximum in the colder months reaching a peak of  $0.857^\circ$  in the November bin. There appears to be a secondary peak in July where the mean refraction reaches  $0.798^\circ$ . This apparent bimodal behaviour was not exhibited in the Sugawa results.

The standard deviation also appears to follow a seasonal trend with the greatest variations for both sunrise and sunset occurring in November and January. The standard deviation is generally greater for sunrise than sunset with only April showing higher values for sunsets. The sunrise standard deviation for the month of February is the second lowest value; this appears to contradict the seasonal trend. As well, the third largest sunrise standard deviation takes place in June. One of the most striking features of the sunset standard deviation plot is the interval from May through October where the values are not only at a minimum but exhibit a high degree of stability, ranging from  $0.019^\circ$  to  $0.033^\circ$ .

More data may be necessary to confirm the seasonal behavior of atmospheric refraction. Many of the monthly bins, especially for sunsets, contain fewer than 10 data points. The trends in the monthly mean and standard deviation of the astronomical refraction appear to be strengthened by the relationship between refraction and observed meteorological conditions, outlined in the following section.

### **3.5 Surface Atmospheric Conditions and Astronomical Refraction.**

To explore the possibility of a simple method to predict astronomical refractive behavior, the relationships between surface conditions and astronomical refraction will be examined. At most sites observers may not have access to surface temperature gradients but should have easy access to surface vertical temperature and pressure data.

So far the results have been examined only in a descriptive or statistical sense. It is well understood that the index of refraction is directly proportional to the density

of the refractive medium (Humphreys, 1964, p. 455). From Snell's Law, the amount of refraction is a function of the difference in refractive index between two media. Therefore, the amount of astronomical refraction should be a function of the density gradient of the atmosphere. From the ideal gas law, the density of the atmosphere  $\rho$  is directly proportional to the atmospheric pressure  $p$  and inversely proportional to the temperature  $T_k$  in degrees Kelvin.

$$\rho = \frac{p}{RT_k} \quad (3.5.1)$$

where R is the gas constant.

Therefore, the amount of refraction is expected to vary with the vertical temperature and pressure gradient of the intervening air. The temperature of the lowest layers in the troposphere is controlled by the radiative properties of the surface, it is expected that the vertical temperature gradient near the surface should vary with the seasonal changes in the surface temperatures. The higher layers of the atmosphere, beyond the planetary boundary layer (about 1 km), show less seasonal variation in temperature (Wallace, J. and Hobbs, P., 1977, p. 27). Therefore, the seasonal variation in surface temperature should be related to the seasonal variation in the vertical density gradient. A plot of surface air density versus the surface temperature gradient appears in Figure 3.5.1. A linear regression analysis fits a line with a correlation coefficient of 0.27 which, according to Taylor (1982, pp. 248-249), has a probability of less than 1% that 369 measurements of two uncorrelated variables will give a correlation coefficient greater than or equal to the value found. According to the criteria outlined in Taylor, this correlation is considered highly significant. A visual inspection of the Figure 3.5.1 appears to show such a linear relationship. Yet, there is a great deal of scatter and any linear relationship must be somewhat imprecise.

In order to test this hypothesis, the refraction was plotted against the surface temperature, pressure and the vertical temperature gradient (see Figures 3.5.2 to 3.5.10).

The water vapor content of the air was ignored since it has a negligible effect on the refractive index of visible light in air. The correction to the index of refraction  $\Delta n$  is given as (C.R.C. Handbook of Chemistry and Physics, 1975, p. E-224):

$$\Delta n = 0.000041(m / 760) \quad (3.5.2)$$

where  $m$  is the vapor pressure in mm of Hg. The typical range of vapor pressures recorded in this study was between about 0.2 mm Hg (50% R.H. at  $-35^\circ$  C) and 15 mm Hg (75% R.H. at  $25^\circ$  C). For a refractive index of  $n-1 = 0.0002929$ , (for light from the Sodium D line at  $0.59\mu\text{m}$ ), the resulting change in the index of refraction is between  $1.1 \times 10^{-8}$  and  $8.1 \times 10^{-7}$ , a difference of 0.004% to 0.3%. Zuev (1982, p. 4) also provides a formula for the refractive index:

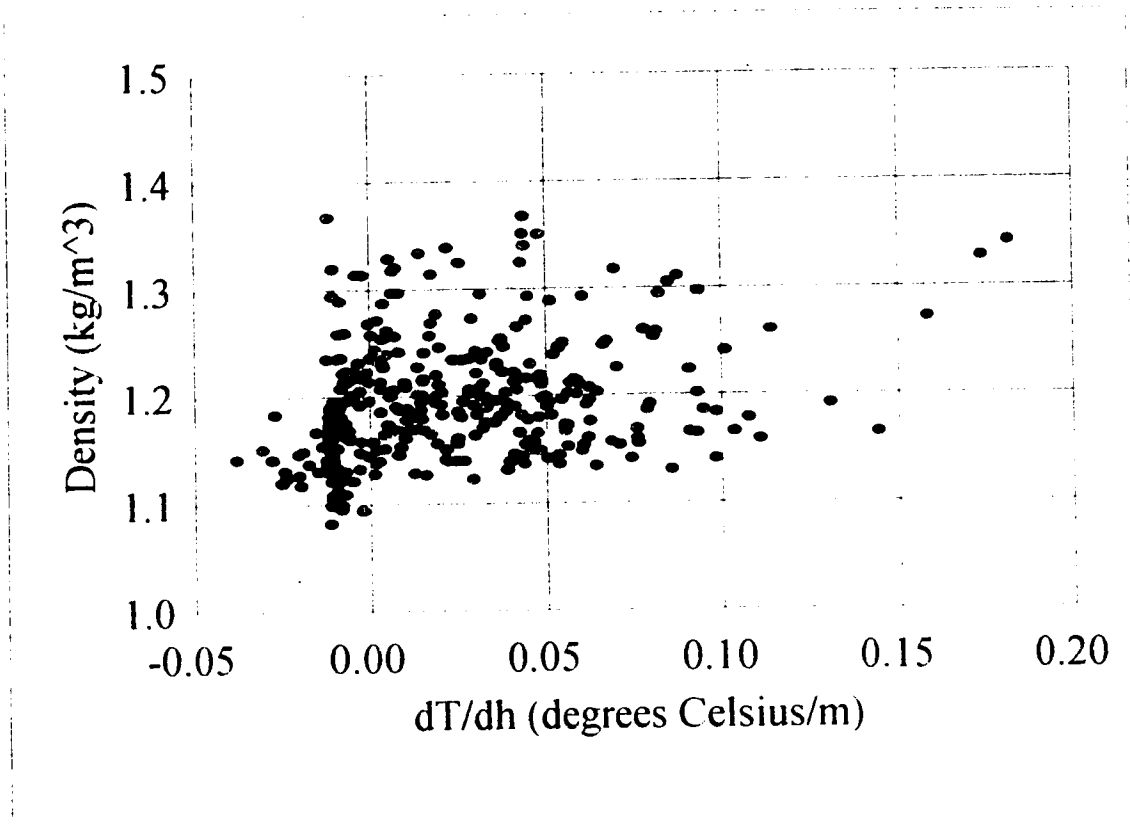


Figure 3.5.1: Surface air density versus the surface vertical temperature gradient at sunrise and sunset.

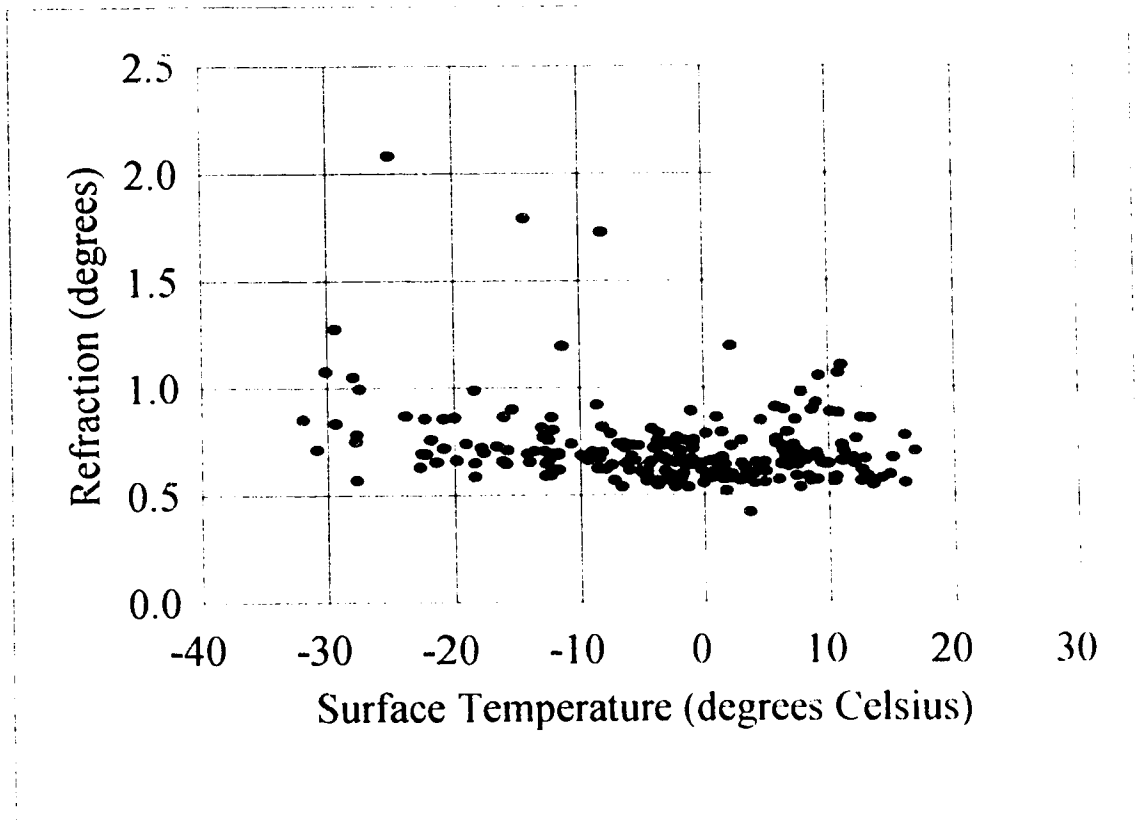


Figure 3.5.2: Surface temperature versus sunrise astronomical refraction.

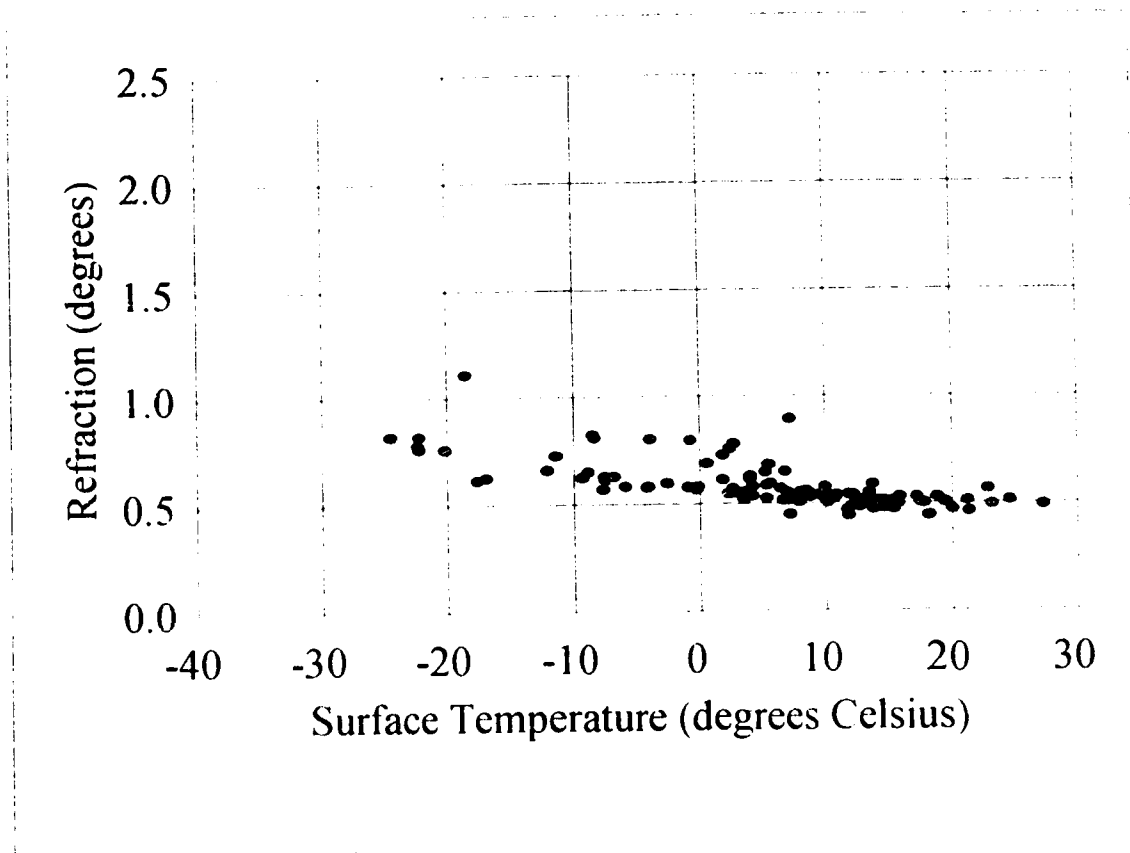


Figure 3.5.3: Surface temperature versus sunset astronomical refraction.

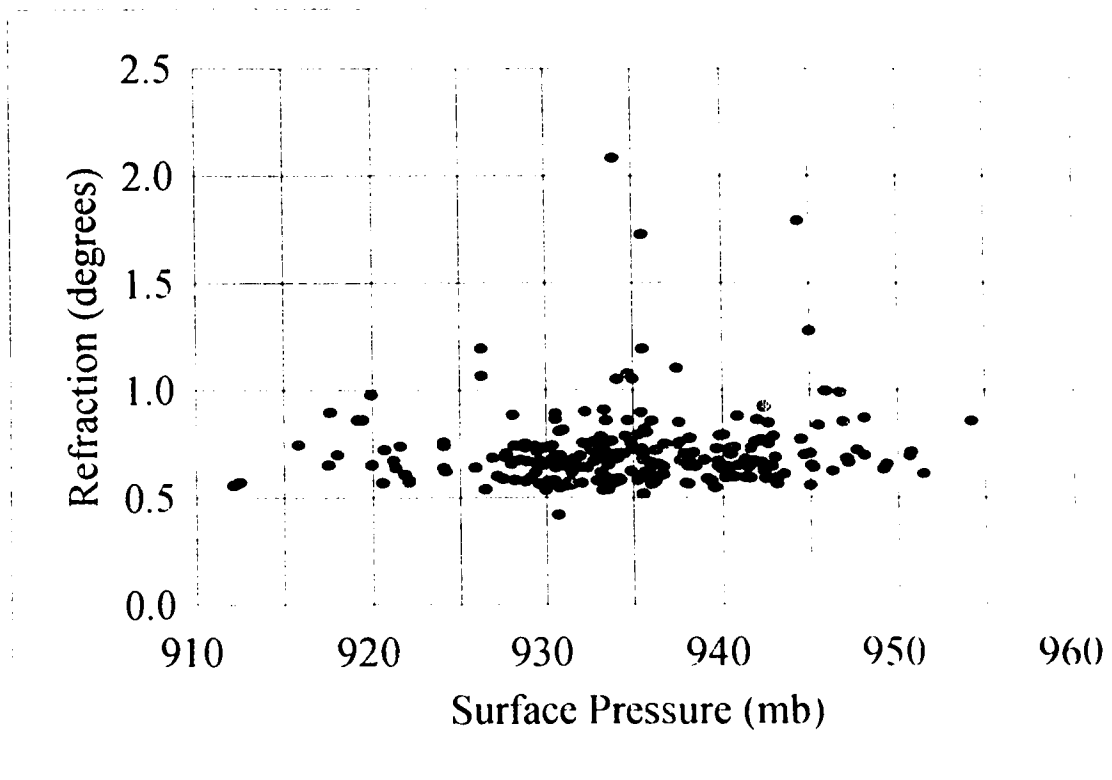


Figure 3.5.4: Surface pressure versus sunrise astronomical refraction

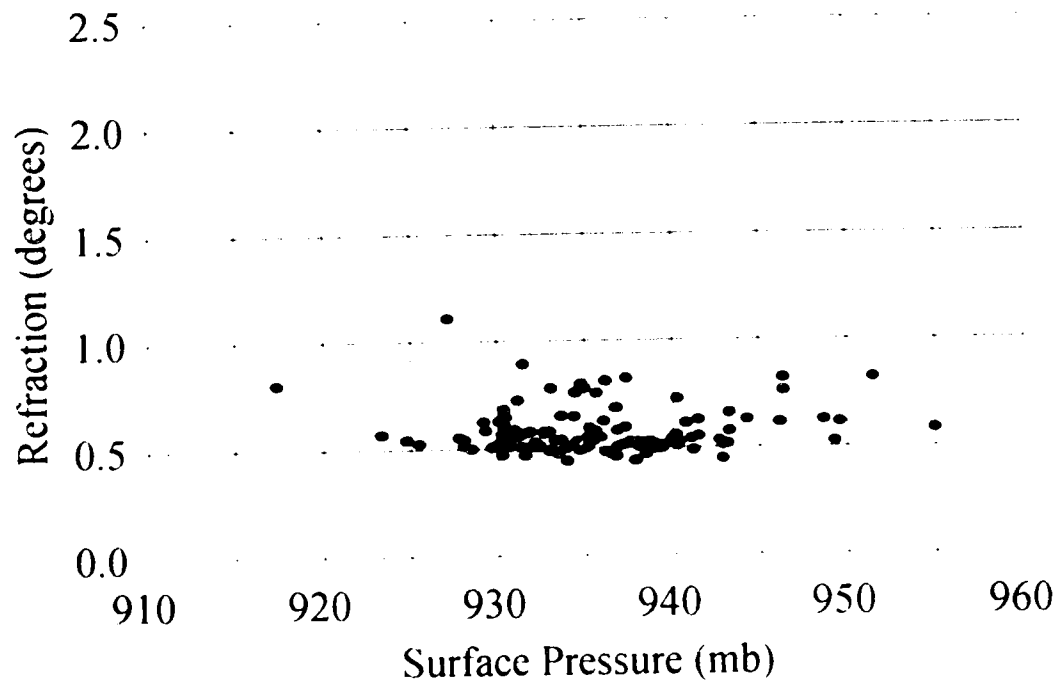


Figure 3.5.5: Surface pressure versus sunset astronomical refraction



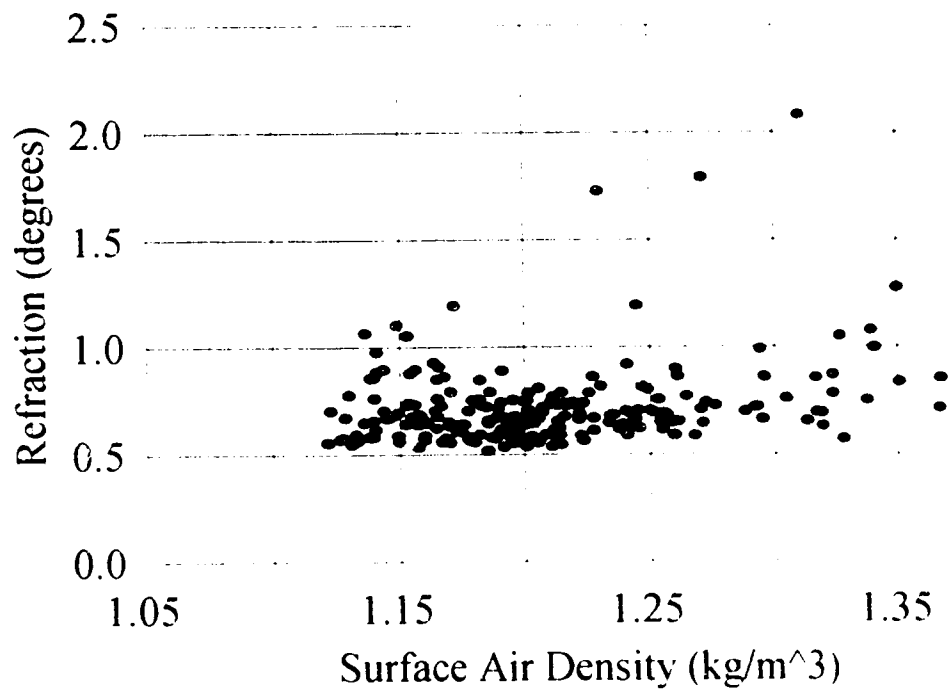


Figure 3.5.6: Surface air density versus sunrise astronomical refraction

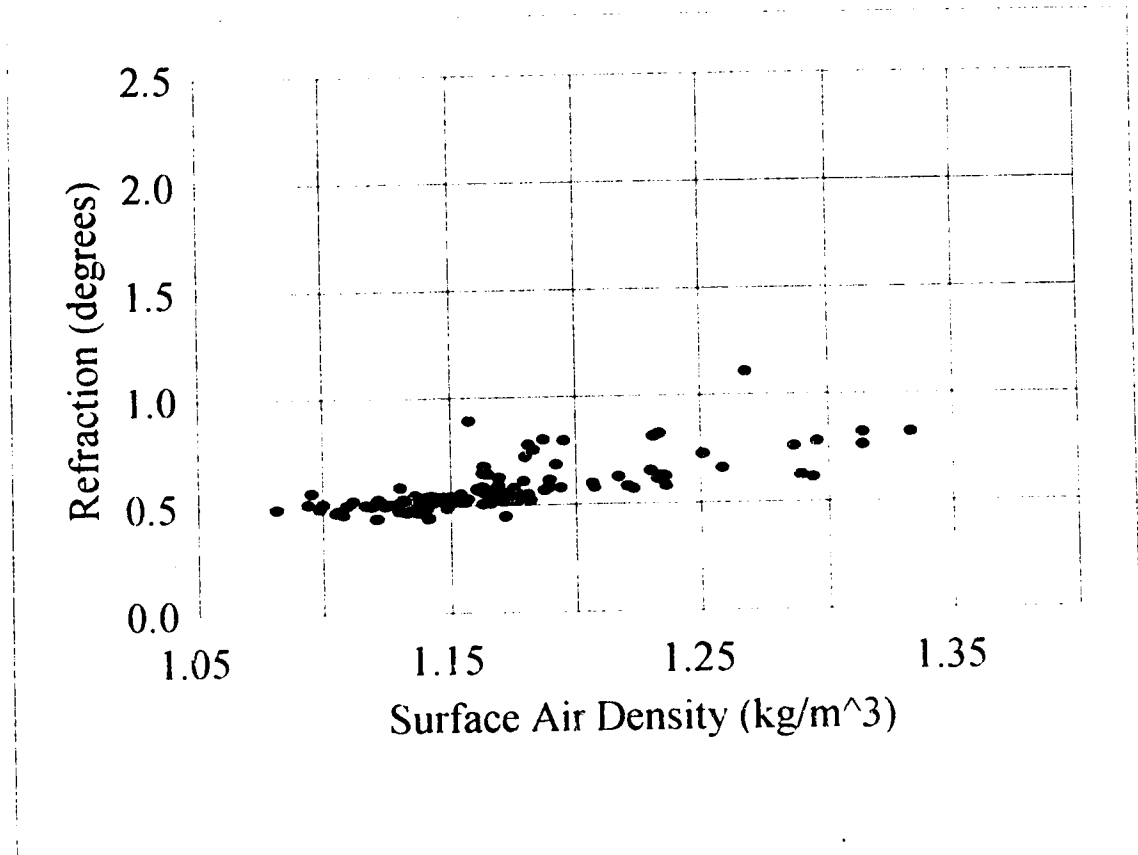


Figure 3.5.7: Surface air density versus sunset astronomical refraction.

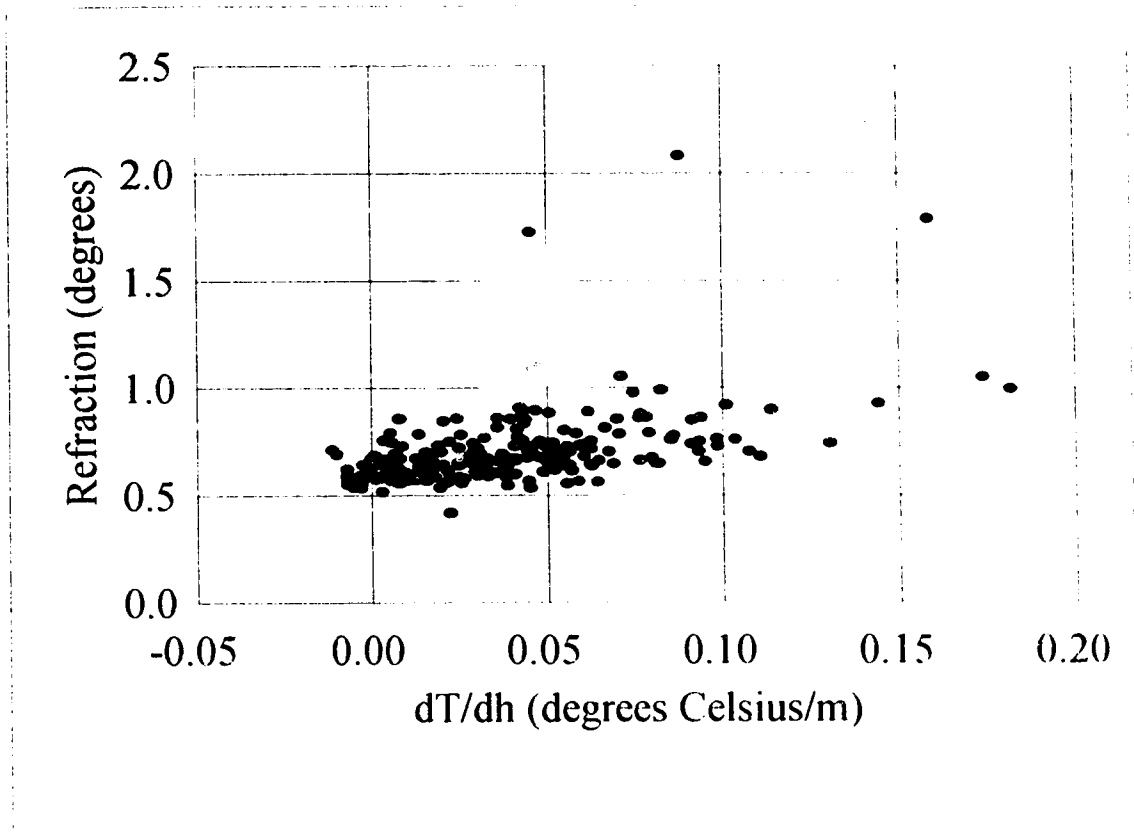


Figure 3.5.8: Surface vertical temperature gradient versus sunrise astronomical refraction.

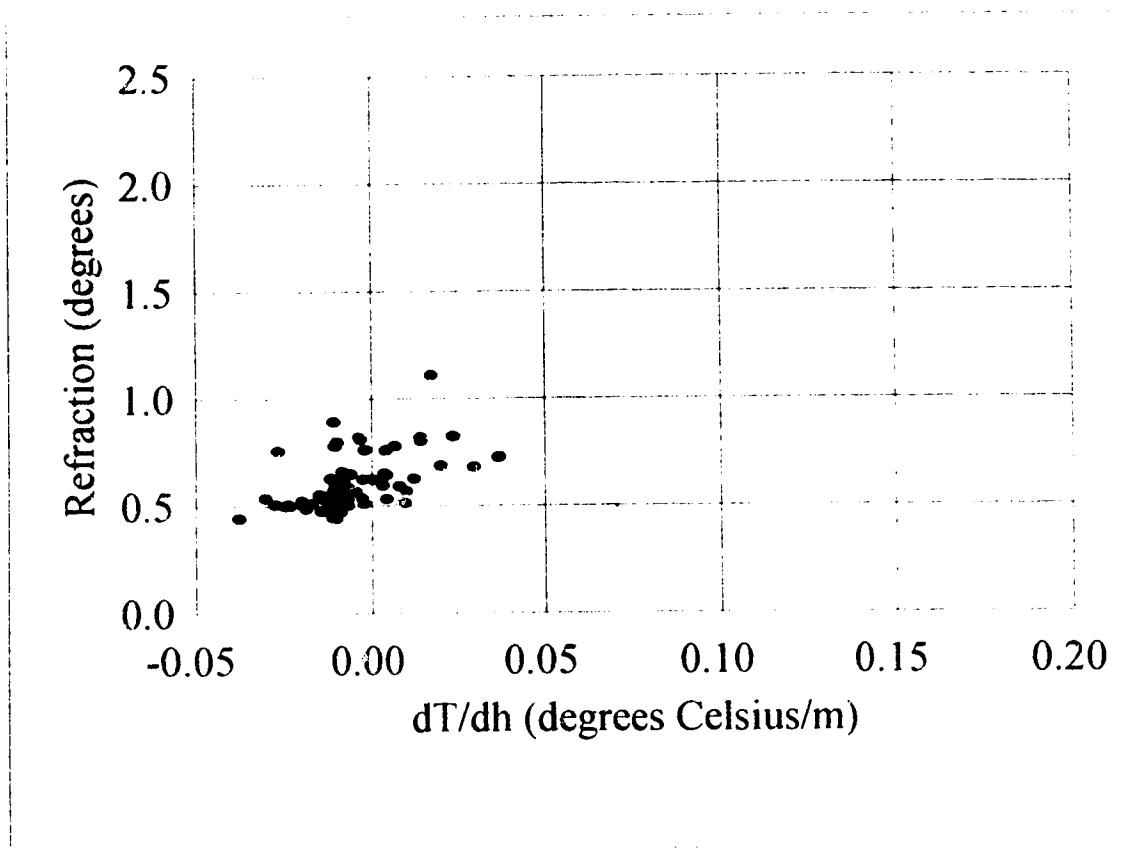


Figure 3.5.9: Surface vertical temperature gradient versus sunset astronomical refraction.

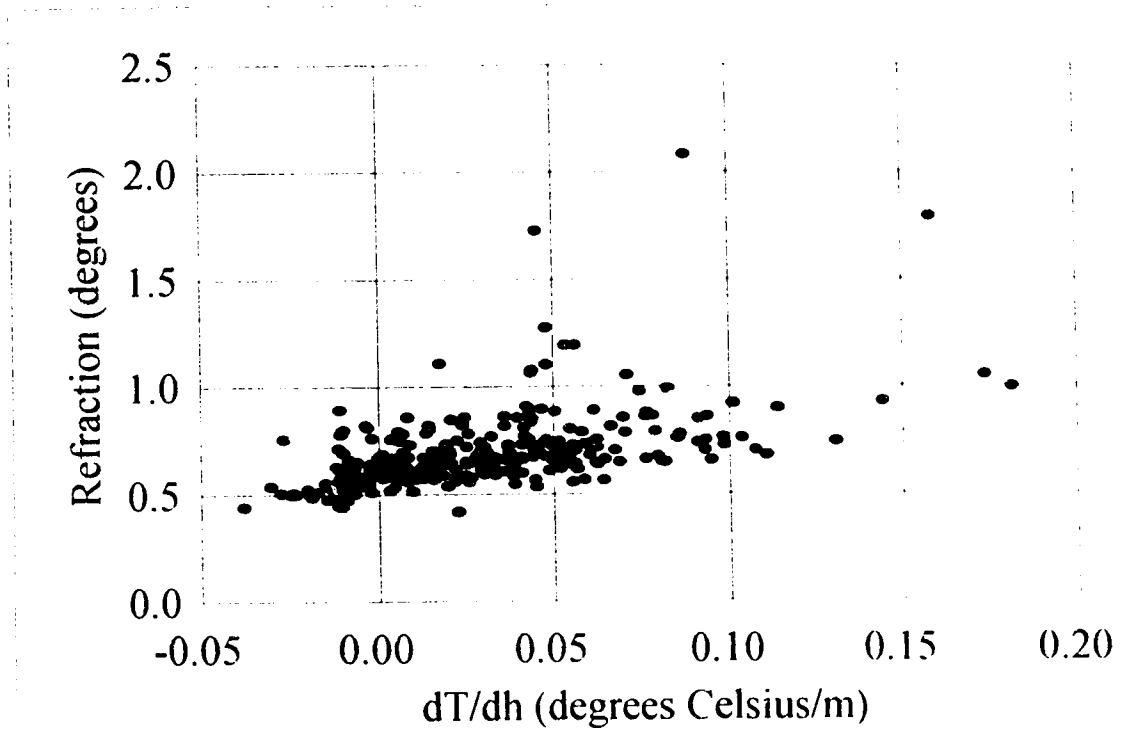


Figure 3.5.10: Surface vertical temperature gradient versus sunrise and sunset astronomical refraction.

$$n - 1 = C_{\lambda} \frac{p}{T} \left( 1 - 0.132 \frac{m}{p} \right) \quad (3.5.3)$$

where  $p$  is the pressure in mm of Hg,  $T$  is the temperature in degrees Kelvin,  $m$  is the vapor pressure in mm of Hg and,  $C_{\lambda}$  is a function of the wavelength of light and is  $1.0485 \times 10^{-4}$  for the Sodium D line. For the vapor pressures mentioned in the previous example, the corresponding correction to the index of refraction, due to the effects of vapor pressure, ranges from 0.003% to 0.3%. Consequently, the vapor pressure was assumed to have a negligible effect on astronomical refraction.

From a visual examination of the graphs it is apparent that the vertical refraction is most significantly correlated with the surface temperature, density and the vertical temperature gradient, and therefore, may help to predict the amount of astronomical refraction at sunrise and sunset. The relatively large amount of scatter and outliers suggests that a linear fit could only be somewhat approximate and other, possibly non-linear, processes may be involved.

As expected, the amount of refraction appears to be inversely proportional to the temperature in degrees Kelvin. There appears to be little or no correlation with the surface pressure. Since the relative range in temperature  $\Delta T/T$  is far greater than the relative range in pressure  $\Delta p/p$ , the density, and hence the refractive index, is more sensitive to variations in temperature than variations in pressure. In this particular study the range in temperature was from about  $253^{\circ}\text{K}$  to  $293^{\circ}\text{K}$ , a total variation of 23.7% compared to a range in surface pressure of 915 mb to 955 mb, a total variation of only 4.4%. A summary of a linear regression analysis of these meteorological relationships is given in Table 3.5.1.

It appears the temperature versus refraction graphs exhibit some power law relationship. However, a linear regression of the logarithmic values of temperature and refraction produced little or no improvement in the correlation coefficients. The only relationship that showed any improvement in correlation was the sunset temperature and refraction graph where the slope was found to be -3.1047, the intercept 7.3480 and the correlation coefficient -0.7461 (an improvement of only 0.0159 from the temperature and refraction graph). A visual examination of the logarithmic sunset graph appears to show only a slightly improved linear regression than the sunset temperature and refraction graph.

It is apparent from this analysis that the use of surface meteorological conditions may be only moderately effective for predicting the exact amount of astronomical refraction. A high degree of scatter in the data limits any method of prediction from surface condition data alone. A summary of possible limitations of the method used in this investigation is as follows:

- 1) The uncertainty in the measurement of the vertical temperature gradient leads to uncertainties in its relationship with terrestrial and astronomical refraction. The response time and accuracy of the radiosonde thermometers, plus the uncertainty in the derived height of the balloon leads to an uncertainty in the vertical temperature gradient, especially at such small distances as those occurring during morning inversion conditions.

	Temp. vs. Ref.	Press. vs. Ref.	Dens. vs. Ref.	$dT/dh$ vs. Ref.
<b>SUNRISES</b>				
Slope	-0.0045	0.0023	0.9256	2.6686
y-intercept	0.7010	-1.3970	-0.4203	0.6121
Correl. Coef.	-0.2650	0.0912	0.2709	0.4838
% Prob.	<0.05	~20	<0.05	<0.05
<b>SUNSETS</b>				
Slope	-0.0072	0.0000	1.4848	5.1142
y-intercept	0.6194	0.6031	-1.1603	0.6140
Correl. Coef.	-0.7259	-0.0014	0.6918	0.5493
% Prob.	<0.05	~100	<0.05	<0.05
<b>BOTH</b>				
Slope	-0.0066	0.0011	1.3475	2.8761
y-intercept	0.6691	-0.3462	-0.9471	0.6023
Correl. Coef.	-0.4397	0.0434	0.4264	0.5787
% Prob.	<0.05	~50	<0.05	<0.05

**Table 3.5.1:** Linear regression analysis of refraction data with respect to surface meteorological parameters. The ordinate (y-axis) is the amount of observed refraction. The third row in each section is the correlation coefficient while the fourth row is the percent probability that  $N$  measurements ( $N = 234$  for sunrises and  $N = 115$  for sunsets) of two uncorrelated variables will give a correlation coefficient greater than or equal to the value found (Taylor, 1982, pp. 248-249). Probabilities less than 1% are considered highly significant.

The uncertainty in the measured temperature is no more than about  $\pm 0.8^{\circ}\text{C}$  (personal communications, R. Beaubien, Edmonton Office of Atmospheric Environment Services, 1994). The uncertainty in the height of the radiosonde is estimated to be about  $\pm 10\%$ .

Using the radiosonde data used for each sunrise and sunset event, an error propagation was performed on the equation used to determine the surface vertical temperature gradient:

$$\frac{dT}{dh} = \frac{\Delta T}{\Delta h} \quad (3.5.4)$$

Where  $\Delta T$  is the difference in temperature (in degrees Celsius) between the surface temperature and the temperature at the first significant layer measured by the radiosonde, and  $\Delta h$  is the difference in height (in m) from the surface and the first significant layer.

The results are listed in Table 3.5.2.

Event	Mean Error ( $^{\circ}\text{C/m}$ )	S.D. ( $^{\circ}\text{C/m}$ )	Min. Error ( $^{\circ}\text{C/m}$ )	Max. Error ( $^{\circ}\text{C/m}$ )
Both	0.0076	0.0064	0.0013	0.0504
Sunrise	0.0094	0.0066	0.0013	0.0504
Sunset	0.0038	0.0038	0.0013	0.0219

**Table 3.5.2:** A summary of the error propagation for the surface vertical temperature gradient from radiosonde data.

The results suggest that sunset vertical temperature gradients have about half as much uncertainty as sunrise vertical temperature gradients.

A graph of the error versus the vertical temperature gradient reveals an apparent bimodal structure with a positive slope for values of the vertical temperature gradient greater than  $-0.01^{\circ}\text{C/m}$  and a negative slope for values less than  $-0.01^{\circ}\text{C/m}$  (see Figure 3.5.11 and 3.5.12). The results suggest that the error in the vertical temperature gradient is a function of the vertical temperature gradient. Strong surface inversion conditions (large positive temperature gradients) have correspondingly larger uncertainties. The smallest apparent error occurs around the dry adiabatic temperature gradient ( $-0.01^{\circ}\text{C/m}$ ). Super-adiabatic conditions also show larger uncertainty. A linear regression through the data with vertical temperature gradient greater than  $-0.01^{\circ}\text{C/m}$  produces a slope of 0.137 and the intercept is 0.0042. For values less than  $-0.01^{\circ}\text{C/m}$  the slope is -0.464 and intercept of -0.0018. The results suggests that the uncertainty increases with the presence of strong inversion and super-adiabatic conditions.



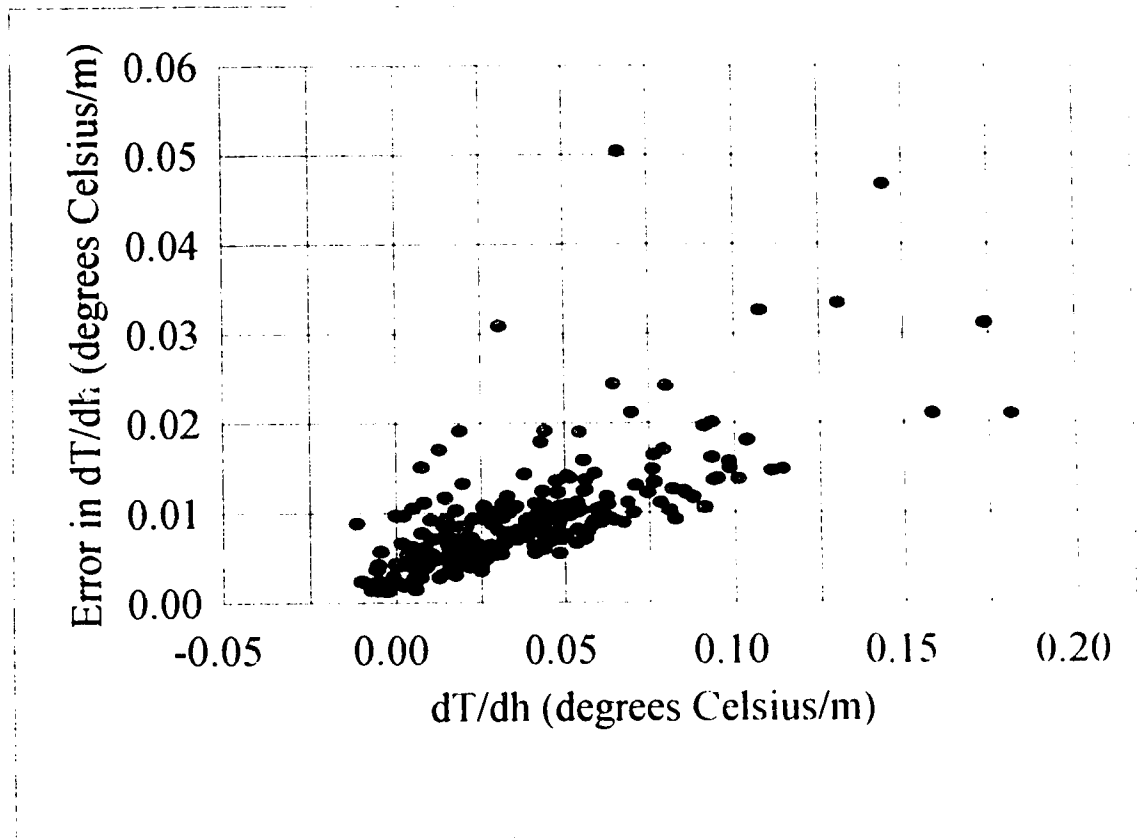


Figure 3.5.11: Uncertainty in the sunrise surface vertical temperature gradient versus the sunrise surface vertical temperature gradient

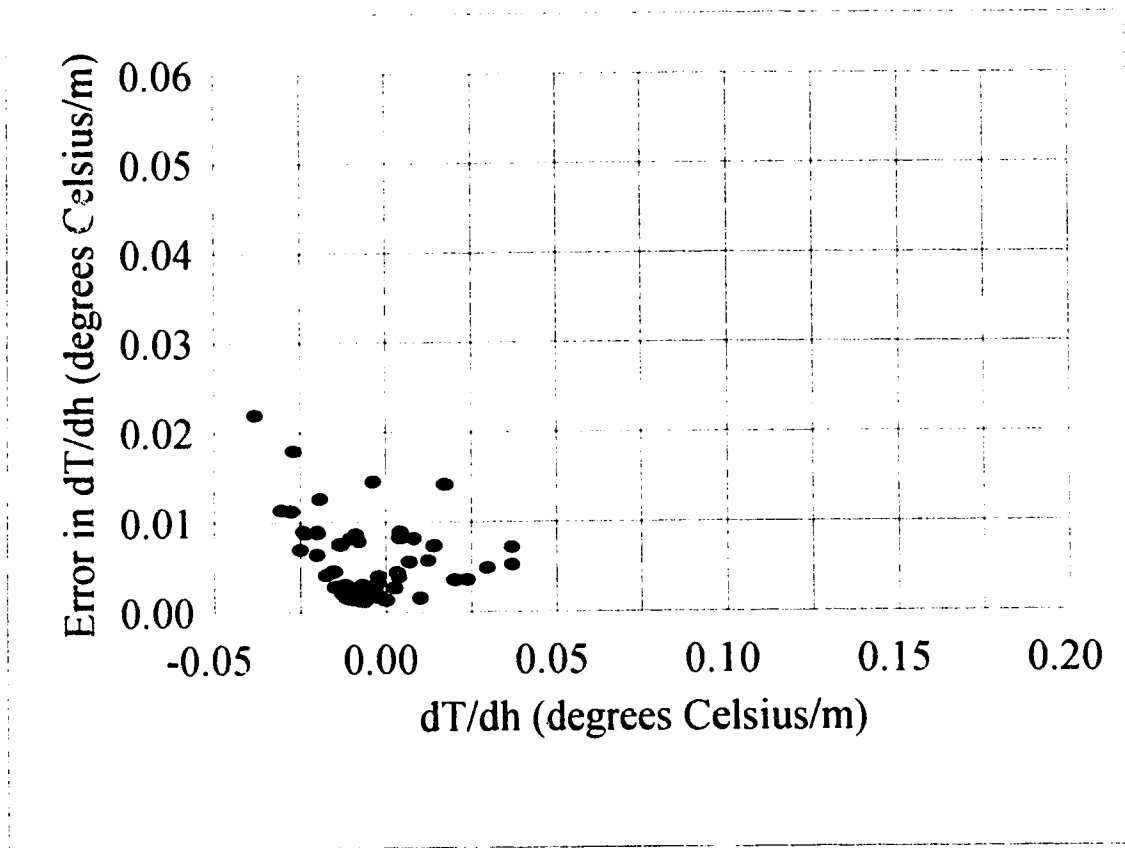


Figure 3.5.12: Uncertainty in the sunset surface vertical temperature gradient versus sunset surface vertical temperature gradient.

The vertical temperature gradients used in this study were checked against temperature gradient derived from minisonde data conducted from a temporary meteorological station located 15 km northeast of Ft. Saskatchewan, about 40 km northeast of observing sites used in this study and about 75 km east northeast of the Stony Plain Upper Air Station (Concord Environmental Corporation, 1993). Minisonde balloons were launched from 1989 to 1992 during various times of the day and year. Four launches were found that coincide with the radiosonde launches used in this study. Instead of recording only significant changes like the radiosondes from the Stony Plain Upper Air Station, the minisondes measured temperatures every 10 seconds during the flight, with an ascent rate of 3.6 m/s for the first minute of the flight. The results appear in Table 3.5.3.

Date	Time (UT) (mini.)	$dT/dh$ (radio.) ( $^{\circ}C/m$ )	$dT/dh$ (radio.) ( $^{\circ}C/m$ )	mini.-radio. ( $^{\circ}C/m$ )	Expected Error (radio.) ( $\pm^{\circ}C/m$ )
01/09/91	14:10	0.0486	0.0440	0.0046	0.0102
01/10/91	14:05	0.0722	0.0880	-0.0158	0.0162
01/11/91	14:20	0.1185	0.1140	0.0045	0.0198
01/14/91	14:20	0.0417	0.0410	0.0007	0.0098

**Table 3.5.3:** Comparison of surface vertical temperature gradients from selected Ft. Saskatchewan minisonde data and corresponding Stony Plain Upper Air Station radiosondes (all radiosondes were launched at 12:00 UT). The fifth column is the difference between the minisonde and radiosonde results. The sixth column is the expected uncertainty using the linear regression results from Figure 3.5.11.

From an examination of the results in Table 3.5.2, the difference between the minisonde and radiosonde data ranges from 2% to 20%. The differences are in reasonable agreement with the results of the linear regression of the uncertainties in Figure 3.5.11 and 3.5.12 and the maximum uncertainties listed in Table 3.5.1.

More accurate measurements using an instrumented tower would be necessary to improve this situation. The times of the radiosonde data were not always the same as the time of sunrise or sunset. The difference of as much as 4 hours could make a larger difference in the vertical temperature profile (Oke, 1992, p. 62). This would be especially important around the solstices when the time difference is at a maximum.

2) Another possible source of error could be the calculated value of the terrestrial refraction. The method outlined in Section 2.5 may not be a reliable and accurate way to determine the altitude of the local horizon. The uncertainties in the vertical temperature gradient as outlined above, and the uncertainties in the exact horizon distance to each sunrise or sunset point would lead to uncertainties in the

calculated terrestrial refraction. It would be more satisfactory to measure the altitude of the horizon using a theodolite at the time of the sunrise or sunset.

The best overall indicator for astronomical refraction  $R_0$  (both sunrise and sunset data combined) appears to be the vertical temperature gradient  $dT/dh$  in the expression:

$$R_0 \pm \Delta R = (0.602 \pm 0.011) + (2.88 \pm 0.27) \frac{dT}{dh} \quad (3.5.5)$$

The uncertainties were determined through a procedure outlined in Appendix B (Taylor, 1982, p. 159).

Sunrise and sunset events appear to show distinct differences in their dependency on surface temperature. The approximate relationship between surface temperature  $T$  (in  $^{\circ}\text{C}$ ) and sunrise refraction can be written:

$$R_{0s} \pm \Delta R = (0.701 \pm 0.015) - (0.0045 \pm 0.0013)T \quad (3.5.6)$$

For surface temperature and sunset refraction  $R_{0s}$ , the relationship is:

$$R_{0s} \pm \Delta R = (0.619 \pm 0.010) - (0.0072 \pm 0.0008)T \quad (3.5.7)$$

To further examine the uncertainty of the astronomical refraction calculated from Equations (3.5.5) to (3.5.7), trial temperatures and surface vertical temperature gradients were placed in the equations with their corresponding estimated uncertainties. Using the error propagation method outlined in Appendix B (Taylor, 1982, pp 45-73) a sample surface temperature of  $15.0^{\circ} \pm 0.1^{\circ}\text{C}$  and a surface vertical temperature gradient of  $-0.010 \pm 0.001^{\circ}\text{C/m}$ , representing the low end of the calculated uncertainty, and  $0.20 \pm 0.05^{\circ}\text{C/m}$  at the higher end produces uncertainties in the resulting astronomical refraction outlined in Table 3.5.4.

Equation	$dT/dh$ ( $^{\circ}\text{C/m}$ )	$T$ ( $^{\circ}\text{C}$ )	$R$ ( $^{\circ}$ )	$\Delta R$ ( $^{\circ}$ )	$\Delta R$ (%)
3.5.5	$-0.010 \pm 0.001$		0.573	$\pm 0.011$	2.0
3.5.5	$0.200 \pm 0.05$		1.178	$\pm 0.154$	13.1
3.5.6		$15 \pm 0.1$	0.634	$\pm 0.025$	4.3
3.5.7		$15 \pm 0.1$	0.511	$\pm 0.016$	3.4

**Table 3.5.4:** Comparison of propagated uncertainties for Equations (3.5.5) through (3.5.7) using test temperatures of  $15.0^{\circ} \pm 0.1^{\circ}\text{C}$  and a vertical temperature gradient of  $-0.010 \pm 0.001^{\circ}\text{C/m}$  and  $0.20 \pm 0.05^{\circ}\text{C/m}$ . Column 4 is the calculated astronomical refraction, column 5 is the uncertainty in degrees and column 6 is the uncertainty in percentage of the calculated refraction.

From this analysis it appears that, Equation (3.5.5) appears to predict the astronomical refraction better than Equations (3.5.6) and (3.5.7) during conditions of lower uncertainty in the surface vertical temperature gradient (i.e. during sunset in dry adiabatic conditions) but performs more poorly under strong surface inversions (i.e. sunrises and cold winter sunsets).

The seasonal variability in the surface vertical temperature gradient and temperature should also be correlated with the seasonal variability of the refraction. As seen in Figures 3.5.13 and 3.5.14, the maximum range in surface temperature at sunrise and sunset appears to occur in the colder months. A more obvious contrast occurs between the seasonal sunrise and sunset vertical temperature gradient (see Figures 3.5.15 and 3.5.16). The range in the sunset vertical temperature gradient appears to be less than the range in sunrise surface vertical temperature gradients. The sunset vertical temperature gradient also exhibits less variation during the warmer portion of the year than during the colder months. The sunrise vertical temperature gradient, on the other hand, shows a high degree of variability throughout the year.

In order to discover a possible relationship between the seasonal variability in meteorological conditions and the seasonal variability in refraction, a linear regression was performed on the monthly values of the standard deviations of the meteorological values versus the monthly standard deviations of the observed refraction. The plots of the data appear in Figures 3.5.17 and 3.5.18 while the results of the linear regression analysis appear in Table 3.5.5.

Standard Deviations	slope	y-int.	Correl. Coef.	Prob. (%)
Refraction vs. T	0.0039	0.0744	0.12	~50
Refraction vs. $dT/dh$	3.75	0.0210	0.63	~0.2

**Table 3.5.5:** Linear regression analysis of the monthly standard deviations of the observed refraction of sunrises and sunsets versus the corresponding monthly standard deviations of surface temperature and surface vertical temperature gradient. The third column is the slope of the best-fit line. The fourth column is the intercept (the ordinate is the monthly standard deviation of refraction). The fifth column is the correlation coefficient while the sixth column is the percent probability that,  $N = 23$ , measurements of two uncorrelated variables will give a correlation coefficient greater than or equal to the value found (Taylor, 1982, pp. 248-249). Probabilities less than 1% are considered highly significant.

The results suggest that the seasonal variability in the vertical temperature gradient is the best indicator of the seasonal variability of sunrise and sunset refraction. This appears to explain why the sunrise refraction has a larger variability

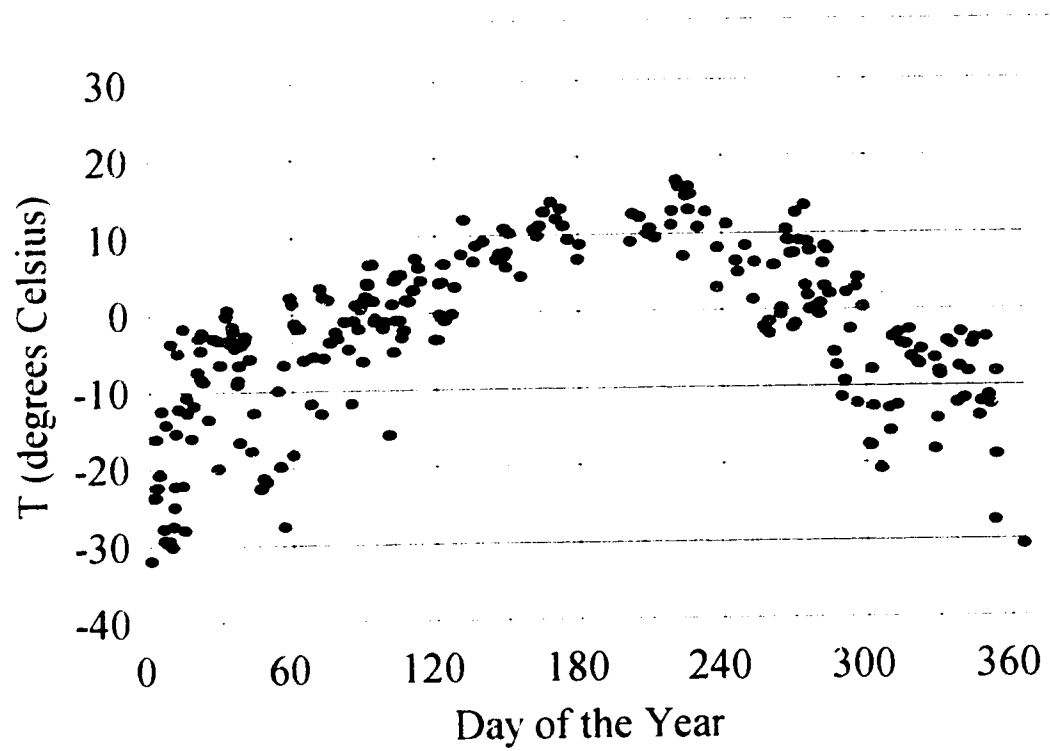


Figure 3.5.13: Sunrise surface temperature versus time of year.

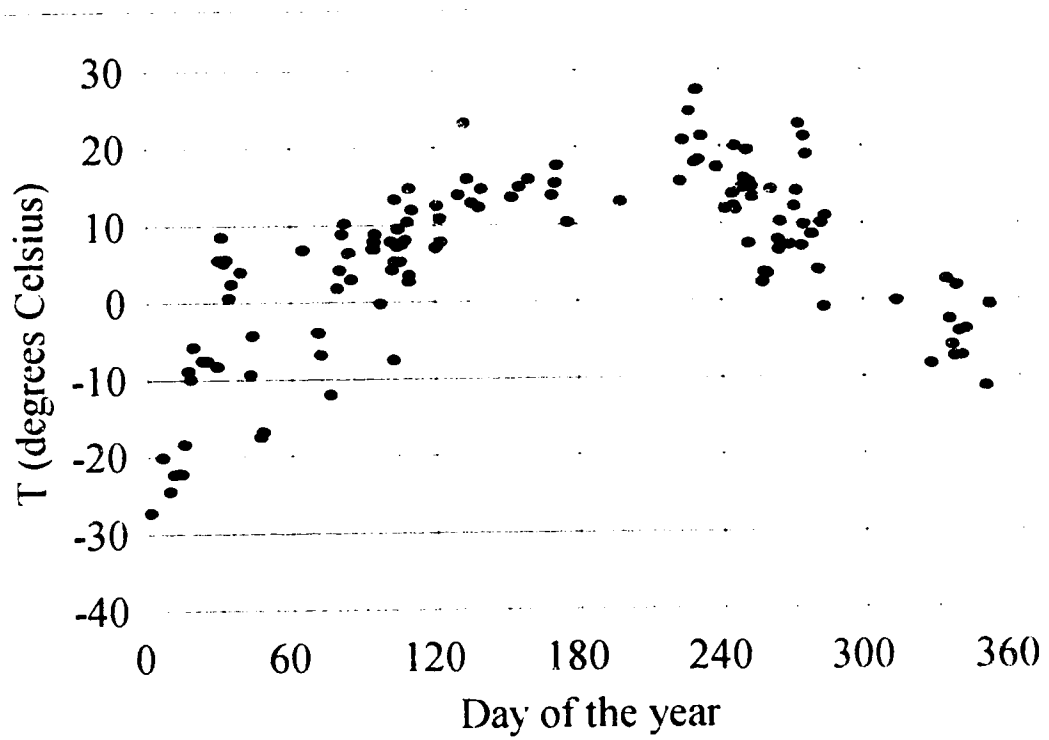


Figure 3.5.14: Sunset surface temperature versus time of year.

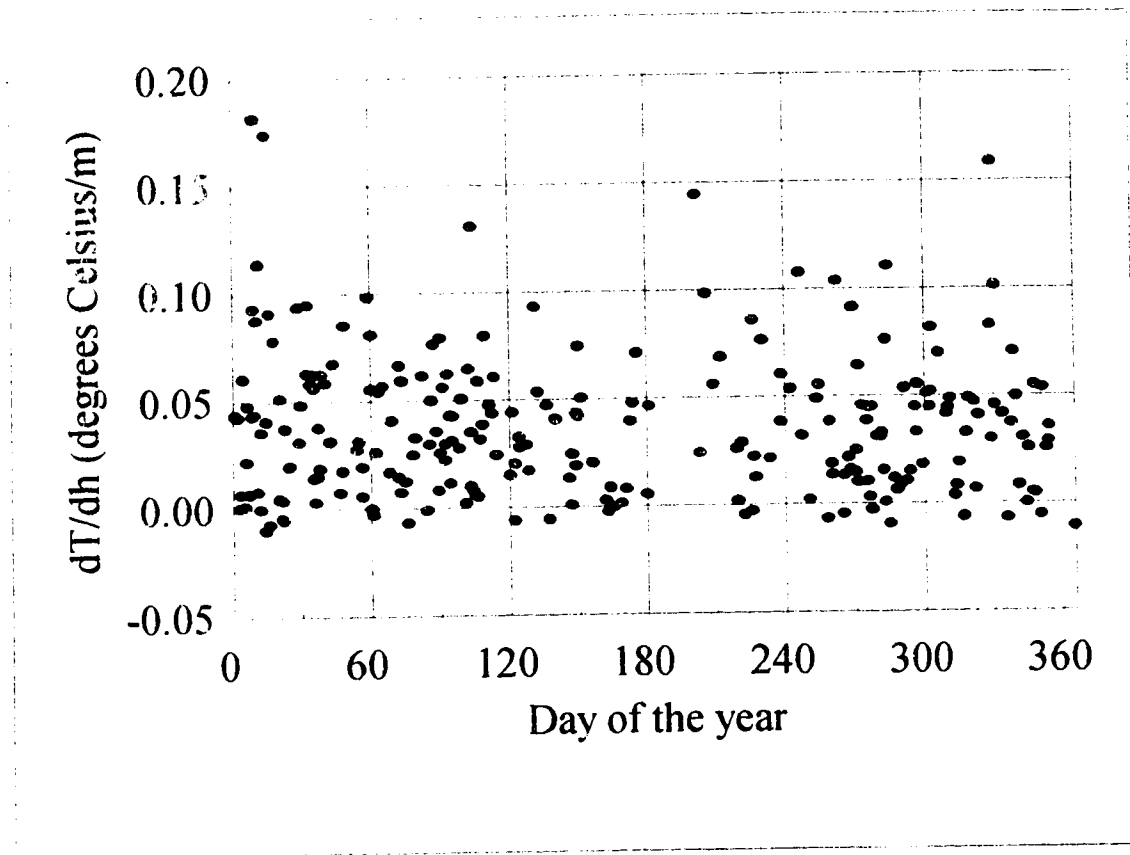


Figure 3.5.15: Sunrise surface vertical temperature gradient versus time of year.



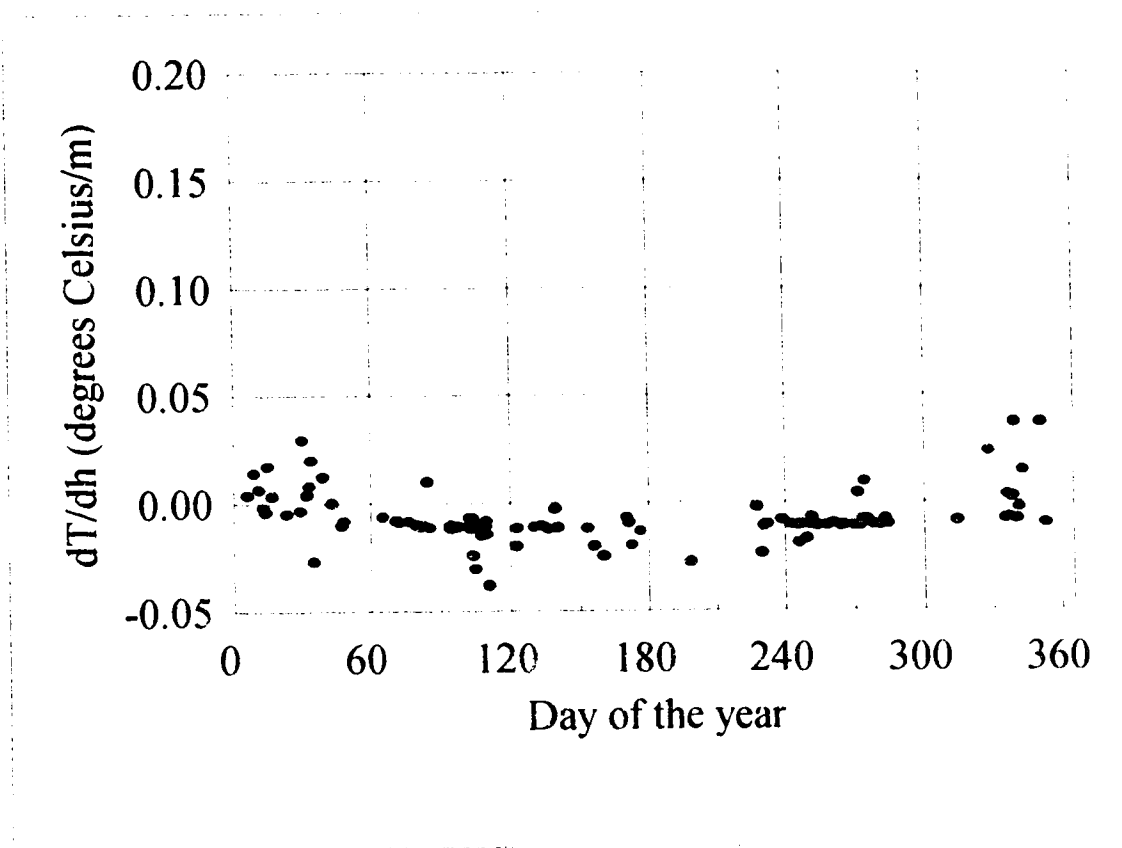


Figure 3.5.16: Sunset surface vertical temperature gradient versus time of year.

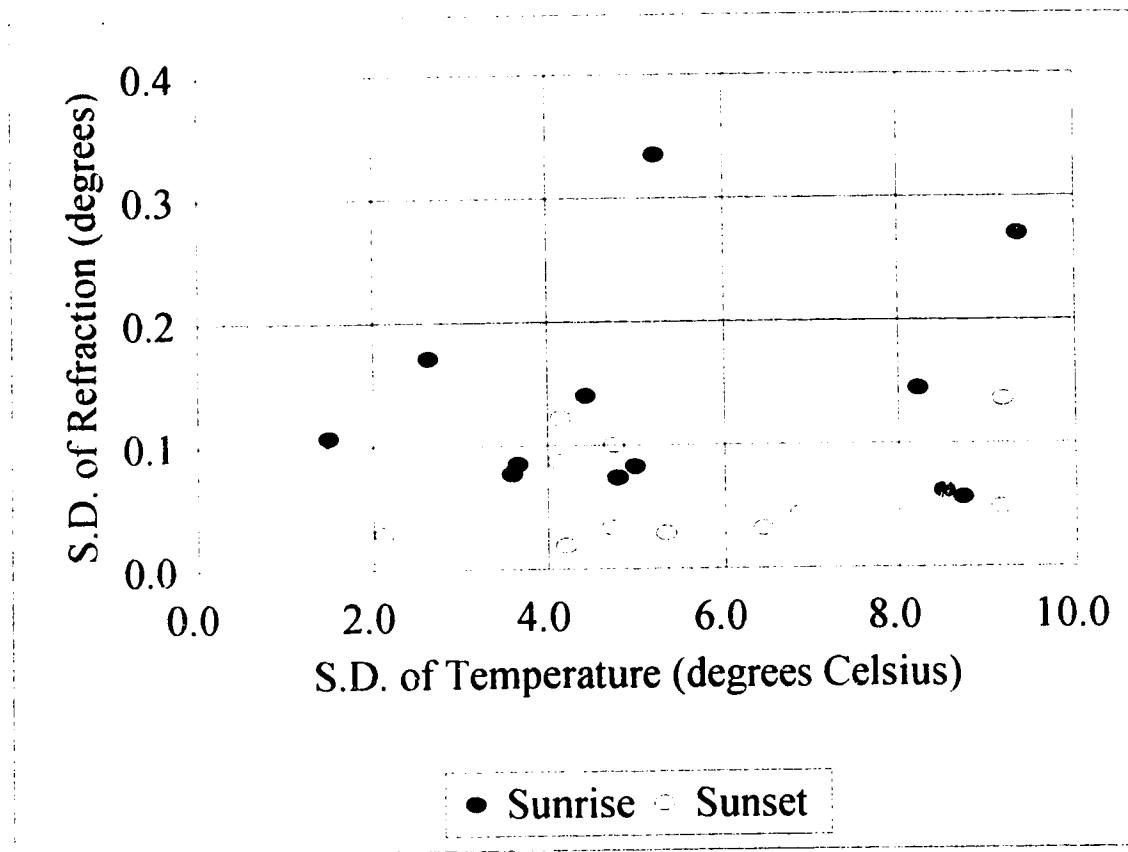


Figure 3.5.17: Monthly standard deviation of surface temperature versus monthly standard deviation of sunrise and sunset astronomical refraction.

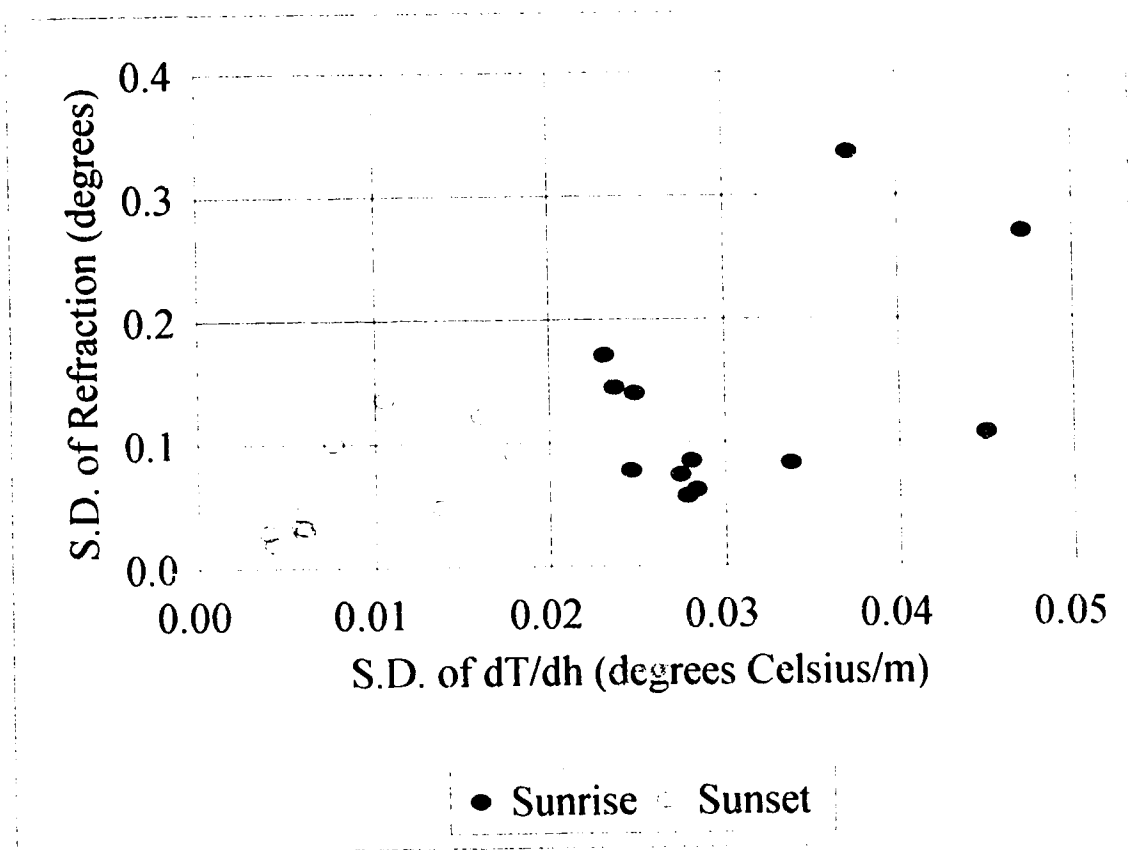


Figure 3.5.18: Monthly standard deviation of surface vertical temperature gradient versus monthly standard deviation of sunrise and sunset astronomical refraction.

than sunset refraction and why summer sunset refraction has less variability than winter sunset refraction. From this result an equation can be written for the standard deviation of astronomical refraction  $SD(R)$ :

$$SD(R) = (0.022 \pm 0.024) + (3.7 \pm 1.0)SD\left(\frac{dT}{dh}\right) \quad (3.5.8)$$

where  $SD(dT/dh)$  is the standard deviation of the monthly surface vertical temperature gradient. The uncertainties were determined using the method outlined by Taylor (1982, pp. 157-159). For a detailed explanation of this method see Appendix A.

The apparent correlation between the standard deviation of the surface vertical temperature gradient with the standard deviation of the astronomical refraction (see Figure 3.5.18) may be due, in part, to the increased uncertainty in the surface vertical temperature gradient as outlined in Table 3.5.2 and Figure 3.5.11. These results suggest that the larger the vertical temperature gradient the larger the corresponding uncertainty. Since the events with the largest range in astronomical refraction occur during sunrise, which typically has correspondingly large surface vertical temperature gradients (see Figure 3.5.8), then the uncertainty due to measurement error of the surface vertical temperature gradient will also be correspondingly large. On the other hand, sunset events typically take place in relatively small vertical temperature gradients and therefore, have correspondingly smaller measurement error. Therefore, the apparently strong correlation exhibited in Figure 3.5.18 may be due, in part, to the relationship between the surface vertical temperature gradient and the corresponding uncertainty in its measurement. Confirmation of these findings will, therefore, require more accurate measurement of the surface vertical temperature gradient.

Taking the linear regression of two standard deviations may appear somewhat needless, yet the poor fit between the standard deviation of the monthly mean surface temperature and the standard deviation of the monthly mean astronomical refraction appears to strengthen the apparent relationship between astronomical refraction and the surface vertical temperature gradient.

### 3.6 Anomalous Astronomical Refractive Events: The Novaya Zemlya Effect.

On rare occasions the Sun appears to rise much earlier than predicted or set much later. In this study, the sunrise of January 10, 1991 was almost 12 minutes earlier than the predictions made from the Tables of Sunrise, Sunset and Twilight (1962).

The first recorded observation of such an extraordinarily early sunrise was made by the third polar expedition of Captain Willem Barents in 1597. The crew was spending the winter on the Island of Novaya Zemlya in the Russian western arctic at a latitude of  $76^{\circ} 12' N$ . On January 24, during the long arctic night, Gerrit de Veer, one of the expedition members, sighted the Sun two weeks earlier than predicted. The geometric altitude of the centre of the Sun at the time of the observation was -

4.9°. This phenomenon has now been called the Novaya Zemlya effect (Lehn, 1979).

In this study, anomalously large astronomical refraction shall be defined as any event having an astronomical refraction more than two standard deviations greater than the line defined by the linear regression of the vertical temperature gradient and the astronomical refraction. This relationship was chosen because of its large correlation coefficient.

The meteorological and refractive data regarding these anomalous sunrise and sunset events appear in Table 3.6.1.

Date	Time (UT)	Temp. (°C)	Press. (mb)	dT/dh (°C/m)	Hor. Alt. (°)	R (°)	R(cor) (°)
<b>Sunrises:</b>							
01/06/91	15:44:56	-29.3	945.0	0.0481	0.203	1.218	1.275
01/09/91	15:45:01	-30.1	934.7	0.0440	0.203	1.022	1.076
01/10/91	15:35:54	-24.9	934.0	0.0880	0.203	2.032	2.114
04/01/91	13:04:30	2.2	926.3	0.0563	0.089	1.167	1.210
05/29/91	11:08:32	10.8	926.3	0.0437	-0.232	1.033	1.062
12/17/91	15:42:10	-11.3	935.6	0.0536	0.205	1.142	1.194
06/22/92	10:57:50	11.1	937.5	0.0482	-0.246	1.060	1.079
11/25/93	15:10:50	-14.3	944.4	0.1586	0.209	1.716	1.837
11/26/93	15:12:00	-8.1	935.6	0.0456	0.209	1.698	1.745
<b>Sunsets:</b>							
01/14/93	23:49:23	-18.4	927.2	0.0175	-0.096	1.104	1.120
04/14/93	02:31:09	7.2	931.5	-0.0107	0.025	0.887	0.889

**Table 3.6.1:** Meteorological condition for anomalous refractive events.

The majority of the events take place in the colder parts of the year. Nine of the eleven events (82%) took place between November 1 and April 30, with January having four events. The average surface temperature for all the events was -7.9°C. All events, except one, occurred during surface temperature inversion conditions. This would suggest that the anomalous refraction tends to be confined to surface inversion conditions. As mentioned earlier, surface inversions tend to occur during times of surface radiative cooling, typically during the night and into the early morning. From Figures 3.5.14 and 3.5.15 it is apparent that inversion conditions in Edmonton frequently occur at sunrises during the entire year, and during the colder months at sunsets.

Even though most of the events take place in the colder part of the year, the data suggest that the Novaya Zemlya effect may not be an exclusively cold weather or arctic phenomenon. Four of the events occurred with surface temperatures greater than 0°C. One event took place two days after the summer solstice. Therefore, it is

possible that the Novaya Zemlya effect could be observed in warmer climates or in the warmer parts of the year.

### 3.7 Horizontal Astronomical Refraction

It has been assumed that the horizontal component of astronomical refraction is relatively small or even negligible (Bomford, 1980, p. 242). This follows from the fact that the atmospheric density gradient is essentially vertical and therefore that the atmospheric density is very close to being horizontally homogeneous.

If horizontal astronomical refraction exists, it should manifest itself as a shift in the measured azimuth of the rising or setting Sun  $A$  as compared to the calculated azimuth of the geometric Sun  $A_0$  at the time of sunrise or sunset. To test this assumption, a sample of sunrise azimuth measurements was taken around the winter solstice, when astronomical refraction is at a maximum. These were then compared with the calculated azimuth of the geometric Sun, at the time of sunrise, found from the equation (Green, 1985, p. 28)

$$\cos A_0 = \frac{\sin \delta - \sin a_0 \sin \phi}{\cos a_0 \cos \phi} \quad (3.7.1)$$

where  $\phi$  is the geographic latitude of the observer,  $\delta$  is the declination of the centre of the solar disc at the time of sunrise (calculated previously), and  $a_0$  is the altitude of the centre of the geometric Sun at the moment of sunrise found through Equation (2.1.3). The results of this investigation appear in Table 3.7.1.

It is apparent from an examination of the results, that the horizontal deviation is typically more than the estimated uncertainty of the observed azimuth and therefore can be considered within the sensitivity of the experiment. Nine (33%) of the observations are less than or equal to the estimated uncertainty of the observed azimuth ( $\pm 0.13^\circ$ ). Out of the 27 observations, 7 were considered to be of the highest possible accuracy using the method described. These sunrises took place directly behind prominent horizon landmarks or between two closely spaced landmarks, and therefore, could be more accurately located with respect to these horizon reference landmarks. Of these, six showed a deviation of  $0.13^\circ$  or more. There is also a systematic behavior in the direction of the deviation. None of the observed azimuths was to the north of the calculated azimuths.

The average horizontal deviation in azimuth is  $+0.19^\circ$  with a standard deviation of  $0.07^\circ$ . The systematic variation in observed azimuth may be caused by a systematic error in the observed or calculated azimuths. It appears unlikely that the error would originate from the reference azimuth (see Section 2.6) since the values found through Cunningham's and Peterson's method agree to within  $0.04^\circ$ . A bias in the observed azimuth may originate from the relatively imprecise method of recording the relative position of sunrise with respect to horizon reference markers. The results suggest that this uncertainty may not explain all of the observed deviations since six of the seven most accurate values show deviations larger than  $0.13^\circ$ .

Date (m/d/y)	$A$ ( $^{\circ} \pm 0.13$ )	$A_0$ ( $^{\circ} \pm 0.01$ )	$A - A_0$ ( $^{\circ}$ )
12/10/91*	129.96	129.74	0.22
12/11/91	130.27	130.02	0.25
12/13/91	130.37	130.15	0.22
12/14/91	130.46	130.34	0.12
12/16/91	130.84	130.67	0.17
12/17/91*	129.96	129.67	0.29
12/20/91	130.59	130.46	0.13
01/05/92	129.18	129.13	0.05
01/07/92*	128.70	128.61	0.09
01/09/92	128.23	128.08	0.15
01/14/92	126.77	126.54	0.23
01/16/92*	126.26	126.00	0.26
12/03/92	128.41	128.23	0.18
12/04/92	128.47	128.35	0.12
12/05/92	128.94	128.78	0.16
12/06/92	129.18	129.06	0.12
12/18/92	130.84	130.48	0.36
12/19/92	130.84	130.59	0.25
12/30/92	130.21	129.99	0.22
12/31/92*	129.80	129.66	0.22
01/02/93*	129.80	129.59	0.21
01/05/93	128.99	128.83	0.16
01/09/93	127.76	127.48	0.28
01/10/93	127.41	127.30	0.11
01/14/93*	126.10	125.80	0.30
12/08/93	129.46	129.33	0.13
12/17/93	130.59	130.46	0.13

**Table 3.7.1:** Azimuth measurements for a sample of sunrises around the winter solstice. The second column is the observed azimuth of the sunrise. The uncertainty was derived by visually estimating the largest error in placing a point between the two landmarks with the largest angular separation ( $1.27^{\circ}$ ). This was done through a pair of 7x20 binoculars, the same instrument used to obtain the original observations. Column three is the calculated azimuth of the geometric Sun. The last column is the difference between the observed and the calculated azimuth. Dates marked with an asterisk are those estimates of the observed relative azimuth of the sunrise with the highest degree of confidence (i.e. about  $\pm 0.05^{\circ}$ ). These appeared directly behind or between two closely spaced horizon landmarks.

Nevertheless, this systematic difference between the observed and the calculated solar azimuths could also be the result of horizontal astronomical refraction, caused by the a horizontal temperature gradient which, in turn, produces a horizontal density gradient. Around winter solstice, the Sun rises in the southeast and therefore the path of the sunlight has both a meridional and zonal component through the atmosphere. According to Snell's Law, the angle of refraction  $\theta_r$  should be less than the angle of incidence  $\theta_i$  as a ray passes from a medium of lesser density into a medium of greater density (see Figure 3.7.1). Typically, the atmospheric temperature decreases with increased latitude and consequently, the density increases. This should produce a southerly shift in the observed azimuthal position of the winter solstice rising Sun.

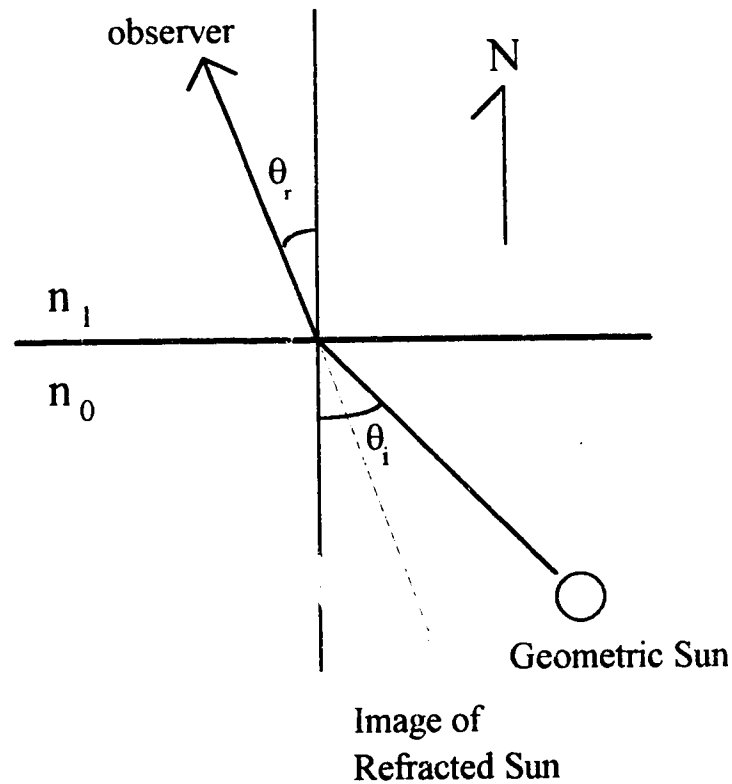


**Figure 3.7.1:** Plan view showing the sense of horizontal refraction due to a meridional temperature gradient. The density and therefore the index of refraction increases from south to north, ( $n_0$  is less than  $n_1$ ). The dashed line is the apparent position of the solar image while the lower solid line indicates the geometric position.



Bomford (1980, p. 242) gives an expression to estimate the amount of horizontal refraction  $R_h$  in arc seconds per m over horizontal distances typically used by surveyors.

$$R_h = 16.3 \frac{p}{T^2} \frac{dT}{dx} \quad (3.7.2)$$

where  $p$  is in millibars,  $T$  is in  $^{\circ}\text{K}$ , and  $dT/dx$  is in  $^{\circ}\text{C/m}$  and is measured horizontally at right angles to the line of sight.

Under certain rare conditions the sunlight during sunrise or sunset can have nearly constant elevation trajectories of 100 to 400 km (Lehn, 1979). If one assumes that the trajectory of the sunlight has a constant altitude just above the surface for 100 km and that the pressure, temperature and horizontal temperature gradient are 940 mb,  $241^{\circ}\text{K}$  and  $0.00005^{\circ}\text{C/m}$  (typical extreme values for the period around winter solstice), then the horizontal refraction is  $1.32 \times 10^{-5} \text{ "/m}$  or  $1.32''$  ( $0.0004^{\circ}$ ) over 100 km. This is almost three orders of magnitude lower than the largest observed discrepancy cited in Table 3.7.1.

It seems reasonable to assume that if horizontal refraction exists it should occur more often during times of maximum astronomical refraction. The path length through the atmosphere is longer with increased astronomical refraction so, therefore, the sunlight would have more opportunity to experience horizontal refraction. A plot of these two values appears in Figure 3.7.2. From a linear regression analysis the resulting correlation coefficient is 0.33 with a probability of 11% that 27 random data points would achieve the same correlation coefficient or greater. An inspection of the plot appears to suggest a relationship, but the scatter in the data prevents any strong conclusions from being drawn.

As well, a histogram of the azimuthal deviation (Figure 3.7.3) shows that the largest single concentration of data occurs in the  $0.10^{\circ}$  to  $0.15^{\circ}$  bin (bin sizes are  $0.05^{\circ}$  starting at  $0.05^{\circ}$ ).

If the experiment is too insensitive to measure horizontal refraction and the overall positive tendency of the deviation originates from a systematic and consistent error, then the distribution of the data around the mean deviation should resemble a Gaussian distribution with a standard deviation of about  $0.13^{\circ}$ . Using the following Gaussian function to determine the expected distribution of the deviation (Taylor, 1982, pp. 99-113):

$$f = e^{-(\Delta A - \overline{\Delta A})^2 / 2\sigma^2} \quad (3.7.3)$$

where,  $f$ , is the expected fraction of observations occurring at a particular value of the azimuthal deviation  $\Delta A$  while  $\overline{\Delta A}$  is the mean deviation ( $0.19^{\circ}$ ), and  $\sigma$  is the uncertainty of the observations ( $\pm 0.13^{\circ}$ ). The resulting graph (Figure 3.7.3) shows the expected distribution and the observed distribution.

In addition, a  $\chi^2$  test of the results in Figure 3.7.3 (with seven degrees of freedom) produces a result of 1.1% (Taylor, 1982, pp.218-233). This indicates that

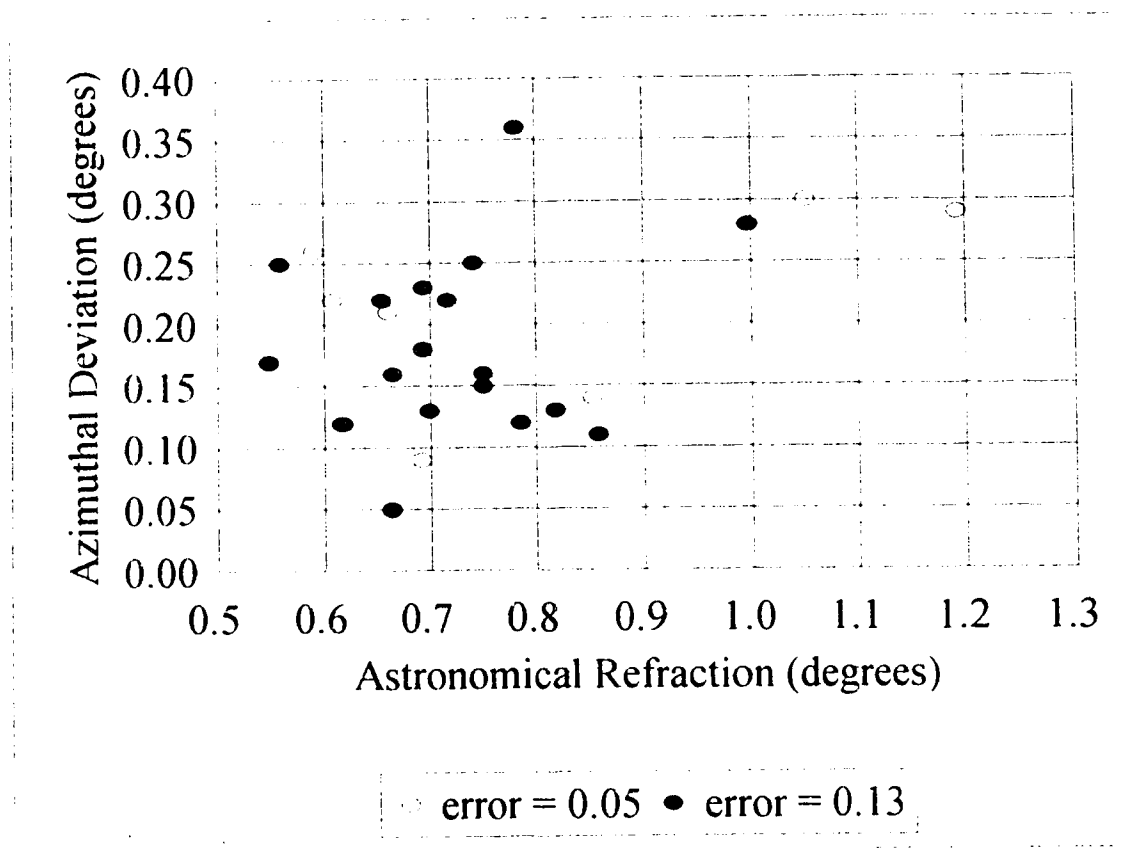


Figure 3.7.2: Azimuthal deviation versus astronomical refraction. Open circles are observations with the greatest accuracy (about  $+0.05^\circ$ ). These sunrises were observed directly behind or between two closely spaced horizon landmarks.

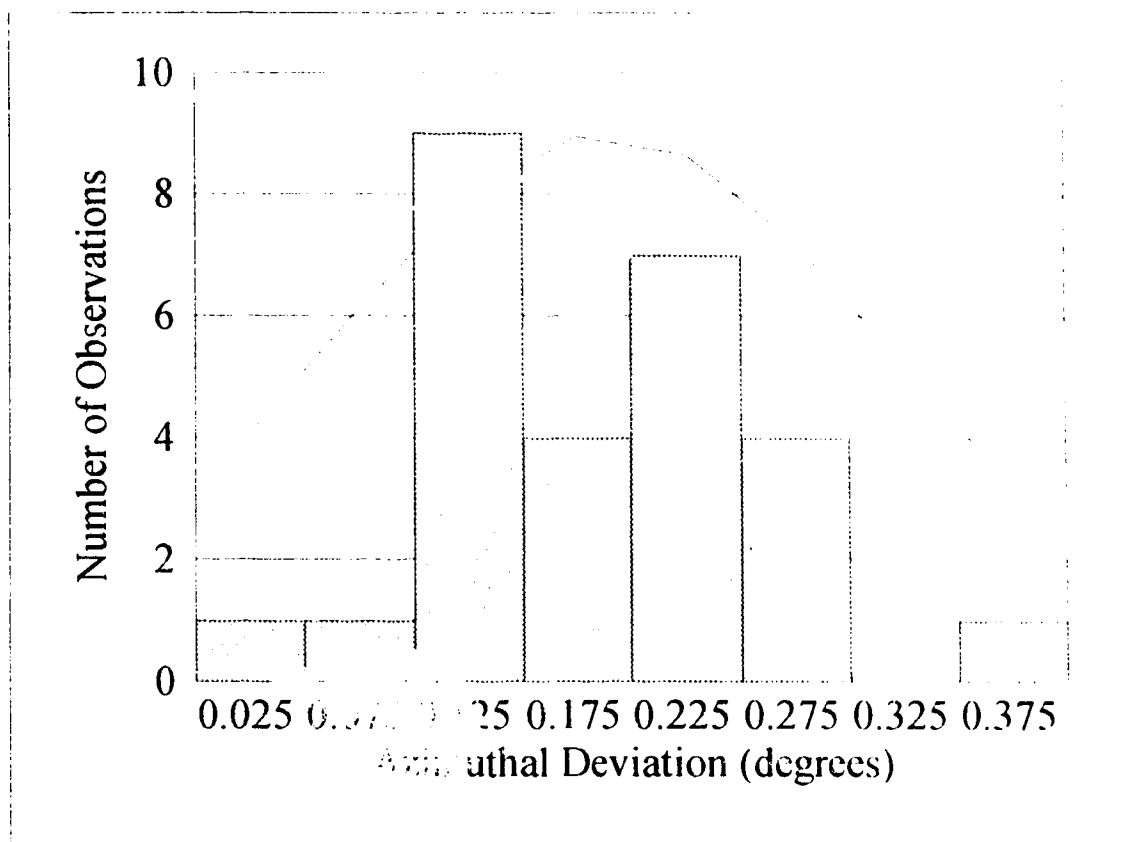


Figure 3.7.3: Histogram showing the distribution of deviations in sunrise azimuth. Bin dimensions are  $0.05^\circ$  wide, starting at  $0.05^\circ$ . The curve represents the expected Gaussian distribution with an uncertainty,  $\sigma$ , of  $+0.13^\circ$  and a mean deviation,  $\Delta A$ , of  $0.19^\circ$ .

there is a 1.1% chance that the expected distribution matches the observed distribution. Therefore, it appears reasonable, that the observed distribution may not be solely the result of random measurement error. On the other hand, if the uncertainty  $\sigma$  is improved to  $\pm 0.10^\circ$  (not unreasonable, since  $\pm 0.13^\circ$  is an upper limit to the uncertainty) the same test produces a probability of 13%, which, according to Taylor, indicates that the expected and observed distributions are a reasonable match. This further suggests that the test may be too sensitive to the initial values to provide conclusive evidence of horizontal refraction. The relatively small sample also prevents any conclusive results being drawn from such an analysis.

Yet, since all the observations show a shift to the south of the geometric azimuth, consistent with a meridional density gradient, it appears possible that these observations provide evidence for significant horizontal refraction. The relatively large deviations shown by six of the seven measurements with the highest accuracy, are perhaps the strongest evidence for the possible existence of significant horizontal refraction. Although the evidence is tantalizing, it is certainly not conclusive. It appears possible that an unknown source of systematic error may be responsible for the observed deviations. Further observations and analysis with a higher degree of accuracy and sophistication will be necessary to clarify this apparent dilemma.

### 3.8 Comparison of the Present Results with Other Predictive Formulae.

Based on the results outlined in Section 3.5 this study suggests that a linear function of surface temperature or surface vertical temperature gradient can be used to predict the astronomical refraction during sunrise and sunset on a zero horizon. For solar altitudes less than  $15^\circ$  the Astronomical Almanac (1992, p. B62) uses the following approximation for astronomical refraction:

$$R_A = \frac{p(0.1594 + 0.0196a + 0.00002a^2)}{(273 + T)(1 + 0.505a + 0.0845a^2)} \quad (3.8.1)$$

where  $p$  is the surface pressure in millibars,  $T$  is the surface temperature in degrees Celsius, and  $a$  is the altitude of the astronomical object above or below a zero horizon (in this case, the altitude of the upper limb of the geometric Sun).

In order to examine the predictive ability of Equation (3.8.1) the surface temperature, surface pressure and the altitude of the upper limb of the Sun during the sunrise and sunset events used in this study, were placed into the equation and then subtracted from the astronomical refraction found in the present study. The average difference between the observed values and calculated values is  $-0.030^\circ$  with a standard deviation of  $0.116^\circ$ . There appears to be a substantial difference between sunrises and sunsets. The average difference between the observed and calculated sunrise values is  $0.009^\circ \pm 0.117^\circ$ , while it is  $-0.110^\circ \pm 0.056^\circ$  for sunsets.

The difference between sunrise and sunset deviations may be the result of the intended use and possible source of the data for Equation (3.8.1). As outlined in Section 3.5, the most apparent difference between sunrise and sunset meteorological

conditions is the vertical temperature gradient. Equation (3.8.1) appears to produce the most accurate results during sunrise (the average sunrise deviation is very close to zero). Therefore, Equation (3.8.1) appears to be formulated assuming a positive vertical temperature gradient, which generally occur at night when most astronomical work is performed. To produce a more universal empirical formula Equation (3.8.1) should include a term involving the surface vertical temperature gradient.

In Section 3.5 the results suggested that astronomical refraction was closely correlated with the surface temperature and surface vertical temperature gradient. It appears reasonable that the deviation, outlined above, should also have a similar correlation. A plot of the deviation for the sunrise astronomical refraction versus surface temperature and pressure appears in Figure 3.8.1 and 3.8.2. For sunsets, the corresponding graphs are Figures 3.8.3 and 3.8.4. A plot of sunrise and sunset deviation versus the surface vertical temperature gradient appears in Figure 3.8.5 and 3.8.6.

An examination of Figures 3.8.1 to 3.8.4 suggests there is little or no dependence on pressure and only a modest dependence on temperature. A linear regression was performed on the above data. The results appear in Tables 3.8.1 to 3.8.3.

Therefore the results suggest that Equation (3.8.1) may require additional corrections with respect to surface temperature and the surface vertical temperature gradient. Specifically, from Table 3.8.1 and 3.8.3 the following correction can be applied to both sunrises and sunsets on a zero horizon:

$$R'_s = R_s - (0.0040 \pm 0.0005)(T + 273) - (1.07 \pm 0.13) + (2.21 \pm 0.13) \frac{dT}{dh} - (0.0811 \pm 0.0055) \quad (3.8.2)$$

where  $T$  is in degrees Celsius, and  $dT/dh$  is in  $^{\circ}\text{C}/\text{m}$ . The uncertainties in the slopes and intercepts were determined using a method outlined in Appendix B and taken from Taylor (1982, pp. 157-159).

Applying Equation (3.8.2) to the data in Table 3.1.1 and 3.1.2. produces an average deviation from the observed values of  $0.030^{\circ} \pm 0.085^{\circ}$ , a decrease of 27% in the standard deviation. With only the correction for surface vertical temperature gradient applied (the last two terms in Equation (3.8.2)), the resulting average deviation was  $0.000^{\circ} \pm 0.086^{\circ}$ . Therefore, the inclusion of the temperature correction term improves the standard deviation but only changes the sign of the average deviation. However, the use of the surface vertical temperature gradient correction alone, reduces the average deviation to negligible amounts and produces nearly the same decrease in the standard deviation. This may be due to the differences in uncertainty in the two linear regressions. The percentage uncertainty in the slope and intercept for the surface temperature correction (about 12.4%) is almost twice the uncertainty in the slope and intercept for the surface vertical temperature gradient (about 6.4%). Since the slope for both sunrises and sunsets in

Table 3.8.3 is actually larger than the slope for either sunrise or sunsets, it appears that the two data sets may have to be considered separately.

These results suggest that astronomical measurements taken near the horizon requiring the highest possible positional accuracy should include the surface vertical temperature gradient in their corrections for astronomical refraction.

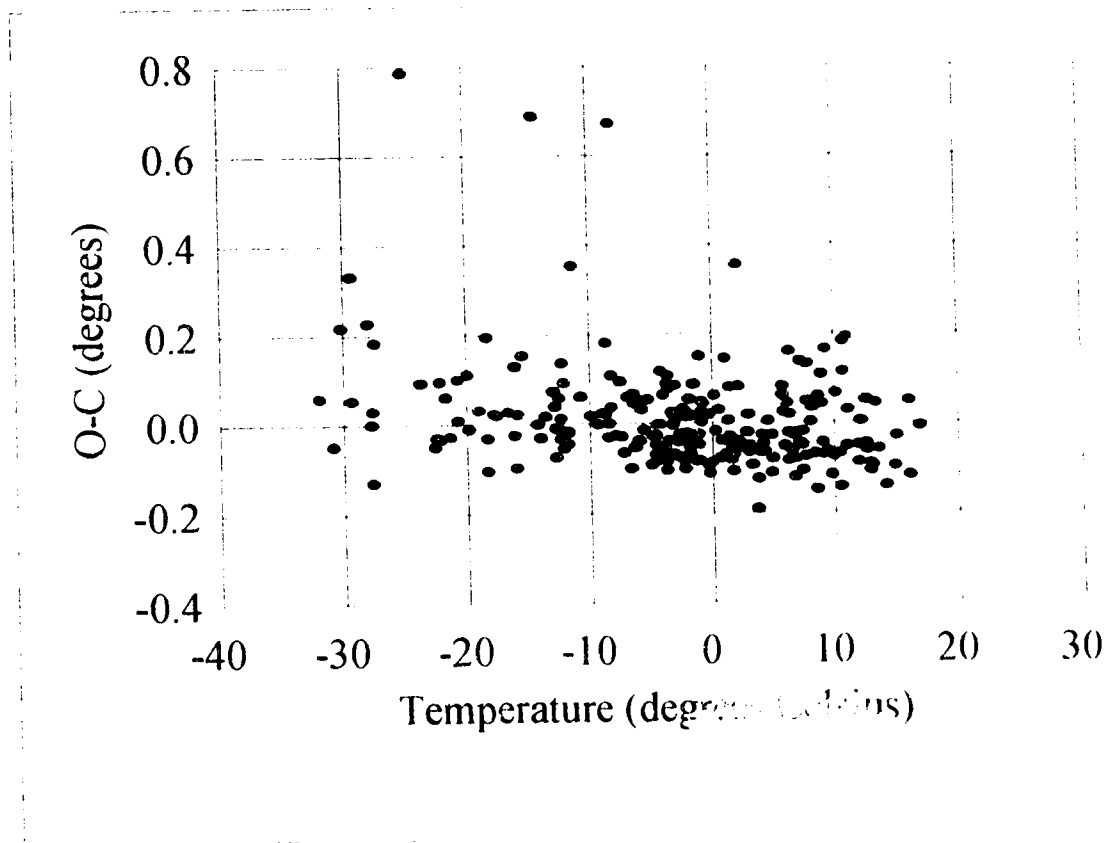


Figure 3.8.1: Observed minus calculated sunrise astronomical refraction (calculated from Equation 3.8.1) versus surface temperature

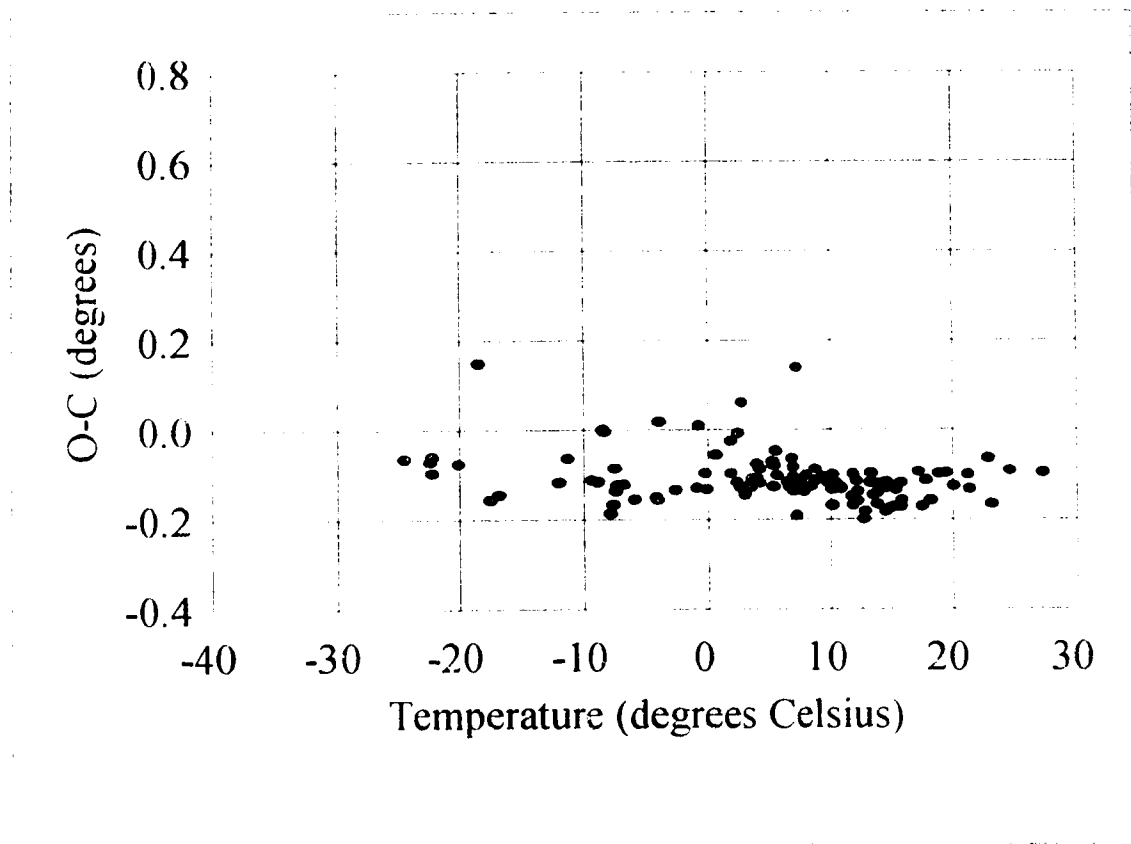


Figure 3.8.2: Observed minus calculated sunset astronomical refraction (calculated from Equation 3.8.1) versus surface temperature.



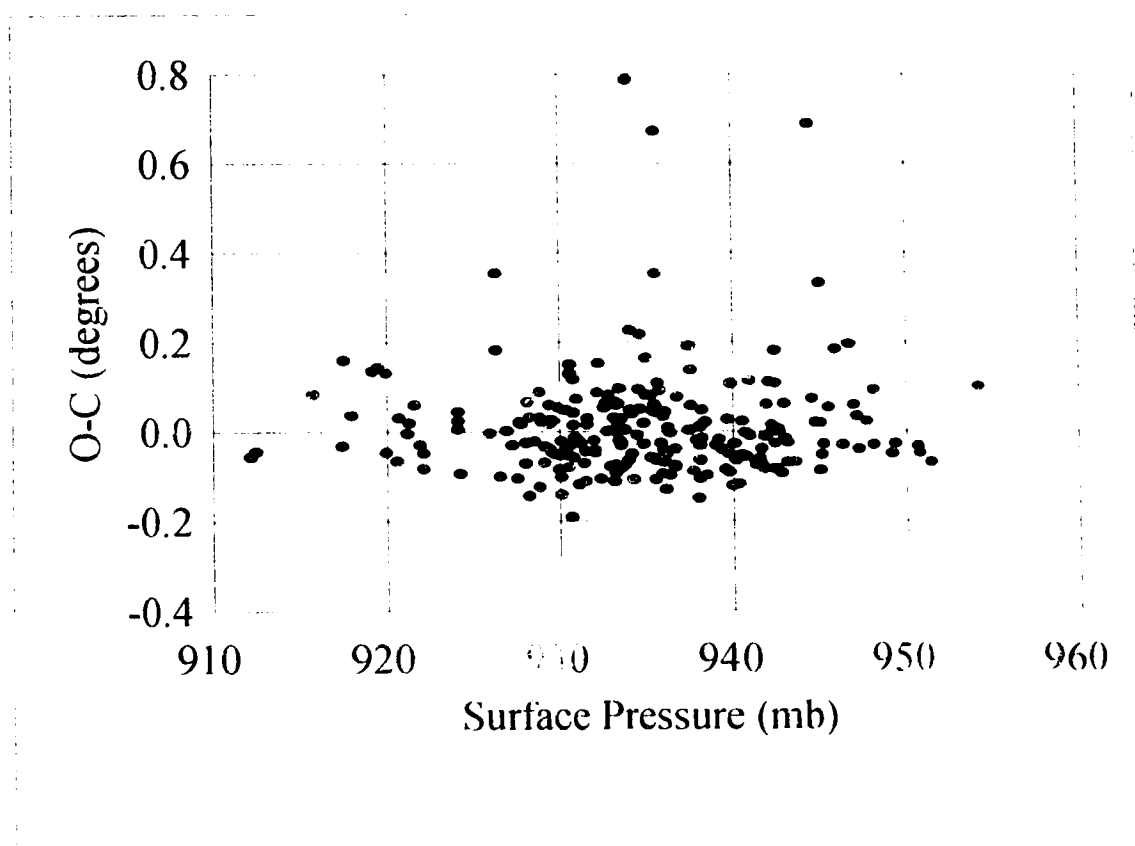


Figure 3.8.3: Observed minus calculated sunrise astronomical refraction (calculated from Equation 3.8.1) versus surface pressure.

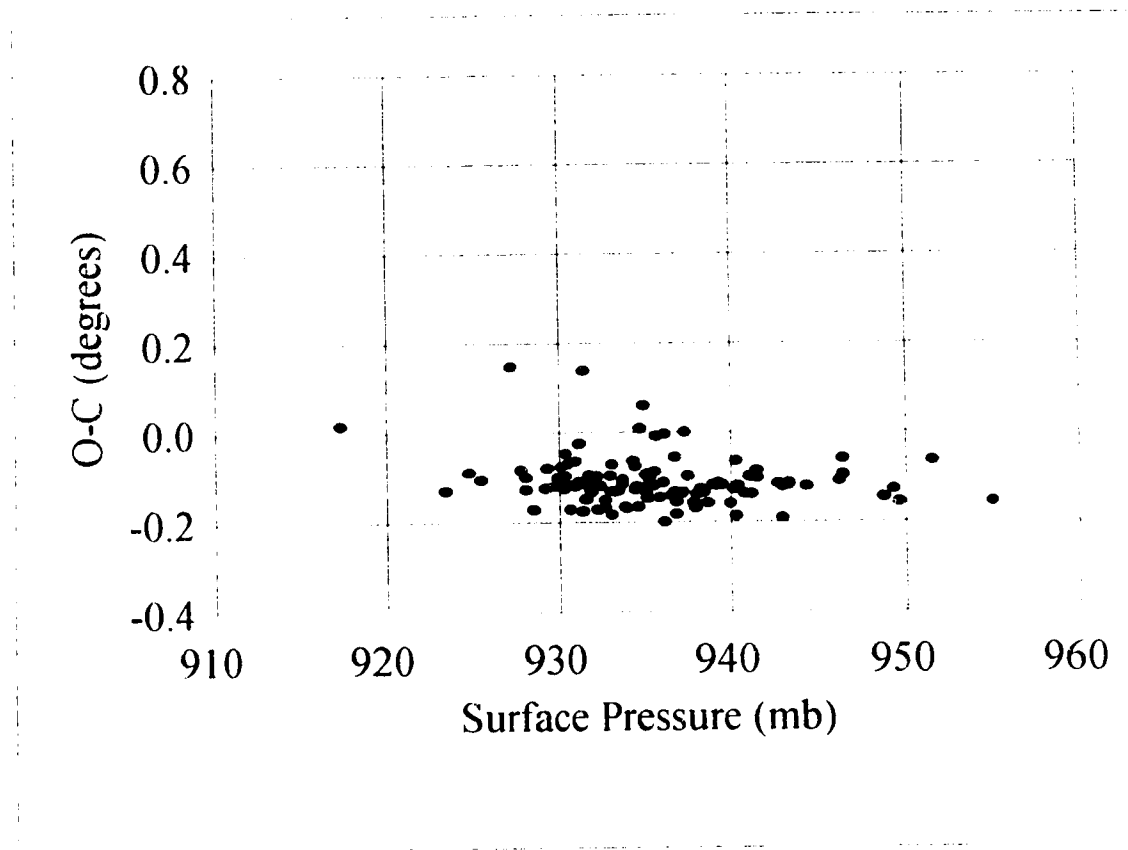


Figure 3.8.4: Observed minus calculated sunset astronomical refraction (calculated from Equation 3.8.1) versus surface pressure.

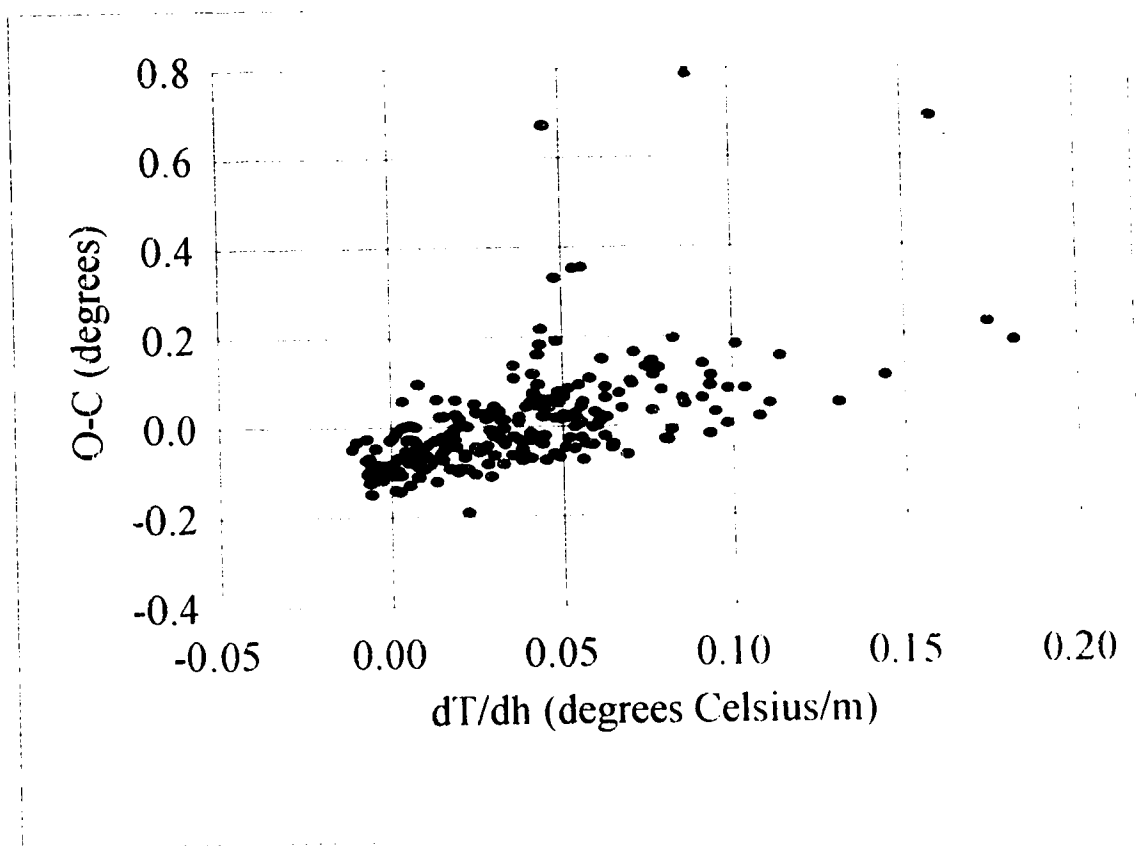


Figure 3.8.5: Observed minus calculated sunrise astronomical refraction (calculated from Equation 3.8.1) versus surface vertical temperature gradient.

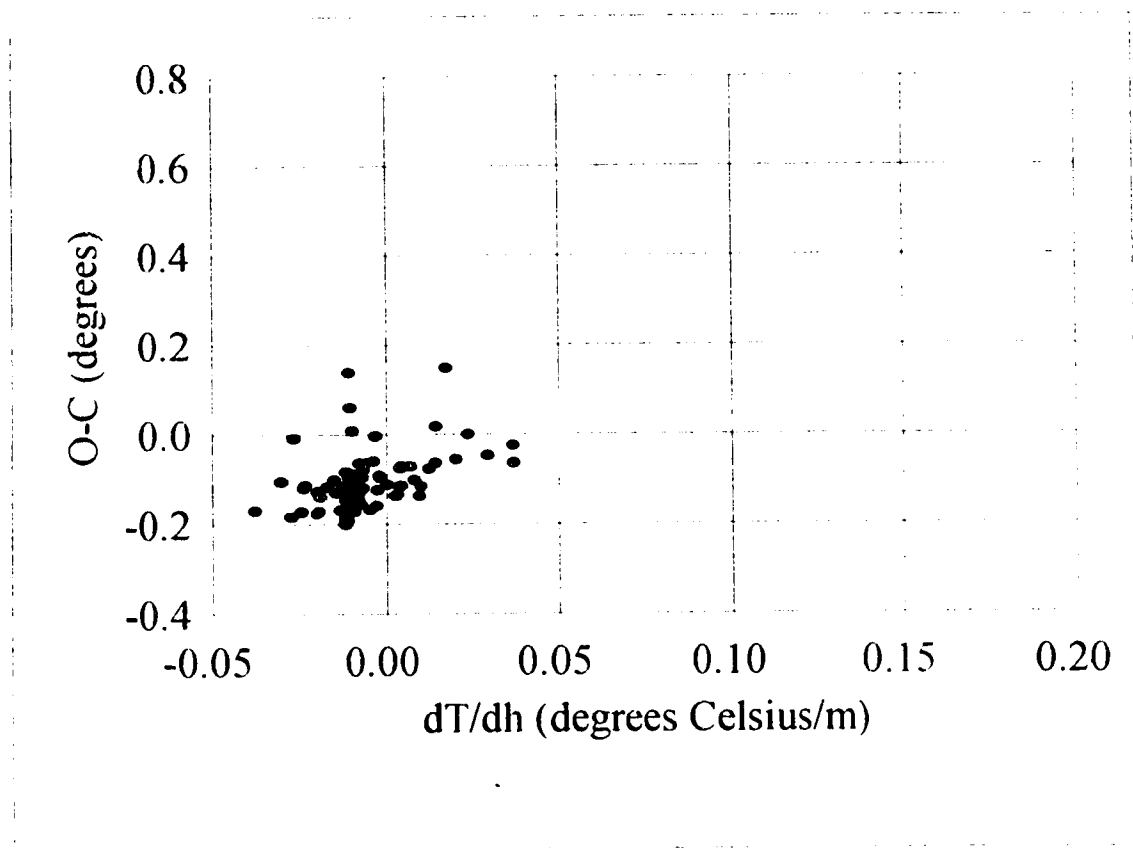


Figure 3.8.6: Observed minus calculated sunset astronomical refraction (calculated from Equation 3.8.1) versus surface vertical temperature gradient.

<b>Parameter/Event</b>	<b>Slope</b>	<b>Intercept (<math>^{\circ}</math>)</b>	<b>Correl. Coeff.</b>	<b>Prob. (%)</b>
Temperature/Both	-0.0040	-0.0300	-0.40	<0.05
Temperature/Sunrise	-0.0033	-0.00013	-0.31	<0.05
Temperature/Sunset	-0.0015	-0.1012	-0.30	<0.05

**Table 3.8.1:** Linear regression results for surface temperature and deviation between Equation (3.8.1) and the astronomical refraction found in this study (see Figures 3.8.1 and 3.8.2).

<b>Parameter/Event</b>	<b>Slope</b>	<b>Intercept (<math>^{\circ}</math>)</b>	<b>Correl. Coeff.</b>	<b>Prob. (%)</b>
Pressure/Both	-0.00085	0.7663	-0.05	~50
Pressure/Sunrise	0.00024	-0.2139	0.02	~90
Pressure/Sunset	-0.0021	1.821	-0.22	~5

**Table 3.8.2:** Linear regression results for surface pressure and deviation between Equation (3.8.1) and the astronomical refraction found in this study (see Figures 3.8.3 and 3.8.4).

<b>Parameter/Event</b>	<b>Slope</b>	<b>Intercept (<math>^{\circ}</math>)</b>	<b>Correl. Coeff.</b>	<b>Prob. (%)</b>
$dT/dh$ /Both	2.2130	-0.0811	0.67	<0.05
$dT/dh$ /Sunrise	1.9677	-0.0656	0.56	<0.05
$dT/dh$ /Sunset	2.0226	-0.0956	0.42	<0.05

**Table 3.8.3:** Linear regression results for vertical temperature gradient and deviation between Equation (3.8.1) and the astronomical refraction found in this study (see Figure 3.8.5).

## CHAPTER 4

### APPLICATIONS TO ARCHEOASTRONOMY

#### 4.1 Neolithic Stone Monuments

It has been suggested that certain British Neolithic stone monuments built during the period 4000 to 1000 B.C. were deliberately aligned with the rising and setting points of the Sun or Moon at key moments in their cyclical movement (Heggie, 1981, Thom, 1971). Since this investigation has focused on the refractive behavior at sunrise and sunset, this portion of the analysis shall concentrate only on the claimed solar alignments. Observable rising and setting events of the moon generally take place at night when meteorological conditions may be different.

It has also been claimed that certain stone markers deliberately point to the solar solstice rising and setting points on a distant horizon. At the solstices, the Sun appears to rise and set at its most southerly and northerly position on a given horizon. The stone monuments or menhirs, are not claimed to be in accurate and precise alignment with these past solstice rising and setting points, rather, they supposedly point to distant horizon features that could be used as precise markers. An observer would stand at the furthest stone and use other stones to point to the crest of a distant hill, a col between two hills or some other convenient horizon marker that would provide a consistent reference for the most southerly or northerly setting or rising point of the Sun. The slow changes in the obliquity of the ecliptic coupled with relatively imprecise dating of the monuments and the rather arbitrary choice of horizon markers makes these claims debatable. These apparent alignments have been used by Thom (1971) as evidence for Neolithic society's advanced understanding of celestial motions of the Sun and the Moon.

Thom suggests that these observations could have been made to determine the day of the winter and summer solstice. For example, as the Earth approaches the summer solstice, the azimuthal position of the rising or setting Sun approaches a maximum northerly position. Depending on the exact time of the solstice, the Sun usually sets at its most northerly point on the day of the summer solstice. If the moment of solstice occurs in the early morning hours then the most northerly sunset can occur on the previous day.

Thom also claimed that these sites could have been used to determine the Sun's solstitial declination and hence the obliquity of the ecliptic (the angular tilt of the Earth's rotational axis with respect to its orbital axis around the Sun). At the moment of the summer or winter solstice the Sun is at its extreme northern or southern declination (about  $+23.4^\circ$  and  $-23.4^\circ$  respectively) and, as mentioned previously, at its most northerly or southerly rising and setting point. Once the azimuth of the most northerly or southerly sunrise or sunset is found, along with the latitude, the altitude of the centre of the geometric Sun, the declination of the Sun at the solstice, and thus the obliquity of the ecliptic, can be found through Equation (3.7.1). This method is limited by the difference between the declination of the Sun at the moment of solstice

and the declination of the Sun at the time of the most southerly or northerly sunrise or sunset. How Neolithic people may have recorded, reduced, and analyzed these azimuthal observations to produce an accurate value for the obliquity is still unexplained and beyond the scope of this paper.

According to Thom, (1971, p. 36) the most noteworthy solstitial observatories occur at sites in Ballochroy and Kintraw, both situated on the west coast of Scotland. From extensive surveys at these and other sites, Thom claims the Neolithic observers could have determined the solar declination at the moment of solstice and hence the obliquity of the ecliptic to an accuracy of about  $\pm 0.012^\circ$ .

Thom deduced this by first assuming that some Neolithic sites were used for sunrise and sunset observations. Sites were then selected which had stone monuments that roughly pointed towards locations on the horizon where the solstitial sunrise or sunset occurred. Thom then measured the altitude and azimuth of the horizon features at these solstitial sunrise or sunset horizon locations. Particular horizon features were then selected that, in Thom's opinion, could produce the most accurate azimuthal measurements of the position of the sunset or sunrise. Thom further assumed that the Neolithic observers used the moment of contact between the upper limb of the Sun and these selected horizon features to determine the azimuthal position of solstitial sunset or sunrise. For example, from the Kintraw site, winter solstice sunset occurred near a V-shaped depression where the slopes of two hills, 45 km away, appeared to intersect. Thom speculated that the Neolithic observers waited until the top limb of the winter solstice setting Sun briefly appeared at the bottom of the depression. At this point the sunset had reached its most southerly azimuthal position and therefore, the Sun was at its most southerly declination. From the altitude and azimuth measurements of the bottom of the depression, Thom could then calculate the past position of the Sun at the moment of winter solstice and hence the obliquity of the ecliptic.

Since the parameters of the Earth's orbit and rotation change over time (the obliquity of the ecliptic has changed by about  $0.013^\circ$  in the last century) the position and apparent size of the Sun and therefore, the position of sunrise and sunset also changes over time. Thom, used these periodic motions to determine an approximate date for the construction of these stone monuments (Thom, 1971, p. 15).

This study will examine the validity of these claims by applying the uncertainty in the astronomical refraction to the azimuthal position of sunrise and sunset and hence the accuracy in determining the date and declination of the solstice (and thus the obliquity of the ecliptic) using a method of sighting sunrises and sunsets.

#### **4.1.1 Application of Observed Astronomical Refraction to the Determination of the Sunrise and Sunset Azimuth and the Value of Solar Declination.**

The uncertainty in the azimuth of the setting Sun was found by applying an error propagation method outlined in Taylor (1982, p. 62) to Equation (3.7.1). This method could not be used for the uncertainty in the declination since Equations (3.7.1) has two terms,  $a$ , and,  $A$ , with uncertainties that are not independent.

Alternatively, a method outlined by Schaefer and Liller (1990) was used where the uncertainty in the declination  $\Delta\delta$  was estimated from the equation

$$\Delta\delta = \Delta R \cos \omega \quad (4.1.1)$$

where  $\Delta R$  is the uncertainty in the astronomical refraction, and  $\omega$  is the interior angle between a great circle of constant right ascension and a great circle of constant azimuth, which intersect at the zero horizon. This is found from the formula (Schaefer and Liller, 1990):

$$\cos \omega = \frac{\sin \phi - \sin \delta \sin \alpha}{\cos \delta \cos \alpha} \quad (4.1.2)$$

Using the uncertainties in astronomical refraction outlined in Table 3.4.1 the resulting uncertainties and half ranges in azimuth and declination for a zero horizon are contained in Table 4.1.1.

Event	$\Delta A$ ( $^{\circ}$ )	Half Range <sub>A</sub> ( $^{\circ}$ )	$\Delta\delta$ ( $^{\circ}$ )	Half Range <sub><math>\delta</math></sub> ( $^{\circ}$ )
sunrise December	0.231	0.578	0.100	0.250
sunrise June	0.318	0.489	0.131	0.201
sunset December	0.156	0.206	0.067	0.089
sunset June	0.053	0.077	0.022	0.032

**Table 4.1.1:** Standard deviations and half ranges for azimuth and declination due to the standard deviation and the half range in refraction (half of the difference between the minimum and maximum values). Columns 2 and 4 are the estimated uncertainties in the azimuth (column 2) and declination (column 3) of the Sun due to the standard deviations of the monthly mean astronomical refraction. Columns 3 and 5 are the half range in azimuth and declination (half the difference between the minimum and maximum value in the monthly astronomical refraction).

The uncertainty and half range in the declination found in this investigation is consistently larger than the accuracy of the obliquity of the ecliptic claimed by Thom. The smallest uncertainty occurs during June sunsets. These have an uncertainty almost twice Thom's value and a half range that is nearly three times as large. Care must be taken when drawing any conclusions from this comparison since Thom's Neolithic sites do not have a horizon at  $0^{\circ}$  altitude, and climatic conditions, that have been shown in this present work to affect refraction, could be significantly different between twentieth century Edmonton and the sites in Neolithic Scotland.



For the Ballochroy site ( $55^{\circ} 42' 44''$  latitude) the present horizon elevations for the winter solstice sunset were found to lie between about  $-0.13^{\circ}$  and  $-0.18^{\circ}$  and for the summer solstice sunset, between  $0.57^{\circ}$  and  $0.90^{\circ}$  (Thom, 1971, pp. 37). No solstice sunrise alignments were mentioned. For the Kintraw ( $56^{\circ} 11' 18''$  latitude) site only the winter solstice sunset horizon was found to be in apparent alignment and it was measured at an altitude  $0.43^{\circ}$ .

According to palaeoclimatic studies, the Neolithic British Isles were only slightly warmer and clearer than today (Lamb, H. H., 1974). The effect of a coastal climate is to moderate seasonal temperature variations, so instead of using the Edmonton December mean refraction and uncertainty the values for October in Edmonton were chosen for the winter solstice sunset evaluation. The mean refraction was adjusted for horizon elevation by using the approximate empirical relationships found earlier. The standard deviation of the mean monthly astronomical refraction was also adjusted, for horizon altitude, in proportion to the adjustments made to the mean astronomical refraction. The results of this analysis appear in Table 4.1.2.

Site	Event	$\Delta A$ ( $^{\circ}$ )	Half Range <sub>A</sub> ( $^{\circ}$ )	$\Delta \delta$ ( $^{\circ}$ )	Half Range <sub><math>\delta</math></sub> ( $^{\circ}$ )
Ballochroy	winter solstice sunset	0.066	0.104	0.026	0.042
Ballochroy	summer solstice sunset	0.052	0.076	0.020	0.029
Kintraw	winter solstice sunset	0.062	0.098	0.023	0.037

**Table 4.1.2:** Standard deviations and half range uncertainties in the solstitial solar azimuth and declination at Ballochroy and Kintraw. These are considered the two most accurate measurements suggested by Thom (1971). Column 3 and 5 are the standard deviation from Table 3.7, and column 4 and 6 are the estimated uncertainties using the half range method.

The propagation of the standard deviation of the refraction suggest that none of the sites could have been used to determine the obliquity of the ecliptic to a precision of  $\pm 0.012^{\circ}$ . The best site appears to be Ballochroy, which shows an uncertainty in declination of  $\pm 0.020^{\circ}$  during the summer solstice sunset. This is 67% larger than the accuracy of the obliquity of the ecliptic claimed by Thom. More realistically, the half range uncertainty at Ballochroy summer sunset, suggests that the method was 2.4 times too inaccurate to produce the claimed value. It is also assumed that to determine the obliquity of the ecliptic, at least two azimuthal positions must be measured, either at the winter solstice sunset position or the summer solstice sunrise position. The only other horizon point mentioned by Thom was the Ballochroy winter solstice sunset position. The standard deviations in the two measurements would then propagate, according to the method described in Taylor (1982, p. 56), to

a combined error of  $\pm 0.033^\circ$  in declination, almost three times larger than the value claimed by Thom. Such an accuracy could have been achieved only if the Neolithic observers could measure the azimuth over a number of solstitial events and then somehow average the results and ignore the inevitable outliers. The two half range uncertainties produce a combined value of  $\pm 0.129^\circ$ , an order of magnitude larger than the figure claimed by Thom.

Even though the summer solstice sunset refraction shows significantly less variation than sunrise refraction and winter sunset refraction, the results of the Ballochroy and Kintraw analysis suggest that the refraction is still not stable enough to determine the obliquity to an accuracy better than about  $\pm 0.1^\circ$  from these sites.

#### **4.1.2 Application of Observed Astronomical Refraction to the Determination of the Date of Solstice Using the Time of Extremes in Sunrise or Sunset Azimuth.**

As mentioned previously, variations in astronomical refraction produce a resulting variation in the azimuthal position of the rising or setting Sun. To determine the exact day of the solstice by observing the rising or setting point of the Sun, an observer must obtain an unambiguous sighting of the most northerly or southerly azimuth of the Sun. The uncertainty of the azimuth of the rising or setting Sun due to refraction determines the accuracy of this measurement. If the uncertainty in azimuth is less than the difference in azimuth from one day to the next, then it is possible to determine the exact date of the solstice. A plot of the azimuth of the setting Sun around summer solstice as seen from Edmonton is given in Figure 4.1.1.

The accuracy of the date of the solstice found through the sunrise and sunset method outlined above is estimated by comparing the uncertainty in azimuth due to refraction with the daily change in azimuth for the period centered on the solstice. The difference in azimuth between a setting or rising Sun on a particular day and the azimuth of the setting or rising Sun at the solstice is then subtracted from the uncertainty in azimuth due to refraction. The period of time when the values are below zero is considered to be a period of ambiguity when the uncertainty in azimuth could potentially produce the most northerly or southerly azimuth. Any one of the days within this period could, therefore, be considered to be the day of the solstice. For the values listed in Table 4.1.1 (conditions specific to the Edmonton sites) the uncertainty in the possible dates for the different solstices are given in Table 4.1.3.

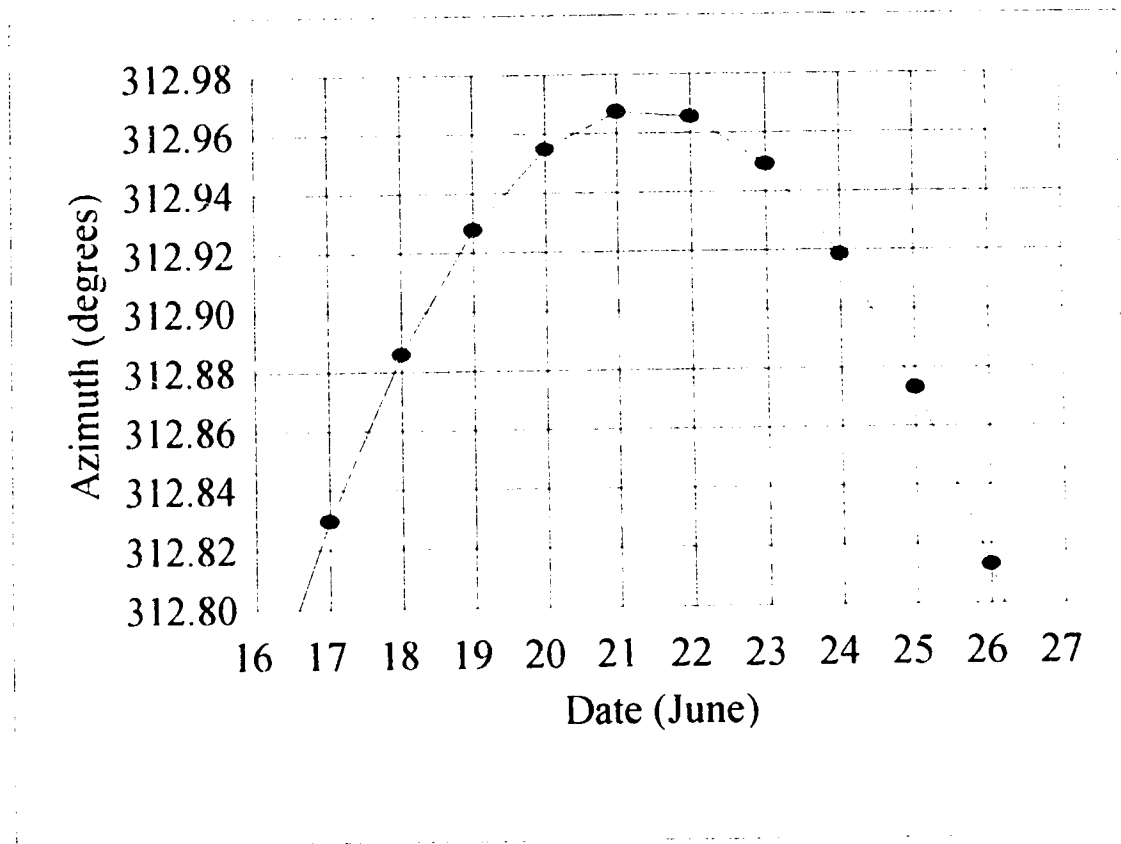


Figure 4.1.1: Azimuth of setting Sun around summer solstice as seen from Edmonton. To determine the azimuth, daily declinations for the Sun and Edmonton's geographic latitude were placed in Equation (3.7.1). For the altitude of the upper limb of the Sun, the mean value for sunset astronomical refraction in June ( $-0.526^\circ$ ) was used.

<b>Event</b>	<b>Accuracy (from SD) (<math>\pm 0.1</math> days)</b>	<b>Accuracy (from half range) (<math>\pm 0.1</math> days)</b>
sunrise winter solstice	11.2	16.9
sunset winter solstice	8.7	10.0
sunrise summer solstice	13.4	16.5
sunset summer solstice	5.4	6.5

**Table 4.1.3:** The estimated uncertainty in determining the date of the solstice at Edmonton's geographical location and climate, using the most northerly or southerly sunrise or sunset to indicate the date of solstice. The second column is the accuracy derived from the standard deviation of the refraction observed in December or June. The third column is the accuracy derived from the half range of observed refraction during the two months.

A case study appears to support the overall conclusion that the time of summer solstice cannot be determined to an accuracy of a single day using the most northerly sunset (see Figure 4.1.2)

The methods outlined previously were then used to determine whether the solstice sunsets at Ballochroy and Kintraw could have been used to find the date of solstice. The results appear in Table 4.1.4.

<b>Site and Event</b>	<b>Accuracy (from SD) (days)</b>	<b>Accuracy (from half range) (days)</b>
Ballochroy, sunset winter solstice	5.3	6.8
Ballochroy, sunset summer solstice	5.2	6.2
Kintraw, sunset winter solstice	5.1	6.4

**Table 4.1.4:** The estimated uncertainty in determining the date of the solstice from Thom's Neolithic solstitial sites. As before, June and October values for refraction were used.

The results in Table 4.1.4 suggest that at the Ballochroy and Kintraw sites, the day of solstice for an individual year could be consistently determined to an accuracy of no better than about 5 days using the method of sighting the azimuth of the most northerly or southerly sunset. This assumes that the meteorological conditions in Neolithic Scotland are not radically different than those used in this study.

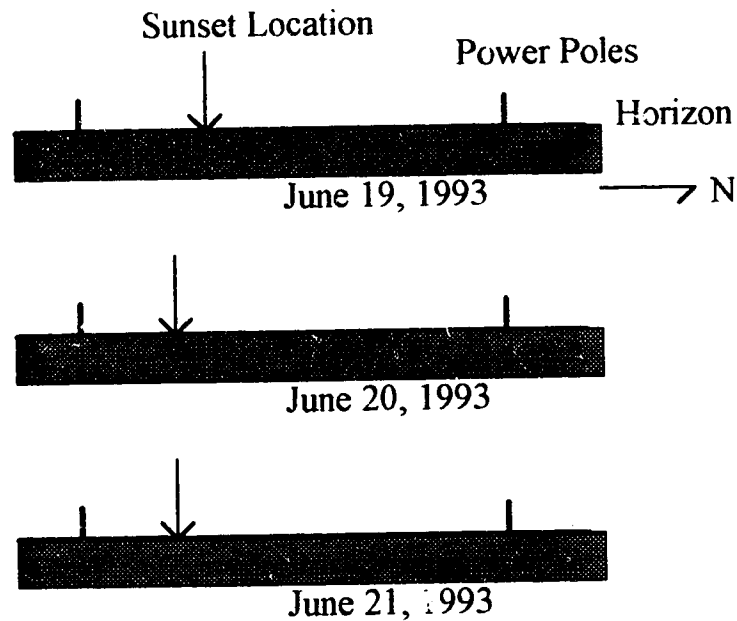


**Figure 4.1.2:** A series of sunsets around summer solstice illustrating the difficulty in determining the date of summer solstice from the date of the most northerly sunset. All observations were made from the roof of the H. M. Tory building. The location and elevation of the observer for all three observations was maintained to an accuracy of about  $\pm 0.1$  meter. The distance to the horizon is over 30 kilometers and the power poles are about 10 kilometers away. The angular distance between the two power poles was estimated to be about  $1.2^\circ$ . Observations were made with a pair of 7x20 binoculars. Dates are in UT, and all three sunsets occurred around 04:08 UT. Summer solstice took place on June 21 at 09:00 UT (The Astronomical Almanac, 1992, p. A1), 2.2 days from the most northerly sunset, which occurred on June 19.

## 4.2 The Pyramids of Egypt.

Many of the great pyramids of Egypt are apparently aligned to the cardinal points to within a precision of less than a degree of azimuth. Numerous attempts have been made to explain how the ancient Egyptians could have found the cardinal points with such accuracy and precision (Zaba, Z., 1953 and Haack, S. C., 1984). Most attempts have concentrated on the sighting of the star  $\alpha$  Draconis which was close to the celestial pole at the time of the Pharaohs. Haack also claims that the sighting of the rising or setting Sun at the equinoxes would lead to a large error, since the daily northward or southward motion of the setting or rising Sun around the equinoxes is at its annual maximum.

One possible alternative method would be to locate north by bisecting the angle subtended by the azimuthal position of the sunrise and sunset on a given day. Since the change in azimuth of the Sun is at a maximum around the equinoxes, this method would have greater accuracy during the solstices. It would also be more convenient during the period around solstice since, as mentioned in Section 4.1.2, there would be a number of sunrises and sunsets at approximately the same azimuth and, as a result, the occasional cloudy day would not be as problematic. During the few days around the solstice when the sunrise or sunset azimuth appears to be nearly stationary, an observer would have numerous attempts to observe and even refine their sight lines. As shown in Section 4.1.1, the mean azimuthal position of the solstice sunrise or sunset is a function of the mean sunrise and sunset refraction during the time of the solstice. The uncertainty in azimuthal position of the most northerly sunrise and sunset is also a function of the standard deviation of the refraction at that particular time of year.

Zaba (1953, pp. 11-12) provides alignments of eight pyramids, three of which are only approximate due to their poor state of preservation. These three alignments were ignored. The alignment errors of the five most accurately measured pyramids are contained in Table 4.2.1.

Pyramid name	Error ( $^{\circ}$ )
The Great Pyramid of Cheops at Giza	0.0147
The Pyramid at Meidum (Huni)	-0.4069
Seneferu's Bent Pyramid at Dahshur	-0.1533
The Pyramid Mycerinus at Giza	0.2347
The Pyramid of Chephren at Giza	-0.0906

**Table 4.2.1:** The error in alignment of five of the pyramids of Egypt. A positive error indicates an alignment to the east of true north. The error for the Great Pyramid of Cheops was determined from the average of the alignment errors of its four sides.

The mean alignment error is  $0.08^\circ$  to the west of true north with a standard deviation of  $0.2^\circ$ . This implies that, on average, these five pyramids are aligned to an azimuthal point of  $359.92^\circ \pm 0.2^\circ$ .

The mean and standard deviation of refraction for June sunrise and sunset were taken from Table 3.7. A latitude of  $30.0^\circ$  N, and a horizon altitude of  $0^\circ$  were used for the calculations. The mean azimuthal position of the rising and setting summer solstice Sun was found through Equation (3.7.1), where the solar declination at summer solstice (for 2500 B.C.) was  $+24.067^\circ$  (Seidelmann, 1992, p. 171) and the altitude of the centre of the solar disc was found by the summation of the mean refraction for June sunrise and sunset and the mean semidiameter of the Sun ( $0.267^\circ$ ). The standard deviations are then determined for this site through the same error propagation methods described in Section 4.1.1. The resulting azimuth is  $359.84^\circ$  with an uncertainty of  $\pm 0.1^\circ$ .

Therefore, the results suggest that if the refractive conditions were similar to those in Edmonton, and if the builders had access to a relatively flat horizon (or a solstitial sunrise and sunset horizon of equal altitudes), then the method outlined above would be consistent with the mean alignment and the standard deviation of the five most accurately measured pyramids. The relatively flat Nile delta is located just to the north of the Pyramids of Giza and may have been used to find the cardinal points. Once a line had been found, it could have been extended to the location of the pyramid by a form of backsighting, where a series of markers would be aligned sequentially with the previous two. This method would obviously introduce its own uncertainty into the final alignment.

Therefore, it appears possible that the builders of the Pyramids used the bisection of the angle described by the azimuthal location of the summer solstice sunrise and sunset to align these structures.

## CHAPTER 5.

### DISCUSSION AND CONCLUSIONS

Observed timings of 244 sunrises and 125 sunsets were used to determine the astronomical refraction of the Sun's upper limb. Once corrected for horizon altitude and terrestrial refraction, the differences between sunrise and sunset refraction, as well as seasonal differences in refraction were examined. Using the physical principles of refraction as a guide, the results were then correlated with available meteorological data. Anomalously large refractive events were examined, with respect to their frequency, seasonal distribution and meteorological correlations. An attempt was made to determine the existence and behavior of horizontal astronomical refraction by comparing the observed sunrise azimuth with the calculated value. Finally, the results were used to examine specific issues in the field of archaeoastronomy. The results of the study are as follows.

1) The analysis showed that the mean sunrise and sunset astronomical refraction for this study was  $0.669^\circ$  with a standard deviation of  $0.175^\circ$  and a total range of between  $0.402^\circ$  and  $2.081^\circ$ . The data suggest that the amount and variability of refraction differs between sunrise and sunset. In this study, the mean sunrise astronomical refraction was found to be  $0.714^\circ$  with a standard deviation of  $0.184^\circ$ , while the mean sunset astronomical refraction was  $0.579^\circ$  (19% less than the sunrise value) with a standard deviation of  $0.108^\circ$  (41% less than the standard deviation for sunrise refraction). The mean sunset astronomical refraction is in close agreement with the value found by Schaefer and Liller, differing by only 3%. The difference in standard deviation between the two studies is considerably more. The Schaefer and Liller data shows 41% greater standard deviation in their sunset astronomical refraction. Direct comparison between these two data sets may be slightly hampered by the absence of any correction for terrestrial refraction in the Schaefer and Liller study.

2) The results also suggest a relatively strong seasonal effect on the monthly mean and monthly standard deviation of the astronomical refraction. Both the mean sunrise and sunset astronomical refraction peak during the colder months. The peak monthly mean sunrise astronomical refraction occurs in November with a value of  $0.857^\circ$  while the sunset value peaks in January at  $0.777^\circ$ . Sunrise astronomical refraction shows a secondary peak in summer, with  $0.779^\circ$  in June and  $0.798^\circ$  in July. Sunset astronomical refraction experiences a broad minimum in the warmer months with the lowest value of  $0.496^\circ$  occurring in August. The monthly mean sunset refraction is consistently less than the sunrise refraction. The difference between the two generally increases during the warmer portion of the year and reaches a maximum difference in June and August.

The seasonal variations in the monthly standard deviation of sunrise and sunset astronomical refraction follow a similar trend. The maximum standard deviation for both sunrise and sunset appears to occur during the colder parts of the year with a secondary maximum for sunrises occurring in June. The largest values occur for



January and November sunrises, where the standard deviation is  $\pm 0.270^\circ$  and  $\pm 0.335^\circ$  respectively. The standard deviation of the sunset astronomical refraction experiences a broad minimum during the warmer months. The average standard deviation for the observations taken during May through October (excluding July due to the lack of sufficient data) is around  $0.028^\circ$  with a range of  $0.019^\circ$  in May to  $0.033^\circ$  in August.

During most of the year, the ranges of the standard deviation for sunrise and sunset overlap. Only in May, June, August and September do the two ranges remain separate. It is, therefore, not unreasonable to conclude that the mean astronomical refraction for both sunrise and sunset during the colder months could be the same. Yet, the consistent difference between the mean monthly sunrise and sunset refraction (sunset refraction is always less) strongly suggests that the difference is real and not an artifact of the data.

3) Astronomical refraction appears to be most strongly correlated with the surface temperature and the surface vertical temperature gradient, with the vertical temperature gradient giving a slightly higher correlation coefficient. Little or no improvement was seen when correlating astronomical refraction with surface air density. The astronomical refraction exhibits very little correlation with the surface pressure.

Empirical formulae for sunrise and sunset refraction based on surface temperature and surface vertical temperature gradient were derived through linear regression. The formulae assume a zero horizon. The correlation coefficients suggest the linear correlation is highly significant. Since the correlation is based on the physical relationship between the vertical temperature gradient and refraction, it appears reasonable to conclude that the results of this investigation indicate a causal relationship and hence, the relationship between the measured surface vertical temperature gradient and the astronomical refraction should be universal in its application. Even though the linear fit between astronomical refraction and the surface vertical temperature gradient may be highly significant, there remains a large amount of variance that can not be explained by the linear fit. Inaccuracies in the calculated surface vertical temperature gradient and differences between the time of radiosonde measurements and the time of sunrise and sunset, limit the accuracy of the relationship and may account for some of the scatter. Since the same surface vertical temperature gradient may occur with a different surface temperatures, further observations from different climatic regions may be necessary to confirm the universality of these relationships. Ray tracing analysis using observed vertical temperature distributions would also help to verify these empirical results.

The monthly standard deviation in sunrise and sunset astronomical refraction is also strongly correlated with the variability in the surface vertical temperature gradient. A linear regression of these two values produces a highly significant correlation. A similar correlation between the standard deviation of the surface temperature and the standard deviation of the refraction produces a relatively poor correlation. This suggests that surface temperature alone is not a satisfactory indicator of astronomical refractive behavior. The surface vertical temperature gradient appears to be the best overall indicator of sunrise or sunset astronomical

refraction. However, this apparently strong correlation may be due, in part, to the strong correlation between the surface vertical temperature gradient and the corresponding measurement uncertainty. Therefore, the correlation between the monthly standard deviation of the refraction and the monthly standard deviation of the surface vertical temperature gradient may be coincidental. Further work, with data of higher resolution, will be necessary to uncover a more conclusive relationship.

The present results may provide a useful archeoastronomical tool for determining the range in astronomical refraction for a particular site, as deduced from the expected range in the surface vertical temperature gradient. It may be possible to determine the range of the surface vertical temperature gradient for a prehistoric site from palaeoclimatic studies and also from comparisons with surface vertical temperature gradient records from similar present day climatic sites.

4) On rare occasions, anomalously large refractive events caused the Sun to rise much earlier than predicted or set much later. These so-called, Novaya Zemlya effects, were extracted from the data by selecting astronomical refraction events more than two standard deviations greater than the line defined by the linear regression of the vertical temperature gradient and the astronomical refraction. It appears the effect is about twice as common at sunrise than at sunset. From a total of 11 events, nine were sunrises (4% of total sunrises) and two were sunsets (2% of total sunsets). All Novaya Zemlya events, except one, took place during surface inversion conditions. The data suggests the Novaya Zemlya is typically, but not exclusively, a cold weather phenomenon. Therefore, the Novaya Zemlya phenomenon may also be visible in warmer climates during surface inversion conditions (i.e. during sunrise).

5) The possibility of horizontal refraction was explored by comparing the observed azimuth of a sample of sunrises taken around the winter solstice to the calculated azimuth of these events. The results suggest the possible existence of horizontal astronomical refraction of  $0.19^\circ \pm 0.08^\circ$  with a minimum azimuthal deviation of  $+0.05^\circ$  and a maximum of  $+0.36^\circ$ . Seven measurements were considered to be of the highest possible accuracy (an uncertainty of less than  $\pm 0.1^\circ$ ). Six of the most accurate measurements showed an azimuthal deviation of  $+0.14^\circ$  or more. The overall southward direction of the observed displacement is consistent with the sense of the refraction which would arise from a meridional temperature gradient. Yet the magnitude of the apparent displacement appears to be far greater than the amount predicted by Bomford's equation (1980). Therefore, it appears that the measured deviation could also be the result of random measurement error, and/or systematic error in the calculation or measurement of the azimuth of the reference horizon landmarks or the sunrises themselves.

It was expected that any significant horizontal refraction should be correlated with significant astronomical (i.e. vertical) refraction. A plot of the horizontal deviation versus astronomical refraction appears to reveal a linear relationship with a modest correlation coefficient of 0.30 (i.e.: there is a probability of 11% that 27 random data points would achieve the same correlation coefficient).

Therefore, confirmation of the existence of significant horizontal astronomical refraction must await a more sensitive and sophisticated study.

6) A comparison of the results of this study and the formula for astronomical refraction in the *Astronomical Almanac* reveals a systematic difference with respect to sunrise and sunset refraction. The altitude of the upper limb of the geometric Sun, the surface temperature and surface pressure at the time of the observed sunrise or sunset were placed into the *Astronomical Almanac* formula and the resulting astronomical refraction was then subtracted from the values found in this study. The average deviation for all the observations was  $-0.030^\circ$  with a standard deviation of  $0.116^\circ$ . For sunrises the average deviation was  $0.009^\circ$  and standard deviation of  $0.117^\circ$ , while for sunset the average deviation was  $-0.110^\circ$  and standard deviation of  $0.056^\circ$ .

A linear regression was performed on the sunrise and sunset deviation versus surface temperature and surface vertical temperature gradient. The results show that the *Astronomical Almanac* formulae require little or no further adjustments for surface temperature and especially the surface vertical temperature gradient. The application of the linear correction term for surface vertical temperature gradient to the *Almanac* formulae decreased the average deviation from the observed astronomical refraction by  $0.030^\circ$  and decreased the corresponding standard deviation by 26%.

Therefore, the results suggest that the surface vertical temperature gradient should be factored into any methods for calculating the expected amount of astronomical refraction near the horizon.

7) The results of the investigation were finally applied to specific issues in archaeoastronomy. The effects of astronomical refraction found in this study were used to examine the claims of A. A. Thom, who suggested that specific Neolithic stone monuments in the British Isles were deliberately aligned with the solstitial rising and setting points of the Sun. Thom claimed that sites at Ballochroy and Kintraw in Scotland, demonstrated that Neolithic observers could determine the exact day of solstice and find the obliquity of the ecliptic to an accuracy of  $\pm 0.012^\circ$  using the azimuthal position of the rising and setting Sun.

8) The results of this study suggest that Neolithic observers could not have used the solstice sunrise or sunset to determine the exact date of the solstice from these two sites. The variability in astronomical refraction produces a variability in the azimuth of the rising or setting solstitial Sun. The results of this study, suggest that at the Ballochroy and Kintraw sites, the day of solstice could be consistently determined to an accuracy of no better than about 5 days using the method of sighting the azimuth of the most northerly or southerly sunset. Actual observations from Edmonton of the most northerly setting point of the Sun around the 1993 solstice, appear to support this conclusion.

The same variability in the astronomical refraction limits the possible measurement accuracy of the obliquity of the ecliptic to about  $\pm 0.1^\circ$  at the Ballochroy or Kintraw sites.

A possible concern with these results is the assumption of similarity between refractive conditions revealed through this study (from late 20th century Edmonton) and the refractive conditions in Neolithic Scotland. The present climate in Edmonton is northern continental while the sites in Scotland have a northern maritime climate. The results of this study point to a possible solution to this problem. If the

relationship between the standard deviation of the monthly refraction and the standard deviation of the monthly surface vertical temperature gradient is universal, and a relationship between regional climate and seasonal/daily surface vertical temperature gradient variability can be established, then the climatic refractive conditions in Neolithic Scotland could be estimated.

9) The present results have also been applied to the alignment of the pyramids of Egypt. Many of these structures are apparently aligned to the cardinal points with an error of less than half a degree of azimuth. The five pyramids with the best measurements (due to their state of preservation) show a mean northern alignment azimuth of  $359.92^\circ$  with a standard deviation of  $\pm 0.21^\circ$ . If the position of true north were determined by bisecting the angle described by the rising and setting point of the Sun around the summer solstice, then the results of this study suggest that the mean monthly astronomical refraction for the June sunrise and sunset would place true north at  $359.83^\circ$  and the standard deviation due to refraction would be  $\pm 0.10^\circ$ . Therefore, the position and uncertainty of true north, estimated by the results of this study, appear to be consistent with the alignment of the five most accurately measured pyramids.

The validity of this conclusion is limited by the unknown refractive conditions during the construction of the pyramids, and the availability of a sufficiently flat horizon near the construction sites. The relatively flat Nile delta is located just to the north of the Pyramids of Giza and may have been used to find the cardinal points. Once a line had been found it could have been extended to the location of the pyramid by a form of backsighting, where a series of markers would be aligned sequentially with the previous two. This method would obviously introduce its own uncertainty into the final alignment. As mentioned previously, a study into the climatic conditions of ancient Egypt and a full examination of the connection between climate, surface vertical temperature gradient variability and astronomical refraction would help to solve the first concern. A full examination of the present local topography around the pyramids and any possible changes that may have occurred would clarify the second.

With these concerns in mind, it is not unreasonable to suggest that these five pyramids could have been aligned to the measured accuracy using the bisection of the angle described by the rising and setting Sun around the summer solstice.

## BIBLIOGRAPHY

- Alberta Bureau of Surveying and Mapping, 1982: 1:40000 Map of Edmonton (including St. Albert).
- Bomford, G., 1980: Geodesy, Fourth Edition, Clarendon Press, Oxford, pp. 855.
- Brinker, R. C. and Wolf, P. R., 1984: Elementary Surveying, Harper & Row, New York, pp. 608.
- Chemical Rubber Company Press, 1975: C.R.C. Handbook of Chemistry and Physics, 56th Edition, Cleveland Ohio, pp. 2351.
- Concord Environmental Corporation, 1993: Summary of Surface and Upper Air Data From the FSRIA Fort Saskatchewan Meteorological Station, 1989-1992, pp. 113 (not including minisonde data supplied on computer disk).
- Green, R. M., 1985: Spherical Astronomy, Cambridge University Press, Cambridge, pp. 520.
- Haack, S. C., 1984: The astronomical orientation of the Egyptian Pyramids, Archaeoastronomy, (supplement to the Journal of the History of Astronomy), 7, S119-S125.
- Henderson-Sellers, A. and Robinson P. J., 1986: Contemporary Climatology, Longman Scientific and Technical, New York, pp. 439.
- Heggie, D. C., 1981: Megalithic Science, Thames and Hudson, London, pp. 256.
- Humphreys, W. J., 1964: Physics of the Air, Dover Publications, New York, pp. 676.
- Huschke, R. E., 1959: Glossary of Meteorology, American Meteorological Society, Boston, pp. 638.
- Illingworth, V. (editor), 1980, The Anchor Dictionary of Astronomy, Anchor Press, New York, pp. 518.
- Lamb, H. H., 1974: Climate, vegetation and forest limits in early civilized times, Philosophical Transactions of the Royal Society of London, A. 276, 195-230.
- Lehn, W. H., 1979: The Novaya Zemlya effect: an arctic mirage, Journal of the Optical Society of America, 69, 776- 781.

Lehn, W. H., 1983: Inversion of superior mirage data to compute temperature profiles, *Journal of the Optical Society of America*, 73, 1622-1625.

Mahan, A. I., 1962: Astronomical refraction - some history and theories, *Applied Optics*, 1, 497-511.

Mac Kie, E. W., 1974: Archaeological tests to supposed prehistoric astronomical sites in Scotland, *Philosophical Transactions of the Royal Society of London*, A. 276, 169-194.

Meeus, J., 1988: *Astronomical Formulae for Calculators*, Willmann-Bell, Inc., Richmond Virginia, pp. 218.

Oke, T. R., 1992: *Boundary Layer Climates*, Routledge, London, pp. 435.

Royal Astronomical Society of Canada, 1993: *Observer's Handbook 1994*, University of Toronto Press, pp. 240.

Schaefer, B. E., 1989: Refraction by the Earth's atmosphere, *Sky & Telescope*, 77, 311.

Schaefer, B. E., Liller, W., 1990: Refraction near the horizon, *Publications of the Astronomical Society of the Pacific*, 102, 796-805.

Seidelmann, K. P., 1992: *Explanatory Supplement to the Astronomical Almanac*, University Science Books, Mill Valley California, pp. 752.

Sugawa, C., 1955: On the Numerical integration of astronomical refraction, *Publications of the Astronomical Society of Japan (Nihon Tenmon Gakkai Publications)*, 7, 163-175.

Surveys and Mapping Branch, Department of Energy Mines and Resources, 1980: 1:50000 Topographic Map: 83 H/5, Leduc.

Surveys and Mapping Branch, Department of Energy Mines and Resources, 1980: 1:50000 Topographic Map: 83 H/6, Cooking Lake.

Surveys and Mapping Branch, Department of Energy Mines and Resources, 1980: 1:50000 Topographic Map: 83 H/11, Edmonton.

Surveys and Mapping Branch, Department of Energy Mines and Resources, 1980: 1:50000 Topographic Map: H/12, St. Albert.

Taylor, J. R., 1982: *An Introduction to Error Analysis*, University Science Books, Mill Valley California, pp. 270.

Thom, A. A., 1958: An empirical investigation of atmospheric refraction, *Empire Survey Review*, XIV, 248-262.

Thom, A. A., 1971: *Megalithic Lunar Observatories*, Clarendon Press, Oxford, pp. 127.

United States Printing Office, 1962: *Tables of Sunrise, Sunset and Twilight*, Washington, DC., pp. 196.

United States Government Printing Office, 1992: *The Astronomical Almanac 1993*, Washington, DC., pp. 539.

Wallace, J. M., Hobbs, P. V., 1977: *Atmospheric Science, An Introductory Survey*, Academic Press, Orlando, Florida, pp. 467.

Zaba, Z., 1953: *L'Orientation Astronomique dans L'Ancienne Egypte et la Precession de L'Axe du Monde*, Editions de L'Academie Tchecoslovaque des Sciences, Prague.

Zuev, V. E., 1982: *Laser Beams in the Atmosphere*, Consultant Bureau, New York, pp. 504.

## APPENDIX A:

### GLOSSARY OF SELECTED TERMS

**Adiabatic Lapse Rate (or Dry-adiabatic Lapse Rate):** A special lapse rate of temperature, defined as the rate of decrease of temperature with height of a parcel of dry air lifted adiabatically (i.e. there is no exchange of energy with the surrounding environment) through an atmosphere in hydrostatic equilibrium (i.e. the state of a fluid whose surfaces of constant pressure and constant mass coincide and are horizontal throughout. Complete balance exists between the force of gravity and the pressure force.) (R. Huschke, 1959, pp. 9, 10, 290)

**Altitude ( $a$ ).** The angular distance of a point or celestial object above or below the horizon (Illingworth, 1980, p. 13). In this study the horizon, the horizontal plane through an observer, shall be called the zero horizon. The zenith has an altitude of  $90^\circ$  above the zero horizon. Altitudes below the zero horizon are negative.

**Astronomical Refraction ( $R_p$ ).** The observed angular displacement, in altitude, of an astronomical object due to the refraction of its light by the atmosphere between the observer and the celestial object ( $R_p$  in Figures 1.1.1, 1.1.2, 1.1.3 and 2.1.2).

**Azimuth ( $A$ ).** The angular distance measured eastwards along the horizon (Illingworth, 1980, p. 44) from a local meridian to the intersection of the object's vertical circle (a great circle passing through the object and the zenith). The cardinal points: north has an azimuth of  $0^\circ$ , east  $90^\circ$ , south  $180^\circ$  and west  $270^\circ$ .

**Declination ( $\delta$ ).** A coordinate used with right ascension in the equatorial coordinate system (see Figure A.1). The declination of a celestial body, is its angular distance (from  $0^\circ$  to  $90^\circ$ ) north (counted positive) or south (counted negative) of the celestial equator (Illingworth, 1980, p. 110).

**Equatorial Coordinate System.** The most widely used astronomical coordinate system in which the fundamental reference circle is the celestial equator with the zero point at the vernal equinox (see Figure A.1). The coordinates are right ascension  $\alpha$  and declination  $\delta$ , which are measured along directions equivalent to those of terrestrial longitude and latitude, respectively (Illingworth, V. 1980, p. 147).



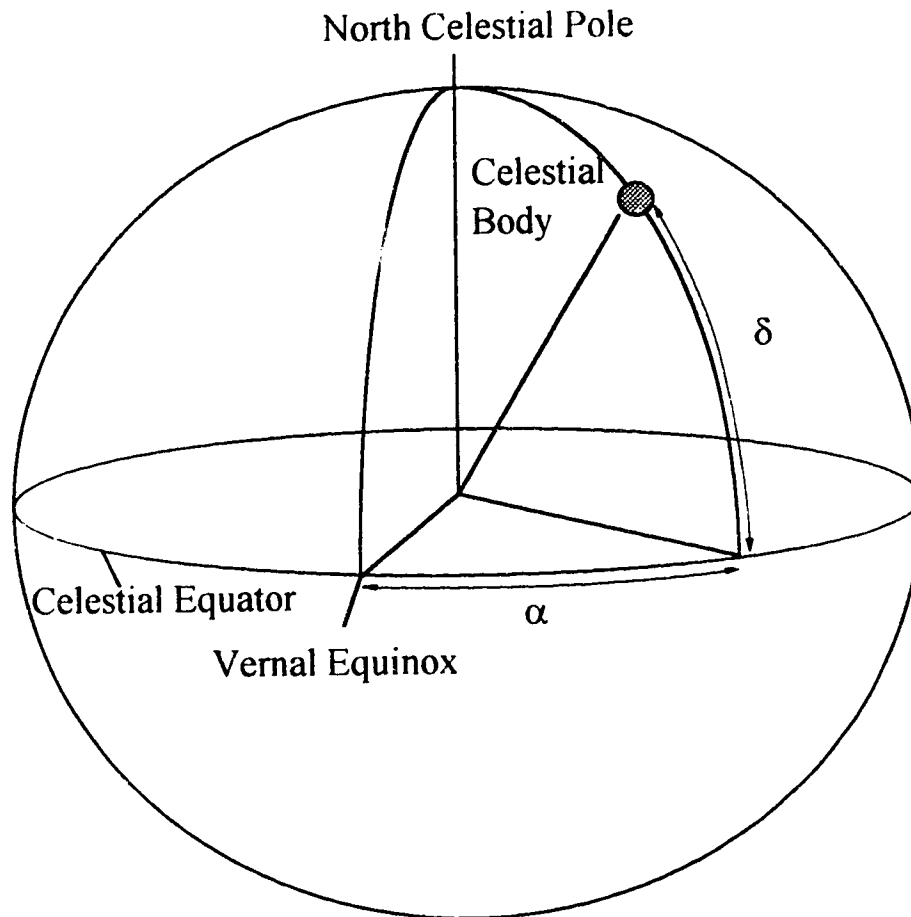


**Figure A.1:** Equatorial coordinate system (Illingworth, 1980, p. 147).

**Geometric Sun.** The apparent position of the solar disc without the effects of refraction (see Figure 1.1.1, 1.1.2, 2.1.2 and 2.1.3).

**Horizontal Refraction.** The displacement of an image in azimuth due to the effects of terrestrial and/or astronomical refraction.

**Hour Angle ( $H$ ).** The angle measured westward along the celestial equator from the observer's meridian to the hour circle (a circle of constant right ascension) of a celestial body (Illingworth, 1980, pp. 206-207).

**Lapse Rate ( $\gamma$ ).** The decrease of an atmospheric variable with height, the variable being temperature, unless otherwise specified (R. Huschke, 1959, p. 334)

**Local Horizon.** The altitude profile of the most distant visible local topography against the open sky.

**Right Ascension ( $\alpha$ ).** A coordinate used with declination in the equatorial coordinate system (see Figure A.1). The right ascension of a celestial body, etc., is its angular distance measured eastwards along the celestial equator from the vernal equinox to the intersection of the hour circle passing through the body (Illingworth, 1980, p. 384).

**Refracted Sun.** The position of the solar disc as seen by an observer after its light passes through the atmosphere (see Figure 1.1.1, 1.1.2, 2.1.2 and 2.1.3).

**Sidereal Time.** The time measured by reference to the rotation of the Earth with respect to the stars, which are regarded as fixed in position (Illingworth, 1980, p. 406).

**Super-adiabatic.** A lapse rate greater than the dry-adiabatic lapse rate or less than the dry-adiabatic vertical temperature gradient.

**Sunrise and Sunset.** The moment the upper limb of the Sun appears (sunrise) or disappears (sunset) at the local horizon (see Figures 1.1.1 and 1.1.2).

**Surface Inversion.** A temperature inversion based at the earth's surface; that is, an increase of temperature with height beginning at the ground level. This condition is due primarily to greater radiative loss of heat at and near the surface than at levels above. Thus, surface inversions are common over land prior to sunrise and in winter over high-latitude continental interiors. (R. Huschke, 1959, p. 559)

**Surface Pressure ( $p$ ).** The atmospheric pressure at a given location on the earth's surface. (R. Huschke, 1959, p. 559)

**Surface Temperature ( $T$ ).** The temperature of the air near the surface of the earth, almost invariably determined by a thermometer in an instrument shelter (i.e. a Stevenson screen) (R. Huschke, 1959, p. 560)

**Surface Vertical Temperature Gradient ( $dT/dh$ ).** The rate of change of temperature with height above the surface (a temperature inversion has a positive vertical temperature gradient).

**Terrestrial Refraction.** The displacement of the image of the local horizon due to refraction of the light from the horizon through the atmosphere between the observer and the horizon ( $R_t$  in Figure 2.1.2 and 2.5.1).

**Zero Horizon.** A hypothetical horizon with an altitude of  $0^\circ$  (see Figure 1.1.1, 1.1.2, 2.1.2 and 2.1.3).

**APPENDIX B:**  
**STATISTICAL METHODS**

Error propagation was based on the general formula (Taylor, 1982, p. 73):

$$\delta q = \sqrt{\left(\frac{\partial q}{\partial x} \delta x\right)^2 + \dots + \left(\frac{\partial q}{\partial z} \delta z\right)^2} \quad (\text{B.1})$$

Where,  $q$ , is a function of several variables  $x, \dots, z$ , with their corresponding uncertainties  $\delta x, \dots, \delta z$  that are independent and random.

Uncertainty in the slope,  $\sigma_B$ , and intercept,  $\sigma_A$ , of a line produced by linear regression was found using the formulae (Taylor, 1982, pp. 157-159):

$$\sigma_A^2 = \sigma_y^2 \frac{\sum x_i^2}{\Delta} \quad (\text{B.2})$$

and

$$\sigma_B^2 = N \frac{\sigma_y^2}{\Delta} \quad (\text{B.3})$$

where,  $x_i$ , are the individual values along the abscissa,  $N$ , is the number of measurements, and,  $\Delta$ , and,  $\sigma_y$ , are found through the formulae

$$\Delta = N(\sum x_i^2) - (\sum x_i)^2 \quad (\text{B.4})$$

and

$$\sigma_y^2 = \frac{1}{N-2} \sum_{i=1}^N (y_i - A - Bx_i)^2 \quad (\text{B.5})$$

where,  $y_i$ , are the values along the ordinate,  $A$ , is the intercept and,  $B$ , is the slope of the line.

All linear regression analysis and correlation coefficients were performed using routines included in Quattro Pro for Windows, version 5.0.

## APPENDIX C:

### FINDING THE DISTANCE TO THE LOCAL HORIZON

The altitude  $a$  of the various contour lines on the topographic map, as seen from the observing site, were found by using equation (2.4.1):

$$\sin a = -\frac{(r_c + h_2)^2 - (r_c + h_1)^2 - d^2}{2d(r_c + h_1)} \quad (\text{C.1})$$

where  $r_c$  is the mean radius of the Earth ( $6\,371\,004 \times 10^6 \text{ m}$ ),  $d$  is the distance to the contour line on the 1:50000 topographic map in m,  $h_1$  is the elevation of the observer in m and,  $h_2$  is the elevation of the contour lines in m. The distance to the point of maximum altitude indicates the approximate distance to the local horizon.

For example, the distance to the radome (azimuth  $129.5^\circ$ ) was found through the series of altitudes listed in Table C.1.

$d$ (m)	$h_2$ (m)	$a$ ( $^\circ$ )
11310	716	0.097
16500	724	0.054
17290	732	0.070
17560	739	0.091
17900	747	0.111
18320	754	0.128
18760	762	0.145
21740	754	0.080
24520	762	0.065

**Table C.1:** Altitude of contour lines. The maximum altitude occurs at 18760 m and, therefore defines the approximate distance to the local horizon. The height of the observer  $h_1$  is 687 m.

**APPENDIX D:  
SUNRISE AND SUNSET DATA**

Date (U.T.)	Time (U.T.)	$T$ (C) (event)	$p$ (mb) (event)	$dT/dh$ (C/m) (event)	$h$ (m) (event)	$T$ (C) (survey)	$p$ (mb) (survey)	$dT/dh$ (C/m) (survey)	$h$ (m) (survey)	$a$ (hor.) (deg.)	$d$ (km)	$R'$ (deg.)
12/29/90	15:49:16	-32.0	950.0			16.5	939.9	-0.0198	91	0.203	18.8	
01/02/91	15:49:40	-23.7	948.1	0.0430	46	16.5	939.9	-0.0198	91	0.203	18.8	0.871
01/03/91	15:50:45	-22.4	948.1	0.0070	296	16.5	939.9	-0.0198	91	0.203	18.8	0.696
01/04/91	15:50:32	-20.7	936.3	0.0607	122	16.5	939.9	-0.0198	91	0.203	18.8	0.718
01/06/91	15:44:56	-29.3	945.0	0.0481	108	16.5	939.9	-0.0198	91	0.203	18.8	1.273
01/08/91	15:47:40	-29.3	945.5	0.0435	69	16.5	939.9	-0.0198	91	0.203	18.8	0.834
01/09/91	15:45:01	-30.1	934.7	0.0440	140	16.5	939.9	-0.0198	91	0.203	18.8	1.075
01/10/91	15:35:54	-24.9	934.0	0.0880	104	16.5	939.9	-0.0198	91	0.203	11.4	2.082
01/11/91	15:45:11	-15.4	932.3	0.1140	84	16.5	939.9	-0.0198	91	0.203	11.4	0.899
01/12/91	15:44:30	-12.2	919.2	0.0360	120	16.5	939.9	-0.0198	91	0.203	11.4	0.860
01/14/91	15:45:00	-1.7	927.2	0.0410	213	16.5	939.9	-0.0198	91	0.203	11.4	0.600
01/20/91	15:38:15	-7.4	945.2	0.0050	76	17.0	936.7	-0.0125		0.209	11.4	0.640
01/22/91	15:36:37	-2.3	933.6	-0.0050	192	17.0	936.7	-0.0125		0.218	11.4	0.538
02/01/91	15:21:14	-0.2	921.3	0.0629	89	20.2	934.0	-0.0097	719	0.253	11.4	0.639
02/04/91	15:15:30	-2.1	928.9	0.0145	69	20.2	934.0	-0.0097	719	0.229	11.4	0.670
02/06/91	15:12:30	-1.9	935.6	0.0563	176	20.2	934.0	-0.0097	719	0.251	11.4	0.704
02/09/91	15:07:22	-8.5	946.3	0.0379	58	20.2	934.0	-0.0097	719	0.256	11.4	0.621

Table D.1: Sunrise data (see Section 3.1 for explanation).

Date (U.T.)	Time (U.T.)	$T$ (C) (event)	$P$ (mb) (event)	$dT/dh$ (C/m) (event)	$h$ (m) (event)	$T$ (C) (survey)	$p$ (mb) (survey)	$dT/dh$ (C/m) (survey)	$h$ (m) (survey)	$a$ (hor.) (deg.)	$d$ (km)	$R'$ (deg.)
02/11/91	15:02:51	-2.8	932.1	0.0588	114	20.2	934.0	-0.0097	719	0.270	11.4	0.568
02/25/91	14:32:59	-5.8	947.1	0.0316	76	22.2	933.0	-0.0216	37	0.307	11.4	0.682
03/01/91	14:23:17	-27.6	936.2	0.0059	606	23.3	937.3	-0.0103	1040	0.197	11.4	0.569
03/05/91	14:13:28	-18.3	917.5	0.0810	126	23.3	937.3	-0.0103	1040	0.170	11.4	0.652
03/09/91	14:04:55	-6.6	926.5	0.0197	61	23.3	937.3	-0.0103	1040	0.164	11.4	0.537
03/11/91	13:59:14	-18.3	927.5	0.0000	82	23.3	937.3	-0.0103	1040	0.135	11.4	0.587
03/13/91	13:53:31	-13.0	931.0	0.0666	16	23.3	937.3	-0.0103	1040	0.129	11.4	0.815
03/14/91	13:51:34	-5.8	928.8	0.0596	94	23.3	937.3	-0.0103	1040	0.118	11.4	0.732
03/19/91	13:39:20	-2.4	920.7	0.0250	252	24.4	938.6	-0.0125		0.100	11.4	0.722
03/20/91	13:37:20	-3.2	921.2	0.0331	124	24.4	938.6	-0.0125		0.111	11.4	0.672
03/26/91	13:22:33	-11.7	932.0	0.0301	83	24.4	938.6	-0.0125		0.104	11.4	0.693
03/29/91	13:15:23	-2.0	930.1	0.0359	131	24.4	938.6	-0.0125		0.089	11.4	0.660
03/30/91	13:13:27	0.7	933.0	0.0086	185	24.4	938.6	-0.0125		0.089	11.4	0.579
03/31/91	13:09:44	1.5	935.3	0.0792	53	24.4	938.6	-0.0125		0.089	11.4	0.791
04/01/91	13:04:30	2.2	926.3	0.0563	71	24.4	938.6	-0.0125		0.089	11.4	1.194
04/02/91	13:07:10	3.7	930.7	0.0225	89	24.4	938.6	-0.0125		0.050	11.4	0.420
04/04/91	13:01:09	1.6	922.1	0.0117	171	24.4	938.6	-0.0125		0.040	25.7	0.574

Table D.1: Sunrise data (see Section 3.1 for explanation).

Date (U.T.)	Time (U.T.)	$T$ (C) (event)	$P$ (mb) (event)	$dT/dh$ (C/m) (event)	$h$ (m) (event)	$T$ (C) (survey)	$P$ (mb) (survey)	$dT/dh$ (C/m) (survey)	$h$ (m) (survey)	$a$ (hor.) (deg.)	$d$ (km)	$R'$ (deg.)
04/05/91	12:57:35	-0.8	924.1	0.0430	79	24.4	938.6	-0.0125		0.031	25.7	0.758
04/08/91	12:50:57	-1.9	936.1	0.0281	96	24.4	938.6	-0.0125		0.019	25.7	0.659
04/09/91	12:48:50	-1.1	932.1	0.0508	61	24.4	938.6	-0.0125		0.019	25.7	0.638
04/12/91	12:41:30	1.2	947.2	0.0647	34	24.4	938.6	-0.0125		-0.005	25.7	0.662
04/13/91	12:39:38	4.3	935.6	0.0354	79	21.8	932.0	-0.0099	705	0.028	25.7	0.604
04/14/91	12:37:10	4.9	931.5	0.0083	144	21.8	932.0	-0.0099	705	-0.019	25.7	0.557
04/15/91	12:33:30	-0.9	937.5	0.0060	166	21.8	932.0	-0.0099	705	-0.019	25.7	0.748
04/16/91	12:31:35	-3.2	940.7	0.0590	61	21.8	932.0	-0.0099	705	-0.019	25.7	0.733
04/17/91	12:28:54	-2.2	942.2	0.0321	140	21.8	932.0	-0.0099	705	-0.020	25.7	0.766
04/18/91	12:27:32	1.7	941.5	0.0389	95	21.8	932.0	-0.0099	705	-0.020	25.7	0.642
04/19/91	12:25:11	1.5	939.0	0.0800	35	21.8	932.0	-0.0099	705	-0.029	25.7	0.674
04/21/91	12:19:46	3.0	934.9	0.0479	71	21.8	932.0	-0.0099	705	-0.052	25.7	0.754
04/22/91	12:18:04	7.0	928.5	0.0441	127	21.8	932.0	-0.0099	705	-0.053	25.7	0.677
04/23/91	12:15:30	5.9	924.1	0.0609	92	21.8	932.0	-0.0099	705	-0.053	25.7	0.737
04/24/91	12:13:42	4.2	920.0	0.0248	137	21.8	932.0	-0.0099	705	-0.060	25.7	0.652
04/30/91	12:00:34	-3.5	941.3	0.0153	131	16.0	938.0	-0.0097	719	-0.080	25.7	0.677
05/01/91	11:58:09	-3.5	941.6	0.0442	43	16.0	938.0	-0.0097	719	-0.099	25.7	0.727

Table D.1: Sunrise data (see Section 3.1 for explanation).



Date (U.T.)	Time (U.T.)	$T$ (C) (event)	$P$ (mb) (event)	$dT/dh$ (C/m) (event)	$h$ (m) (event)	$T$ (C) (survey)	$P$ (mb) (survey)	$dT/dh$ (C/m) (survey)	$h$ (m) (survey)	$a$ (hor.) (deg.)	$d$ (km)	$R'$ (deg.)
05/02/91	11:56:32	-0.3	942.8	0.0205	112	16.0	938.0	-0.0097	719	-0.105	25.7	0.648
05/04/91	11:52:16	-1.0	941.8	0.0282	149	16.0	938.0	-0.0097	719	-0.124	25.7	0.669
05/07/91	11:46:51	-0.2	933.2	0.0292	178	16.0	938.0	-0.0097	719	-0.126	25.7	0.617
05/08/91	11:44:50	3.3	924.2	0.0174	321	16.0	938.0	-0.0097	719	-0.126	25.7	0.624
05/11/91	11:39:11	7.5	937.9	0.0933	45	16.0	938.0	-0.0097	719	-0.119	25.7	0.705
05/12/91	11:37:36	12.0	929.7	0.0537	82	16.0	935.3	-0.0098	706	-0.123	25.7	0.649
05/16/91	11:30:20	6.6	935.6	0.0476	63	16.0	935.3	-0.0098	706	-0.158	25.7	0.677
05/17/91	11:29:11	8.6	938.0	-0.0055	219	16.0	935.3	-0.0098	706	-0.176	25.7	0.568
05/20/91	11:23:41	9.2	928.0	0.0409	166	16.0	935.3	-0.0098	706	-0.213	25.7	0.673
05/27/91	11:14:36	7.5	932.4	0.0247	154	16.0	935.3	-0.0098	706	-0.218	25.7	0.639
05/29/91	11:08:32	10.8	926.3	0.0437	119	16.0	935.3	-0.0098	706	-0.232	25.7	1.067
05/30/91	11:08:28	7.8	920.0	0.0747	83	16.0	935.3	-0.0098	706	-0.232	25.7	0.977
05/31/91	11:08:09	10.2	928.1	0.0506	83	16.0	935.3	-0.0098	706	-0.232	25.7	0.883
06/05/91	11:04:00	4.6	942.6	0.0206	97	16.5	940.9	-0.0170	211	-0.242	25.7	0.847
07/29/91	11:42:38	10.7	936.6			16.0	938.0	-0.0097	719	-0.135	25.7	
07/31/91	11:45:58	9.5	938.1	0.0689	91	16.0	938.0	-0.0097	719	-0.135	25.7	0.648
08/07/91	11:57:58	12.9	934.3	0.0020	394	16.0	938.0	-0.0097	719	-0.124	25.7	0.583

Table D.1: Sunrise data (see Section 3.1 for explanation).

Date (U.T.)	Time (U.T.)	$T$ (C) (event)	$p$ (mb) (event)	$dT/dh$ (C/m) (event)	$h$ (m) (event)	$T$ (C) (survey)	$p$ (mb) (survey)	$dT/dh$ (C/m) (survey)	$h$ (m) (survey)	$a$ (hor.) (deg.)	$d$ (km)	$R'$ (deg.)
08/09/91	12:00:38	16.9	934.5	0.0291	151	16.0	938.0	-0.0097	719	-0.120	25.7	0.703
08/10/91	12:03:16	16.1	931.1	-0.0046	347	16.0	938.0	-0.0097	719	-0.127	25.7	0.557
08/13/91	12:08:15	14.9	936.4	-0.0028	575	16.0	938.0	-0.0097	719	-0.120	25.7	0.594
08/14/91	12:10:20	13.1	936.0	0.0226	195	16.0	938.0	-0.0097	719	-0.099	25.7	0.587
08/21/91	12:22:42	12.7	935.7	0.0217	138	21.8	932.0	-0.0099	705	-0.053	25.7	0.616
08/26/91	12:31:28	8.1	926.9	0.0605	119	21.8	932.0	-0.0099	705	-0.012	25.7	0.684
08/30/91	12:38:35	11.2	933.6	0.0538	130	21.8	932.0	-0.0099	705	0.028	25.7	0.702
09/03/91	12:45:48	6.4	945.0	0.1077	26	24.4	938.6	-0.0125	705	0.019	25.7	0.703
09/07/91	12:53:04	8.4	929.1	0.0023	428	24.4	938.6	-0.0125	705	0.027	11.4	0.588
09/10/91	12:58:25	1.3	943.5	0.0490	98	24.4	938.6	-0.0125	705	0.052	11.4	0.611
09/11/91	12:59:38	6.2	935.5	0.0556	72	24.4	938.6	-0.0125	705	0.089	11.4	0.726
09/17/91	13:10:58	-3.1	951.5	0.0138	94	24.4	938.6	-0.0125	705	0.113	11.4	0.612
09/19/91	13:13:42	5.8	932.8	0.1037	54	24.4	938.6	-0.0125	705	0.121	11.4	0.759
09/22/91	13:18:23	0.2	942.9	0.0135	282	24.4	938.6	-0.0125	705	0.091	11.4	0.787
09/24/91	13:23:27	10.5	936.1	0.0218	239	24.4	938.6	-0.0125	705	0.094	11.4	0.562
09/26/91	13:25:13	7.3	937.6	0.0913	46	24.4	938.6	-0.0125	705	0.100	11.4	0.850
09/27/91	13:28:41	7.4	934.2	0.0250	312	24.4	938.6	-0.0125	705	0.110	11.4	0.589

Table D.1: Sunrise data (see Section 3.1 for explanation).

Date (U.T.)	Time (U.T.)	$T$ (C) (event)	$P$ (mb) (event)	$dT/dh$ (C/m) (event)	$h$ (m) (event)	$T$ (C) (survey)	$P$ (mb) (survey)	$dT/dh$ (C/m) (survey)	$h$ (m) (survey)	$a$ (hor.) (deg.)	$d$ (km)	$R'$ (deg.)
09/28/91	13:30:46	12.6	929.6	0.0645	121	24.4	938.6	-0.0125		0.120	11.4	0.564
10/02/91	13:37:57	3.1	934.0	0.0106	151	23.3	937.3	-0.0103	1040	0.149	11.4	0.569
10/03/91	13:40:05	1.8	935.6	0.0034	177	23.3	937.3	-0.0103	1040	0.149	11.4	0.517
10/04/91	13:41:39	0.0	945.0	-0.0026	350	23.3	937.3	-0.0103	1040	0.156	11.4	0.556
10/08/91	13:48:45	0.8	936.7	0.0333	114	23.3	937.3	-0.0103	1040	0.172	11.4	0.603
10/09/91	13:50:45	6.0	936.2	0.0157	153	23.3	937.3	-0.0103	1040	0.172	11.4	0.571
10/10/91	13:52:14	8.2	936.0	0.0764	55	23.3	937.3	-0.0103	1040	0.197	11.4	0.664
10/11/91	13:54:02	7.8	934.1	0.1108	83	23.3	937.3	-0.0103	1040	0.197	11.4	0.679
10/18/91	14:07:20	-9.3	942.2	0.0538	93	23.3	937.3	-0.0103	1040	0.241	11.4	0.663
10/19/91	14:09:42	2.2	939.4	0.0105	114	23.3	937.3	-0.0103	1040	0.241	11.4	0.577
10/23/91	14:17:52	-12.3	929.1	0.0333	84	22.2	933.0	-0.0216	37	0.326	11.4	0.590
10/28/91	14:26:29	-17.6	944.7	0.0515	97	22.2	933.0	-0.0216	37	0.299	11.4	0.700
10/29/91	14:27:59	-17.8	947.7	0.0449	89	20.2	934.0	-0.0097	719	0.270	11.4	0.722
10/30/91	14:30:32	-12.7	940.9	0.0819	83	20.2	934.0	-0.0097	719	0.270	11.4	0.648
11/02/91	14:34:40	-20.7	954.3	0.0700	40	20.2	934.0	-0.0097	719	0.256	11.4	0.854
11/06/91	14:43:19	-15.8	938.4	0.0444	81	20.2	934.0	-0.0097	719	0.253	11.4	0.710
11/07/91	14:44:50	-3.6	936.8	0.0488	86	20.2	934.0	-0.0097	719	0.240	11.4	0.748

Table D.1: Sunrise data (see Section 3.1 for explanation).

Date (U.T.)	Time (U.T.)	$T$ (C) (event)	$p$ (mb) (event)	$dT/dh$ (C/m) (event)	$h$ (m) (event)	$T$ (C) (survey)	$p$ (mb) (survey)	$dT/dh$ (C/m) (survey)	$h$ (m) (survey)	$a$ (hor.) (deg.)	$d$ (km)	$R'$ (deg.)
11/09/91	14:48:33	-12.5	937.6	0.0038	158	20.2	934.0	-0.0097	719	0.248	11.4	0.756
11/14/91	14:58:43	-2.7	930.8	0.0329	70	20.2	934.0	-0.0097	719	0.232	11.4	0.658
11/15/91	14:59:45	-6.2	929.9	0.0490	157	20.2	934.0	-0.0097	719	0.197	11.4	0.734
11/18/91	15:06:36	-7.2	920.6	0.0068	293	20.2	934.0	-0.0097	719	0.209	11.4	0.567
11/19/91	15:07:12	-5.3	932.6	0.0410	78	20.2	934.0	-0.0097	719	0.209	11.4	0.730
12/10/91	15:40:19	-4.6	921.9	0.0000	365	16.5	939.9	-0.0198	91	0.205	18.8	0.608
12/11/91	15:41:57	-3.9	912.2	0.0258	89	16.5	939.9	-0.0198	91	0.201	18.8	0.559
12/13/91	15:43:08	-14.0	938.1	0.0051	311	16.5	939.9	-0.0198	91	0.203	18.8	0.654
12/14/91	15:44:26	-12.1	940.3	0.0047	127	16.5	939.9	-0.0198	91	0.203	18.8	0.616
12/16/91	15:46:45	-3.7	939.6	-0.0054	661	16.5	939.9	-0.0198	91	0.203	18.8	0.548
12/17/91	15:42:10	-11.3	935.6	0.0536	207	16.5	939.9	-0.0198	91	0.205	18.8	1.192
12/20/91	15:47:25	-8.2	935.7	0.0360	111	16.5	939.9	-0.0198	91	0.203	18.8	0.818
01/05/92	15:50:25	-12.4	930.9	0.0017	119	16.5	939.9	-0.0198	91	0.205	18.8	0.663
01/07/92	15:49:19	-14.2	933.2	0.0073	300	16.5	939.9	-0.0198	91	0.204	18.8	0.591
01/09/92	15:48:10	-3.7	928.8	0.0934	61	16.5	939.9	-0.0198	91	0.214	18.8	0.750
01/12/92	15:46:39	-4.9	934.9	0.0000	183	16.5	939.9	-0.0198	91	0.210	11.4	0.622
01/14/92	15:44:25	-22.1	950.7	-0.0098	368	16.5	939.9	-0.0198	91	0.217	11.4	0.694

Table D.1: Sunrise data (see Section 3.1 for explanation).

Date (U.T.)	Time (U.T.)	$T$ (C) (event)	$P$ (mb) (event)	$dT/dh$ (C/m) (event)	$h$ (m) (event)	$T$ (C) (survey)	$P$ (mb) (survey)	$dT/dh$ (C/m) (survey)	$h$ (m) (survey)	$a$ (hor.) (deg.)	$d$ (km)	$R'$ (deg.)
01/16/92	15:43:23	-12.7	941.6	-0.0068	674	16.5	939.9	-0.0198	91	0.217	11.4	0.591
01/22/92	15:35:54	-8.4	932.8	0.0042	191	17.0	936.7	-0.0125		0.218	11.4	0.668
01/27/92	15:28:32	-3.1	922.7			17.0	936.7	-0.0125		0.197	11.4	
01/29/92	15:26:01	-3.3	929.6	0.0313	179	20.2	934.0	-0.0097	719	0.232	11.4	0.673
02/03/92	15:17:39	-3.2	938.5			17.0	936.7	-0.0125		0.248	11.4	
02/04/92	15:15:24	-1.5	932.2	0.0625	80	17.0	936.7	-0.0125		0.229	11.4	0.754
02/05/92	15:14:08	-4.3	936.4	0.0034	148	20.2	934.0	-0.0097	719	0.218	11.4	0.654
02/06/92	15:12:07	-9.0	940.5	0.0155	181	20.2	934.0	-0.0097	719	0.235	11.4	0.701
02/07/92	15:10:13	-16.6	939.7	0.0190	168	20.2	934.0	-0.0097	719	0.251	11.4	0.727
02/12/92	15:01:23	-17.7	934.5			20.2	934.0	-0.0097	719	0.270	11.4	
02/23/92	14:37:32	-9.9	933.4	0.0279	138	23.3	937.3	-0.0103	1040	0.241	11.4	0.684
02/28/92	14:26:02	2.2	935.0	0.0986	71	23.3	937.3	-0.0103	1040	0.232	11.4	0.729
02/29/92	14:24:02	1.4	924.1	0.0557	183	23.3	937.3	-0.0103	1040	0.197	11.4	0.637
03/01/92	14:22:18	-1.3	930.0	-0.0027	634	23.3	937.3	-0.0103	1040	0.197	11.4	0.536
03/02/92	14:19:45	-1.8	930.5	0.0264	148	23.3	937.3	-0.0103	1040	0.197	11.4	0.579
03/03/92	14:16:38	-1.8	931.6	0.0545	44	23.3	937.3	-0.0103	1040	0.172	11.4	0.677
03/05/92	14:12:21	-6.0	929.4	0.0570	142	23.3	937.3	-0.0103	1040	0.168	11.4	0.616

Table D.1: Sunrise data (see Section 3.1 for explanation).

Date (U.T.)	Time (U.T.)	$T$ (C) (event)	$P$ (mb) (event)	$dT/dh$ (C/m) (event)	$h$ (m) (event)	$T$ (C) (survey)	$P$ (mb) (survey)	$dT/dh$ (C/m) (survey)	$h$ (m) (survey)	$a$ (hor.) (deg.)	$d$ (km)	$R'$ (deg.)
03/08/92	14:04:39	-11.7	943.0	0.0172	116	23.3	937.3	-0.0103	1040	0.164	11.4	0.688
03/09/92	14:02:26	-5.6	938.2	0.0409	93	23.3	937.3	-0.0103	1040	0.156	11.4	0.662
03/12/92	13:55:35	3.3	935.3	0.0149	107	23.3	937.3	-0.0103	1040	0.135	11.4	0.582
03/13/92	13:53:01	2.2	940.7	0.0076	53	23.3	937.3	-0.0103	1040	0.129	11.4	0.597
03/15/92	13:48:17	1.8	931.4	0.0126	318	23.3	937.3	-0.0103	1040	0.118	11.4	0.573
03/16/92	13:45:43	-3.7	938.1	-0.0065	402	23.3	937.3	-0.0103	1040	0.092	11.4	0.563
03/22/92	13:29:13	-1.0	930.6	0.0617	107	24.4	938.6	-0.0125		0.111	11.4	0.890
03/24/92	13:26:17	-4.6	942.5	-0.0007	267	24.4	938.6	-0.0125		0.115	11.4	0.588
03/26/92	13:20:36	-0.9	929.5	0.0503	143	24.4	938.6	-0.0125		0.104	11.4	0.714
03/27/92	13:17:12	1.1	919.5	0.0762	63	24.4	938.6	-0.0125		0.103	11.4	0.863
03/30/92	13:11:11	-6.3	945.1	0.0260	77	24.4	938.6	-0.0125		0.089	11.4	0.649
04/01/92	13:06:44	3.9	940.2	0.0302	106	24.4	938.6	-0.0125		0.089	11.4	0.592
04/02/92	13:03:46	6.3	931.1	0.0624	109	24.4	938.6	-0.0125		0.052	11.4	0.645
04/03/92	12:59:30	6.4	917.6	0.0431	102	24.4	938.6	-0.0125		0.040	11.4	0.897
04/04/92	12:58:44	-1.1	928.1	0.0315	89	24.4	938.6	-0.0125		0.031	25.7	0.668
04/10/92	12:44:25	-15.9	938.5	0.0024	82	24.4	938.6	-0.0125		0.019	25.7	0.645
04/12/92	12:40:00	-5.0	933.3	0.0101	179	24.4	938.6	-0.0125		0.014	25.7	0.605

Table D.1.: Sunrise data (see Section 3.1 for explanation).

Date (U.T.)	Time (U.T.)	$T$ (C) (event)	$p$ (mb) (event)	$dT/dh$ (C/m) (event)	$h$ (m) (event)	$T$ (C) (survey)	$p$ (mb) (survey)	$dT/dh$ (C/m) (survey)	$h$ (m) (survey)	$\alpha$ (hor.) (deg.)	$d$ (km)	$R'$ (deg.)
04/13/92	12:37:24	-0.9	930.4	0.1308	26	21.8	932.0	-0.0099	705	0.028	25.7	0.743
04/15/92	12:32:44	5.0	936.7	0.0055	438	21.8	932.0	-0.0099	705	-0.019	25.7	0.608
05/01/92	11:57:27	3.8	928.8	-0.0059	639	16.0	938.0	-0.0097	719	-0.099	25.7	0.578
05/02/92	11:54:48	4.0	936.8			16.0	938.0	-0.0097	719	-0.117	25.7	
05/03/92	11:53:01	6.3	942.4	0.0328	116	16.0	938.0	-0.0097	719	-0.120	25.7	0.640
05/25/92	11:16:05	6.8	940.0	0.0135	113	16.0	935.3	-0.0098	706	-0.218	25.7	0.633
05/26/92	11:14:20	6.9	930.5	0.0011	190	16.0	935.3	-0.0098	706	-0.218	25.7	0.687
05/28/92	11:11:42	7.2	930.3	0.0192	219	16.0	935.3	-0.0098	706	-0.224	25.7	0.735
05/29/92	11:09:10	5.8	933.4	0.0424	118	16.0	935.3	-0.0098	706	-0.232	25.7	0.908
06/10/92	11:03:06	10.6	928.2	0.0030	401	16.5	940.9	-0.0170	211	-0.242	25.7	0.583
06/11/92	11:02:09	9.8	940.3	-0.0023	607	16.5	940.9	-0.0170	211	-0.242	25.7	0.643
06/12/92	11:01:06	11.1	940.5	0.0090	201	16.5	940.9	-0.0170	211	-0.242	25.7	0.729
06/14/92	11:01:10	12.9	939.8	0.0000	191	16.5	940.9	-0.0170	211	-0.242	25.7	0.668
06/17/92	11:01:47	14.2	930.1	0.0016	383	16.5	940.9	-0.0170	211	-0.242	25.7	0.578
06/19/92	11:01:02	12.0	937.7	0.0083	72	16.5	940.9	-0.0170	211	-0.246	25.7	0.672
06/21/92	10:59:52	13.3	936.1	0.0396	101	16.5	940.9	-0.0170	211	-0.246	25.7	0.856
06/22/92	10:57:50	11.1	937.5	0.0482	83	16.5	940.9	-0.0170	211	-0.246	25.7	1.102

Table D.1: Sunrise data (see Section 3.1 for explanation).

Date (U.T.)	Time (U.T.)	$T$ (C) (event)	$P$ (mb) (event)	$dT/dh$ (C/m) (event)	$h$ (m) (event)	$T$ (C) (survey)	$P$ (mb) (survey)	$dT/dh$ (C/m) (survey)	$h$ (m) (survey)	$a$ (hor.) (deg.)	$d$ (km)	$R'$ (deg.)
06/24/92	10:59:10	9.3	935.0	0.0712	73	16.5	940.9	-0.0170	211	-0.246	25.7	1.052
06/28/92	11:03:16	6.7	940.1	0.0057	282	16.5	940.9	-0.0170	211	-0.246	25.7	0.793
06/29/92	11:03:12	8.7	935.5	0.0467	90	16.5	940.9	-0.0170	211	-0.246	25.7	0.896
07/20/92	11:27:17	9.0	942.4	0.1444	18	16.0	938.0	-0.0097	719	-0.218	25.7	0.929
07/21/92	11:28:39	12.6	934.7	0.0245	277	16.0	938.0	-0.0097	719	-0.218	25.7	0.859
07/24/92	11:34:32	12.2	933.8	0.0985	65	16.0	938.0	-0.0097	719	-0.213	25.7	0.761
07/27/92	11:40:29	10.0	936.7	0.0563	64	16.0	938.0	-0.0097	719	-0.158	25.7	0.644
08/06/92	11:57:07	11.1	930.0	0.0265	196	16.0	938.0	-0.0097	719	-0.124	25.7	0.656
08/11/92	12:04:52	7.1	947.0			16.0	938.0	-0.0097	719	-0.124	25.7	
08/13/92	12:08:38	16.1	938.2	0.0860	93	16.0	938.0	-0.0097	719	-0.120	25.7	0.776
08/14/92	12:10:58	15.1	933.6	0.0128	47	16.0	938.0	-0.0097	719	-0.099	25.7	0.672
08/17/92	12:15:09	10.8	940.9	0.0767	73	16.0	938.0	-0.0097	719	-0.081	25.7	0.878
08/25/92	12:31:14	3.0	939.8	0.0385	96	21.8	932.0	-0.0099	705	-0.012	25.7	0.646
09/03/92	12:47:06	4.9	933.6	0.0320	125	24.4	938.6	-0.0125		0.019	25.7	0.654
09/14/92	13:07:15	-2.2	930.1	-0.0065	643	24.4	938.6	-0.0125		0.090	11.4	0.553
09/15/92	13:08:58	-2.7	933.8	0.0385	96	24.4	938.6	-0.0125		0.103	11.4	0.585
09/16/92	13:10:22	-1.5	930.6	0.0188	96	24.4	938.6	-0.0125		0.113	11.4	0.639

Table D.1: Sunrise data (see Section 3.1 for explanation).



Date (U.T.)	Time (U.T.)	$T$ (C)	$p$ (mb)	$\Delta T/dh$ (C/m)	$h$ (m)	$T$ (C)	$p$ (mb)	$dT/dh$ (C/m)	$h$ (m)	$a$ (hor.) (deg.)	$d$ (km)	$R'$ (deg.)
		(event)	(event)	(event)	(event)	(survey)	(survey)	(survey)	(survey)			
09/24/92	13:24:50	9.1	912.5	0.0160	225	22.2	933.0	-0.0216	37	0.110	11.4	0.572
09/26/92	13:27:53	-2.3	933.6	0.0149	87	22.2	933.0	-0.0216	37	0.118	11.4	0.653
09/27/92	13:30:06	-1.8	941.3	0.0103	87	23.3	937.3	-0.0103	1040	0.129	11.4	0.593
09/29/92	13:33:04	9.0	930.8	0.0459	157	23.3	937.3	-0.0103	1040	0.135	11.4	0.695
10/01/92	13:37:36	13.6	930.8	0.0388	129	23.3	937.3	-0.0103	1040	0.131	11.4	0.546
10/03/92	13:41:24	7.7	933.3	0.0452	93	23.3	937.3	-0.0103	1040	0.149	11.4	0.536
10/22/92	14:17:30	2.9	933.5	0.0448	116	23.3	937.3	-0.0103	1040	0.319	11.4	0.567
10/25/92	14:22:56	0.3	939.2	0.0182	132	23.3	937.3	-0.0103	1040	0.309	11.4	0.589
11/10/92	14:52:39	-4.5	925.9	0.0190	210	20.2	934.0	-0.0097	719	0.225	11.4	0.638
11/12/92	14:57:04	-4.6	943.1	-0.0062	642	20.2	934.0	-0.0097	719	0.232	11.4	0.564
11/24/92	15:17:27	-6.4	935.4	0.0302	86	16.5	939.9	-0.0198	91	0.220	11.4	0.721
11/26/92	15:19:20	-8.6	942.4	0.1012	86	16.5	939.9	-0.0198	91	0.220	11.4	0.920
11/29/92	15:24:50	-4.2	930.8	0.0416	113	16.5	939.9	-0.0198	91	0.217	11.4	0.809
12/01/92	15:29:17	-4.6	935.9	-0.0068	558	16.5	939.9	-0.0198	91	0.214	11.4	0.624
12/03/92	15:31:51	-12.3	938.1	0.0373	118	16.5	939.9	-0.0198	91	0.214	18.8	0.693
12/04/92	15:32:30	-7.5	934.6	0.0705	112	16.5	939.9	-0.0198	91	0.204	18.8	0.785
12/05/92	15:34:47	-3.1	929.4	0.0497	151	16.5	939.9	-0.0198	91	0.204	18.8	0.664

Table D.1: Sunrise data (see Section 3.1 for explanation).

Date (U.T.)	Time (U.T.)	$T$ (C) (event)	$p$ (mb) (event)	$dT/dh$ (C/m) (event)	$h$ (m) (event)	$T$ (C) (survey)	$p$ (mb) (survey)	$dT/dh$ (C/m) (survey)	$h$ (m) (survey)	$a$ (hor.) (deg.)	$d$ (km)	$R'$ (deg.)
12/06/92	15:36:19	-11.7	931.5	0.0085	213	16.5	939.9	-0.0198	91	0.204	18.8	0.618
12/13/92	15:42:51	-12.1	935.8	0.0549	91	16.5	939.9	-0.0198	91	0.207	18.8	0.801
12/18/92	15:46:56	-27.6	933.2	0.0256	78	16.5	939.9	-0.0198	91	0.203	18.8	0.782
12/19/92	15:47:56	-19.0	928.2	0.0289	83	16.5	939.9	-0.0198	91	0.203	18.8	0.741
12/30/92	15:51:06	-30.8	950.8	-0.0110	91	16.5	939.9	-0.0198	91	0.206	18.8	0.713
12/31/92	15:50:07	-31.9	946.9	0.0438	192	16.5	939.9	-0.0198	91	0.207	18.8	0.853
01/02/93	15:51:10	-16.1	928.0	0.0006	193	16.5	939.9	-0.0198	91	0.207	18.8	0.659
01/05/93	15:49:29	-27.7	942.6	0.0222	117	16.5	939.9	-0.0198	91	0.204	18.8	0.750
01/09/93	15:45:45	-27.4	945.9	0.1818	77	16.5	939.9	-0.0198	91	0.214	11.4	0.997
01/10/93	15:45:39	-22.2	933.5	0.0083	72	16.5	939.9	-0.0198	91	0.215	11.4	0.858
01/14/93	15:41:20	-27.9	934.1	0.1742	31	16.5	939.9	-0.0198	91	0.215	11.4	1.051
01/15/93	15:42:39	-10.7	921.6	0.0912	148	16.5	939.9	-0.0198	91	0.215	11.4	0.738
01/17/93	15:39:34	-16.0	930.6	0.0784	102	16.5	939.9	-0.0198	91	0.220	11.4	0.864
01/18/93	15:38:25	-11.8	926.4			16.5	939.9	-0.0198	91	0.220	11.4	
01/20/93	15:36:53	-3.0	915.8	0.0516	62	16.5	939.9	-0.0198	91	0.209	11.4	0.745
01/21/93	15:36:54	-4.6	922.1	-0.0043	141	17.0	936.7	-0.0125		0.220	11.4	0.581
01/22/93	15:34:50	-8.7	927.6	0.0375	112	17.0	936.7	-0.0125		0.218	11.4	0.689

Table D.1: Sunrise data (see Section 3.1 for explanation).

Date (U.T.)	Time (U.T.)	$T$ (C) (event)	$p$ (mb) (event)	$dT/dh$ (C/m) (event)	$h$ (m) (event)	$T$ (C) (survey)	$p$ (mb) (survey)	$dT/dh$ (C/m) (survey)	$h$ (m) (survey)	$a(\text{hor.})$ (deg.)	$d$ (km)	$R'$ (deg.)
01/24/93	15:31:55	-13.6	927.7	0.0200	160	17.0	936.7	-0.0125		0.214	11.4	0.704
01/28/93	15:25:09	-19.9	942.0	0.0938	81	17.0	936.7	-0.0125		0.232	11.4	0.859
01/29/93	15:24:18	-6.5	933.2	0.0484	308	20.2	934.0	-0.0097	719	0.230	11.4	0.743
02/01/93	15:20:15	0.6	931.6	0.0950	80	20.2	934.0	-0.0097	719	0.248	11.4	0.657
02/02/93	15:17:27	-3.6	939.9	0.0582	122	17.0	936.7	-0.0125		0.248	11.4	0.788
02/06/93	15:10:36	-6.6	933.3	0.0190	42	20.2	934.0	-0.0097	719	0.248	11.4	0.730
02/07/93	15:08:57	-4.0	932.7	0.0626	115	20.2	934.0	-0.0097	719	0.253	11.4	0.719
02/08/93	15:06:12	-3.4	928.7			22.2	933.0	-0.0216	37	0.256	11.4	
02/12/93	14:59:34	-12.8	934.2	0.0676	136	22.2	933.0	-0.0216	37	0.283	11.4	0.705
02/15/93	14:53:58	-22.6	949.2	0.0077	104	22.2	933.0	-0.0216	37	0.305	11.4	0.631
02/16/93	14:51:45	-21.3	949.4	0.0177	79	22.2	933.0	-0.0216	37	0.309	11.4	0.655
02/17/93	14:49:04	-21.7	941.9	0.0854	89	22.2	933.0	-0.0216	37	0.309	11.4	0.760
02/23/93	14:36:31	-19.8	941.8	0.0315	89	22.2	933.0	-0.0216	37	0.307	11.4	0.662
10/20/93	14:12:57	-2.6	943.1	0.0152	112	23.3	937.3	-0.0103	1040	0.309	11.4	0.591
10/23/93	14:18:58	4.1	931.2	0.0556	54	23.3	937.3	-0.0103	1040	0.309	11.4	0.556
10/29/93	14:29:37	-7.9	942.4	0.0522	92	23.3	937.3	-0.0103	1040	0.256	11.4	0.619
11/05/93	14:42:02	-12.9	944.5	0.0418	91	20.2	934.0	-0.0097	719	0.270	11.4	0.771

Table D.1: Sunrise data (see Section 3.1 for explanation).

Date (U.T.)	Time (U.T.)	$T$ (C)	$T$ (event)	$p$ (mb)	$dT/dh$ (C/m)	$h$ (m)	$h$ (event)	$T$ (C)	$p$ (mb)	$dT/dh$ (C/m)	$h$ (m)	$a$ (hor.) (deg.)	$d$ (km)	$R'$ (deg.)
11/17/93	15:04:29	-6.9	929.4	0.0471	121	20.2	934.0	-0.0097	719	0.214	11.4	0.738		
11/24/93	15:15:00	-18.3	946.7	0.0827	191	16.5	939.9	-0.0198	91	0.220	11.4	0.989		
11/25/93	15:10:14	-14.3	944.4	0.1586	58	16.5	939.9	-0.0198	91	0.209	11.4	1.788		
11/26/93	15:12:00	-8.1	935.6	0.0456	121	16.5	939.9	-0.0198	91	0.209	11.4	1.728		
12/08/93	15:37:55	-8.2	918.0	0.0308	26	16.5	939.9	-0.0198	91	0.207	18.8	0.699		
12/17/93	15:46:18	-12.4	938.6			16.5	939.9	-0.0198	91	0.203	18.8			

Table D.1: Sunrise data (see Section 3.1 for explanation).

Date (U.T.)	Time (U.T.)	$T$ (C) (event)	$p$ (mb) (event)	$dT/dh$ (C/m) (event)	$h$ (m) (event)	$T$ (C) (survey)	$p$ (mb) (survey)	$dT/dh$ (C/m) (survey)	$h$ (m) (survey)	$a$ (hor.) (deg.)	$d$ (km)	$R'$ (deg.)
04/05/91	02:13:33	7.9	924.4			18.5	935.3	-0.0093		0.060	15.8	
04/12/91	02:26:36	7.9	949.3	-0.0108	831	20.7	930.1	-0.0118	692	0.033	15.8	0.525
04/14/91	02:30:14	13.3	929.7	-0.0239	92	20.7	930.1	-0.0118	692	0.025	15.8	0.508
04/15/91	02:32:11	9.5	933.7	-0.0301	73	18.5	935.3	-0.0093		0.040	15.8	0.538
04/16/91	02:33:50	5.3	938.3	-0.0100	643	18.5	935.3	-0.0093		0.040	15.8	0.523
04/17/91	02:35:41	7.5	940.4	-0.0101	99	18.5	935.3	-0.0093		0.040	15.8	0.526
04/18/91	02:37:43	8.0	941.5	-0.0149	188	18.5	935.3	-0.0093		0.039	15.8	0.553
04/19/91	02:39:11	10.4	939.0	-0.0123	486	18.5	935.3	-0.0093		0.050	15.4	0.516
04/20/91	02:40:41	14.7	933.5	-0.0143	335	18.5	935.3	-0.0093		0.060	36.4	0.479
04/21/91	02:42:24	11.9	934.0	-0.0378	37	18.5	935.3	-0.0093		0.060	36.4	0.443
05/01/91	03:01:28	7.0	936.2			18.5	935.3	-0.0093		-0.005	11.6	
05/03/91	03:04:59	7.8	940.3	-0.0115	556	18.5	935.3	-0.0093		-0.014	11.6	0.509
09/03/91	02:21:06	12.3	941.2	-0.0188	64	18.5	935.3	-0.0093		0.039	15.8	0.489
09/09/91	02:06:36	7.4	943.2	-0.0104	770	18.5	935.3	-0.0093		0.072	15.8	0.519
09/11/91	02:01:54	13.4	937.6	-0.0108	723	18.5	935.3	-0.0093		0.060	15.8	0.528
03/21/92	01:48:06	4.2	935.6	-0.0098	702	16.5	940.9	-0.0170	211	0.036	14.0	0.578
03/22/92	01:49:43	8.8	930.2	-0.0105	664	16.5	940.9	-0.0170	211	0.021	14.0	0.528

Table D.2: Sunset data (see Section 3.1 for explanation).

Date (U.T.)	Time (U.T.)	T (C) (event)	P (mb) (event)	dT/dh (C/m) (event)	h (m) (event)	T (C) (survey)	P (mb) (survey)	dT/dh (C/m) (survey)	h (m) (survey)	a(hor.) (deg.)	d (km)	R' (deg.)
03/23/92	01:51:36	10.2	928.1	-0.0099	646	16.5	940.9	-0.0170	211	0.025	14.0	0.539
04/04/92	02:13:10	6.9	925.5	-0.0100	603	18.5	935.3	-0.0093		0.065	15.8	0.526
04/12/92	02:28:38	-7.5	941.5	-0.0115	296	20.7	930.1	-0.0118	692	0.041	15.8	0.627
04/13/92	02:30:17	5.3	929.3	-0.0067	269	20.7	930.1	-0.0118	692	0.025	15.8	0.585
04/19/92	02:40:34	3.5	938.3	-0.0080	676	18.5	935.3	-0.0093		0.049	36.4	0.520
05/02/92	03:04:40	10.8	934.5	-0.0198	91	16.5	939.9	-0.0198	91	-0.014	11.6	0.524
08/11/92	03:11:33	15.5	944.9			16.5	939.9	-0.0198	91	-0.020	11.6	
08/12/92	03:09:22	20.9	943.0			16.5	939.9	-0.0198	91	-0.005	11.6	
08/15/92	03:02:41	24.6	935.2	-0.0020	201	16.5	939.9	-0.0198	91	0.024	36.4	0.512
08/17/92	02:58:08	17.9	939.3	-0.0234	94	16.5	939.9	-0.0198	91	0.060	36.4	0.499
08/18/92	02:55:53	27.3	933.0	-0.0107	748	16.5	939.9	-0.0198	91	0.052	36.4	0.489
08/26/92	02:38:20	17.3	935.1	-0.0080	728	18.5	935.3	-0.0093		0.039	15.8	0.528
09/03/92	02:19:07	11.8	931.6	-0.0102	684	18.5	935.3	-0.0093		0.039	15.8	0.468
09/14/92	01:53:12	2.3	930.8	-0.0106	650	16.5	940.9	-0.0170	211	0.012	14.0	0.548
09/15/92	01:50:48	3.6	931.2	-0.0108	658	16.5	940.9	-0.0170	211	0.012	14.0	0.555
09/16/92	01:47:59	3.5	934.6	-0.0104	555	16.5	940.9	-0.0170	211	0.039	14.0	0.532
09/21/92	01:35:44	6.6	928.1	-0.0107	616	16.5	940.9	-0.0170	211	0.021	14.0	0.515

Table D.2: Sunset data (see Section 3.1 for explanation).

Date (U.T.)	Time (U.T.)	$T$ (C) (event)	$P$ (mb) (event)	$dT/dh$ (C/m) (event)	$h$ (m) (event)	$T$ (C) (survey)	$P$ (mb) (survey)	$dT/dh$ (C/m) (survey)	$h$ (m) (survey)	$a$ (hor.) (deg.)	$d$ (km)	$R'$ (deg.)
09/30/92	01:14:11	22.9	931.0	-0.0078	717	16.5	940.9	-0.0170	211	0.003	14.0	0.563
10/02/92	01:08:56	21.3	929.9	-0.0079	737	16.5	940.9	-0.0170	211	0.011	16.0	0.512
10/05/92	01:02:42	8.5	940.2	-0.0101	750	13.7	932.0	0.0000	128	-0.058	16.0	0.557
11/09/92	23:46:31	-0.1	931.9	-0.0084	655	13.7	932.0	0.0000	128	-0.077	16.0	0.580
11/23/92	23:28:38	-8.4	937.4	0.0238	294	13.7	932.0	0.0000	128	-0.099	16.0	0.823
11/30/92	23:20:01	2.6	923.4	-0.0077	557	13.7	932.0	0.0000	128	-0.087	16.0	0.571
12/01/92	23:19:29	-2.6	937.3	0.0033	182	13.7	932.0	0.0000	128	-0.090	16.0	0.597
12/02/92	23:18:42	-5.9	936.9	-0.0071	677	13.7	932.0	0.0000	128	-0.088	16.0	0.581
12/03/92	23:18:20	-7.4	940.8	0.0027	300	13.7	932.0	0.0000	128	-0.088	16.0	0.615
12/04/92	23:18:36	1.8	931.2	0.0369	217	13.7	932.0	0.0000	128	-0.088	16.0	0.724
12/05/92	23:17:05	-4.1	932.7	-0.0078	359	13.7	932.0	0.0000	128	-0.095	16.0	0.578
12/06/92	23:17:02	-7.3	929.2	-0.0024	250	13.7	932.0	0.0000	128	-0.095	16.0	0.626
12/31/92	23:28:40	-27.2	941.9			13.7	932.0	0.0000	128	-0.082	16.0	
01/05/93	23:33:03	-20.1	934.5	0.0041	97	13.7	932.0	0.0000	128	-0.089	16.0	0.760
01/08/93	23:37:38	-24.5	951.5	0.0144	111	13.7	932.0	0.0000	128	-0.087	16.0	0.821
01/10/93	23:40:25	-22.3	933.1	0.0069	144	13.7	932.0	0.0000	128	-0.100	16.0	0.782
01/12/93	23:43:24	-22.2	946.4	-0.0017	473	13.7	932.0	0.0000	128	-0.100	16.0	0.763

Table D.2: Sunset data (see Section 3.1 for explanation).

Date (U.T.)	Time (U.T.)	T (C) (event)	P (mb) (event)	dT/dh (C/m) (event)	h (m) (event)	T (C) (survey)	P (mb) (survey)	dT/dh (C/m) (survey)	h (m) (survey)	a(hor.) (deg.)	d (km)	R' (deg.)
01/13/93	23:45:30	-22.2	946.4	-0.0036	55	13.7	932.0	0.0000	128	-0.100	16.0	0.822
01/14/93	23:49:23	-18.4	927.2	0.0175	57	13.7	932.0	0.0000	128	-0.096	16.0	1.108
01/16/93	23:49:04	-8.8	933.7	0.0038	206	13.7	932.0	0.0000	128	-0.101	16.0	0.652
01/17/93	23:51:48	-9.9	930.5			13.7	932.0	0.0000	128	-0.099	16.0	
01/18/93	23:54:42	-5.8	922.9			13.7	932.0	0.0000	128	-0.085	16.0	
01/22/93	23:59:04	-7.6	932.7	-0.0045	357	13.7	932.0	0.0000	128	-0.099	16.0	0.568
01/25/93	00:04:10	-7.6	925.6			13.7	932.0	0.0000	128	-0.080	16.0	
01/29/93	00:12:07	-8.3	936.2	-0.0030	308	13.7	932.0	0.0000	128	-0.080	16.0	0.811
01/30/93	00:12:59	5.5	930.4	0.0297	209	13.7	932.0	0.0000	128	-0.087	16.0	0.679
01/31/93	00:15:21	8.5	934.0			13.7	932.0	0.0000	128	0.025	16.0	
02/01/93	00:16:36	5.2	930.5	0.0044	90	13.7	932.0	0.0000	128	-0.077	16.0	0.645
02/02/93	00:17:57	5.6	935.3	0.0082	98	13.7	932.0	0.0000	128	-0.054	16.0	0.593
02/03/93	00:20:43	0.6	936.8	0.0203	276	13.7	932.0	0.0000	128	-0.071	16.0	0.686
02/04/93	00:23:20	2.4	935.7	-0.0266	45	13.7	932.0	0.0000	128	-0.067	16.0	0.755
02/08/93	00:30:05	4.0	930.1	0.0125	144	13.7	932.0	0.0000	128	-0.058	16.0	0.630
02/12/93	00:37:49	-9.3	936.1	0.0003	609	13.7	932.0	0.0000	128	-0.034	16.0	0.626
02/13/93	00:39:14	-4.3	936.1			13.7	932.0	0.0000	128	-0.032	16.0	

Table D.2: Sunset data (see Section 3.1 for explanation).



Date (U.T.)	Time (U.T.)	$T$ (C) (event)	$P$ (mb) (event)	$dT/dh$ (C/m) (event)	$h$ (m) (event)	$T$ (C) (survey)	$P$ (mb) (survey)	$dT/dh$ (C/m) (survey)	$h$ (m) (survey)	$a(\text{hor.})$ (deg.)	$d$ (km)	$R'$ (deg.)
02/16/93	00:45:40	-17.5	949.6	-0.0100	437	13.7	932.0	0.0000	128	-0.034	16.0	0.613
02/17/93	00:47:42	-16.8	948.7	-0.0080	748	13.7	932.0	0.0000	128	-0.032	16.0	0.625
03/06/93	01:21:02	6.8	934.4	-0.0060	704	13.7	932.0	0.0000	128	-0.063	16.0	0.649
03/12/93	01:31:57	-4.0	955.0	-0.0078	102	13.7	932.0	0.0000	128	-0.072	16.0	0.583
03/13/93	01:34:04	-6.8	944.3	-0.0086	93	13.7	932.0	0.0000	128	-0.063	16.0	0.629
03/17/93	01:41:48	-12.0	943.3	-0.0083	530	13.7	932.0	0.0000	128	-0.074	16.0	0.661
03/20/93	01:46:55	1.8	930.4	-0.0096	719	13.7	932.0	0.0000	128	-0.058	16.0	0.613
03/25/93	01:55:49	6.4	931.6	0.0102	665	13.7	932.0	0.0000	128	-0.064	16.0	0.570
03/26/93	01:57:34	3.0	935.9	-0.0110	692	13.7	932.0	0.0000	128	-0.064	16.0	0.549
04/04/93	02:12:51	6.9	927.8	-0.0116	571	18.4	934.6	-0.0127	640	0.072	15.8	0.552
04/05/93	02:14:45	8.8	924.8	-0.0108	610	18.4	934.6	-0.0127	640	0.055	15.8	0.545
04/07/93	02:18:35	-0.2	930.3	-0.0108	637	18.4	934.6	-0.0127	640	0.051	15.8	0.568
04/12/93	02:27:36	4.2	935.5	-0.0067	687	20.7	930.1	-0.0118	692	0.033	15.8	0.535
04/14/93	02:31:09	7.2	931.5	-0.0107	657	20.7	930.1	-0.0118	692	0.025	15.8	0.894
04/15/93	02:32:59	7.6	932.2	-0.0112	679	20.7	930.1	-0.0118	692	0.040	15.8	0.528
04/19/93	02:41:55	2.7	935.0	-0.0104	666	20.7	930.1	-0.0118	692	0.060	36.4	0.781
05/01/93	03:02:08	12.5	935.4			20.7	930.1	-0.0118	692	-0.005	11.6	

Table D.2: Sunset data (see Section 3.1 for explanation).

Date (U.T.)	Time (U.T.)	$T$ (C) (event)	$p$ (mb) (event)	$dT/dh$ (C/m) (event)	$h$ (m) (event)	$T$ (C) (survey)	$p$ (mb) (survey)	$dT/dh$ (C/m) (survey)	$h$ (m) (survey)	$a$ (hor.) (deg.)	$d$ (km)	$R'$ (deg.)
05/10/93	03:19:10	13.9	933.9	-0.0109	698	13.7	932.0	0.0000	128	-0.106	34.9	0.502
05/13/93	03:24:36	23.2	934.7	-0.0103	755	13.7	932.0	0.0000	128	-0.149	34.9	0.492
05/14/93	03:26:35	15.9	938.7	-0.0105	763	13.7	932.0	0.0000	128	-0.148	34.9	0.531
05/16/93	03:29:34	12.8	936.2	-0.0117	581	13.7	932.0	0.0000	128	-0.154	34.9	0.482
05/19/93	03:34:43	12.3	940.0	-0.0026	470	13.7	932.0	0.0000	128	-0.144	34.9	0.538
05/20/93	03:36:00	14.6	933.1	-0.0114	719	13.7	932.0	0.0000	128	-0.145	34.9	0.493
06/02/93	03:54:35	13.6	935.2	-0.0115	590	13.7	932.0	0.0000	128	-0.149	34.9	0.550
06/05/93	03:57:34	14.9	931.4	-0.0198	131	13.7	932.0	0.0000	128	-0.148	34.9	0.505
06/09/93	04:01:19	15.8	928.5	-0.0246	122	13.7	932.0	0.0000	128	-0.138	34.9	0.502
06/19/93	04:08:16	13.8	931.0	-0.0067	688	13.7	932.0	0.0000	128	-0.157	34.9	0.586
06/20/93	04:07:53	15.3	930.7	-0.0091	679	13.7	932.0	0.0000	128	-0.157	34.9	0.509
06/21/93	04:08:12	17.6	932.3	-0.0194	93	13.7	932.0	0.0000	128	-0.157	34.9	0.506
06/25/93	04:08:32	10.2	938.0	-0.0130	108	13.7	932.0	0.0000	128	-0.133	34.9	0.526
07/17/93	03:54:58	12.9	936.9	-0.0274	73	13.7	932.0	0.0000	128	-0.144	34.9	0.507
08/19/93	02:54:08	18.3	937.9	-0.0102	761	13.7	932.0	0.0000	128	0.052	36.4	0.442
08/20/93	02:52:02	21.4	936.8	-0.0100	760	13.7	932.0	0.0000	128	0.058	36.4	0.462
08/30/93	02:29:49	11.9	941.1	-0.0104	769	15.0	934.0	-0.0104	610	0.040	15.8	0.543

Table D.2: Sunset data (see Section 3.1 for explanation).

Date (U.T.)	Time (U.T.)	$T$ (C) (event)	$p$ (mb) (event)	$dT/dh$ (C/m) (event)	$h$ (m) (event)	$T$ (C) (survey)	$p$ (mb) (survey)	$dT/dh$ (C/m) (survey)	$h$ (m) (survey)	$a$ (hor.) (deg.)	$d$ (km)	$R'$ (deg.)
09/02/93	02:22:10	13.9	936.6	-0.0105	323	15.0	934.0	-0.0104	610	0.048	15.8	0.472
09/03/93	02:19:52	20.1	930.3	-0.0099	703	15.0	934.0	-0.0104	610	0.039	15.8	0.473
09/06/93	02:12:59	14.6	939.5	-0.0170	212	15.0	934.0	-0.0104	610	0.035	15.8	0.511
09/07/93	02:10:21	15.8	939.4	-0.0104	771	15.0	934.0	-0.0104	610	0.050	15.8	0.498
09/08/93	02:07:48	19.5	931.8	-0.0068	413	15.0	934.0	-0.0104	610	0.072	15.8	0.504
09/09/93	02:05:12	15.4	938.5	-0.0090	736	15.0	934.0	-0.0104	610	0.067	15.8	0.473
09/10/93	02:02:57	14.7	939.1	-0.0106	775	15.0	934.0	-0.0104	610	0.065	15.8	0.496
09/18/93	01:43:55	14.4	932.4	-0.0098	711	15.0	934.0	-0.0104	610	0.009	14.0	0.513
09/21/93	01:36:25	7.9	938.1	-0.0111	721	15.0	934.0	-0.0104	610	0.021	14.0	0.506
09/22/93	01:33:54	10.2	935.1	-0.0107	709	15.0	934.0	-0.0104	610	0.026	14.0	0.503
09/26/93	01:23:57	7.2	942.9	-0.0110	765	15.0	934.0	-0.0104	610	-0.003	14.0	0.449
09/28/93	01:19:30	12.2	942.7	0.0044	90	15.0	934.0	-0.0104	610	0.009	14.0	0.532
09/29/93	01:16:50	14.2	942.9	-0.0108	758	15.0	934.0	-0.0104	610	0.027	14.0	0.512
10/01/93	01:12:07	7.0	937.2	0.0097	716	15.0	934.0	-0.0104	610	0.002	14.0	0.515
10/02/93	01:09:47	9.8	935.3	-0.0090	712	15.0	934.0	-0.0104	610	0.011	14.0	0.530
10/03/93	01:07:22	18.9	932.2	-0.0086	720	15.0	934.0	-0.0104	610	0.009	14.0	0.527
10/08/93	00:56:38	4.0	946.2	-0.0106	727	13.7	932.0	0.0000	128	-0.075	16.0	0.613

Table D.2: Sunset data (see Section 3.1 for explanation).

Date (U.T.)	Time (U.T.)	$T$ (C) (event)	$p$ (mb) (event)	$dT/dh$ (C/m) (event)	$h$ (m) (event)	$T$ (C) (survey)	$p$ (mb) (survey)	$dT/dh$ (C/m) (survey)	$h$ (m) (survey)	$a$ (hor.) (deg.)	$d$ (km)	$R'$ (c.g.)
10/09/93	00:53:55	10.0	943.3	-0.0104	383	13.7	932.0	0.0000	128	-0.062	16.0	0.576
10/10/93	00:51:34	-0.9	933.0	-0.0079	712	13.7	932.0	0.0000	128	-0.062	16.0	0.579
10/11/93	00:48:57	10.9	933.3	-0.0101	695	13.7	932.0	0.0000	128	-0.062	16.0	0.538
12/08/93	23:17:50	-3.9	917.4	0.0146	516	13.7	932.0	0.0000	128	-0.090	16.0	0.801
12/16/93	23:16:34	-11.3	940.3	0.0370	130	13.7	932.0	0.0000	128	-0.080	16.0	0.727
12/18/93	23:17:55	-0.7	934.8	-0.0098	368	13.7	932.0	0.0000	128	-0.080	16.0	0.797

Table D.2: Sunset data (see Section 3.1 for explanation).